

Thermochemical characterisation of the gas circulation in the relevant cement industry processes

Doctoral Thesis

To be awarded the degree

Doctor rerum naturalium (Dr. rer. nat.)

submitted by

Kamila Anna Armatys

from Wrocław, Poland

approved by the Faculty of Natural and Material Science

Clausthal University of Technology

Date of oral examination

7 October

Gedruckt mit Unterstützung des Deutschen Akademischen Austauschdienst

The work was written in the Institute for Nonmetallic Materials, Clausthal University of Technology.

Chairperson of the board of examiners: Prof. Dr.-Ing. habil. Joachim Deubener

Chief reviewer: Prof. Dr. rer. nat. Albrecht Wolter

Reviewer: Prof. Dr.-Ing. habil. Mirosław Miller

Acknowledgements

In completing this piece of research I would like to acknowledge the kind assistance of the following people:

Prof. Dr. A. Wolter, TU Clausthal, Institute for Non-metallic Materials for suggesting the subject, supervising this work and valuable suggestions,

Prof. Dr. M. Miller, TU Wrocław, EIT+ Research Center for supervising the work, many years of patience, suggestions, invaluable discussions, infinite encouragement, guidance, and support,

Dipl. Chem. D. Kobertz, FZ Juelich, for introducing me into the complicated KEMS world, many discussions, helpful suggestions and a lot of patience,

Dr. L. Bencze for the help by the thermodynamic calculations and a lot of discussions and suggestions,

Dr. A. Matraszek for many suggestions, patience and supporting me at that time,

Dipl. Ing. Seelbach for technical support,

All colleagues in the Institute for Non Metallic Materials, especially Mr. Zellmann for XRF/XRD analyses, Mrs. Luer and Mr. Rust for chemical analyses, A. Blasig for years of support by KEMS, J.P. Fouda, Ch. Ott, Ch. Mehling, T. Bohne, Mrs. Behfeld, Mr. Putzig and Mr. Holly, Mrs. Bringe-Schubert, and Mr. Schaaf,

DAAD (Scholarship No. A0878364) and Klaus-Dyckerhoff Stiftung for the financial support, further support came from Forschungsinstitute der Zementindustrie in Düsseldorf (i.e. materials for Knudsen cells)

My family and friends for a lot of support and patience.

Table of content

INTRODUCTION

1. Fundamentals	6
1.1 Manufacture of cement clinker	7
1.2 Material cycle	9
2. Knudsen effusion mass spectrometry	13
2.1 Principle of the method	14
2.2 Hardware aspects	16
2.3 Partial pressures	18
2.3.1. Calibration procedure	20
2.4 Thermodynamic properties of the condensed phase	21
2.5 Congruent effusion	24
3. The aims of the work	26

EXPERIMENTAL SECTION

4. Investigation methods, apparatus	27
4.1. KEMS	27
4.1.1 Calibration of the mass spectrometer	29
4.2 Additional methods	31
4.2.1. XRD	31
4.2.2. XRF	31
5. Alkali sulphates	32
5. 1.Fundamentals	32
5.2. Vaporisation of Na_2SO_4	35
5.3. Vaporisation of K_2SO_4	40
5.4. Vaporisation of CaSO_4	47

5.5. System $\text{Na}_2\text{SO}_4 - \text{CaSO}_4$	50
5.5.1. Thermodynamic activities for the system $\text{Na}_2\text{SO}_4 - \text{CaSO}_4$	52
5.6. System $\text{K}_2\text{SO}_4\text{-CaSO}_4$	55
5.6.1. Thermodynamic activities for the system $\text{K}_2\text{SO}_4\text{-CaSO}_4$	57
5.7. System $\text{Na}_2\text{SO}_4\text{-K}_2\text{SO}_4$	61
5.8. Discussion	66
6. Industrial samples	70
6.1. The fundamentals of the experiment	70
6.2 Characterization of the industrial materials	73
6.2.1 Humidity and volatile matter	73
6.2.2. XRF Results	74
6.2.2.1 The degree of sulphatisation	76
6.2.3. XRD Results	78
6.3 Analysis of the vaporisation of industrial samples by KEMS	80
6.3.1. The investigation procedure	80
6.3.2 The assignment of the ions to the neutral precursors	82
6.3.3. The comparison of the materials vaporisation	84
6.3.3.1. Materials from different part of the kiln	85
6.3.3.2. Materials from different cement plants	98
6.3.4. Lead vaporisation	106
6.3.5. Mixed and polymeric species	109
6.4. Discussion	111
7. Outlook	117
8. Conclusions	120
9. References	122

INTRODUCTION

1. Fundamentals

The present investigations were undertaken due to the serious industry problems with obtaining cement clinker. Raw materials and fuels used for clinker production contain significant amounts of sulphates, chlorides, alkali, alkali earth compounds as well as heavy metal compounds. These substances can react under technological conditions, giving volatile species that vaporize completely and subsequently condense in colder reactor parts. Simultaneously, raw materials flow continuously introduced into reactor causes secondary steering of volatile species to the high temperature reactor area. During that process, the evaporation/condensation cycle of volatile species produced in the technological regime takes place, leading to unsteady kiln operation, increased refractory consumption and clinker quality, clogging and finally the necessity of production breaks aimed in reactor cleaning from substances deposited at its walls. In investigating the mechanism of such processes of particular importance are the vapour pressure investigation and determination of the thermodynamic properties. The typical methods used in cement chemistry for the investigation of the alkali circulation and clogging phenomenon are x-ray diffraction, x-ray fluorescence, SEM, and other analytical methods describing mostly the condensed phase, along with the modelling of chemical reactions of the alkalis in the cement kiln. The mechanism of vaporisation of the gaseous species in the cement kiln has not been investigated directly so far. A very versatile method of analysis of high-temperature vapours and such complex processes should be therefore the Knudsen effusion mass spectrometry (KEMS) that enables the identification of the gaseous species and determination of their partial pressures as well as thermochemical characteristics of chemical processes going on in the cement kiln. The present study widely implemented KEMS for studying the cement – clinker processes following investigations completed in the research group of Prof. Albrecht Wolter (Institut für Nichtmetallische Werkstoffe TU Clausthal) by Graciela Eguia [1].

1.1 Manufacture of cement clinker

The clinker used for cement production is produced by using the most readily available and cheapest raw materials. It is composed of different oxides that are typically 67% CaO, 22% SiO₂, 5% Al₂O₃, and 3% Fe₂O₃. The remaining 3% are other oxides and nonoxide components. It is common in cement chemistry to use an abbreviation for the formulae of the commoner oxides as single letters, according to table 1.1. The chemical formula can be written further as a sum of particular oxides, which indicates that the constituent oxides have no separate existence within the structure.

Table 1.1 The abbreviations used in cement chemistry for oxide description

Oxide	Abbreviation
CaO	C
SiO ₂	S
Al ₂ O ₃	A
Fe ₂ O ₃	F
MgO	M
K ₂ O	K
SO ₃	\bar{S}
Na ₂ O	N

Apart from the main oxide components, there also occur secondary elements such as chemical species, which participate in the transformation process of the raw metal into the clinker. They distribute differently to the clinker phases at high temperatures and determine a possible displacement of the equilibrium among the phases. Alkali are the technologically less desirable compounds among the secondary ones [2]. The content of the secondary, minor and trace elements in clinker are presented in table 1.2 [3].

Table 1.2. Concentration ranges (by mass content) of main, secondary, and trace elements in cement clinker [3]

Definition	Element	Content
Main elements	Ca, Si, Al, Fe, O, C, N	> 5%
Secondary elements	Mn, Mg, K, Na, Ti, P, Ba, Sr, Cr, S	1 – 5 %
Minor and trace elements	Cd, Sb, As, Co, Ni, Te, Zn, Pb, Cr, V, Ti	< 1%

The main four phases of the clinker are alite (Ca_3SiO_5), belite (Ca_2SiO_4), tricalcium aluminate ($\text{Ca}_3\text{Al}_2\text{O}_6$) and dicalcium aluminoferrite ($\text{Ca}_2\text{AlFeO}_5$). A small amount of alkalis, up to about 2%, and up to over 2% of sulphate occurs in clinker, as coming from raw meal and fuels. The total alkali content is in cement chemistry calculated as per cent by mass Na_2O equivalent, according to formula (1.1), the sulphate content is calculated as SO_3 .

$$\%_{\text{by mass}} \text{Na}_2\text{O}_{\text{equivalent}} = 0.658 \cdot \%_{\text{by mass}} \text{K}_2\text{O} + \%_{\text{by mass}} \text{Na}_2\text{O} \quad (1.1)$$

Table 1.3 summarizes main phase content in clinker and their abbreviations according to table 1.1 [4].

Table 1.3 Main phases content in clinker and their abbreviation terms [4],

Phase	Chemical composition	% in clinker	Industrial term
alite	Ca_3SiO_5	50 – 70	C_3S
belite	Ca_2SiO_4	15 – 30	C_2S
aluminate	$\text{Ca}_3\text{Al}_2\text{O}_6$	5 – 10	C_3A
aliminoferrite	$\text{Ca}_2\text{AlFeO}_5$	5 – 15	C_4AF
Compound			
alkalis	K_2O	0.4 – 1.8	K
	Na_2O	0.05 – 0.5	N
sulphate	SO_3	< 2%	$\bar{\text{S}}$

In producing clinker, different types of fuels are used. They mostly include hard coal, lignite, heavy fuel oil and natural gas. Additionally, more and more commonly, waste fuels are used as alternatives; among them are old car tyres, acid sludge, bleaching clay, used oils, shredded and domestic refuse [5].

The clinker is burned in the rotary kiln that is a refractory – lined tube, which is inclined at up 3.5° and rotates at 1.5 to 3 revolutions per minute about its longitudinal axis. The material feeds in the upper part of a kiln and runs counter-current towards the flame located at the end of a tube. The temperature of a flame reaches $1800 - 2000^\circ\text{C}$; the kiln feed reaches temperatures $1350 - 1500^\circ\text{C}$. To heat the material before introducing it into the kiln, cyclone preheaters are applied. They are combined with the rotary kiln so that the exhaust gas passes through the cyclone from the bottom to the top. In this manner, the material is initially heated from $810 - 840^\circ\text{C}$, and the exhausted gas is cooled down to $330 - 380^\circ\text{C}$ when it leaves the cyclone stage [5]. The scheme of clinker production is presented in figure 1.1 [6].

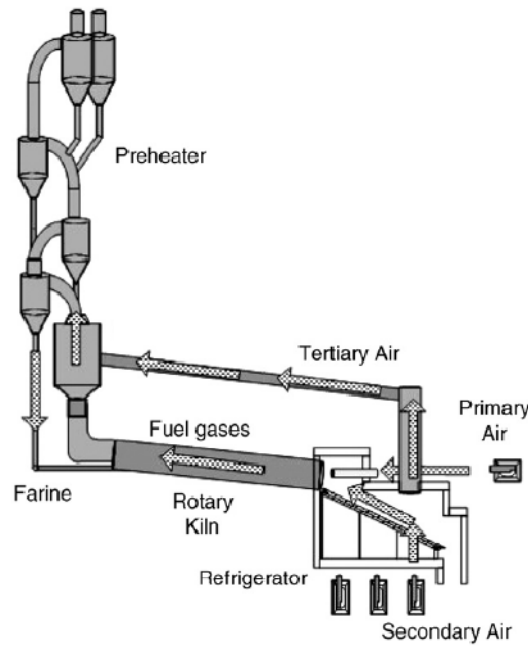


Figure 1.1. A schematic draft of the cement production installation; the rotary kiln is combined with cyclone preheater.

1.2 Material cycle

The information about the recirculation behaviour of the species in relation to the clinker production could be described by using mass flow diagram, called Sankey diagram, on which the flows of the incoming, recirculated and discharged masses of the relevant constituent are presented (figure 1.2.) Raw materials (1) and fuels (2) are inputs to the mass flow diagram that supply the kiln plant. As outputs are identified the quantities, which are removed from the kiln system, such as clinker (a), volatilities (c) that are removed along with clinker. The recirculation can be also reduced by removing alkali-rich dust or by drawing off some of the gas by using bypass (b), which is considered as discharging masses. The external balance provides no information about the nature and extent of the recirculation system [5].

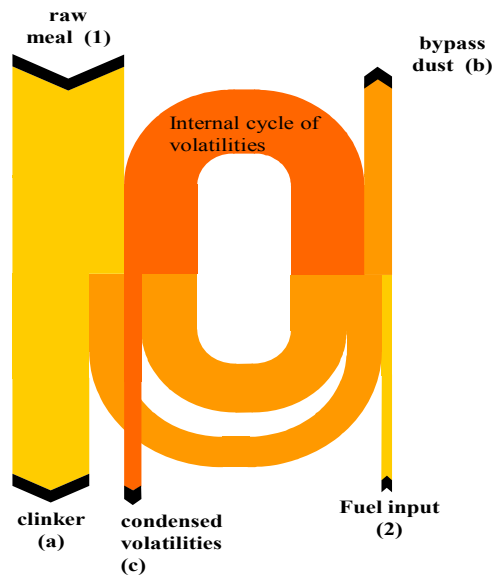


Figure 1.2. A mass flow diagram of the volatile species during clinker production

Alkali sulphates and chlorides are the most important recirculating constituents which are responsible for corrosional coating formation. Coatings occur around different parts of a kiln system in the forms of blades of the exhausted gas and intermediate gas fans, two bottom stages of cyclone preheater or in the rotary kiln in the form of rings. Coatings also cause operating problems by delaying the flow of the kiln feed and kiln gas into the reactor and reducing the output from the cement kiln. Moreover, balls of a kiln feed of the size up to a diameter of 1 meter could be created and through their weight the kiln brickwork and clinker cooler can be damaged. The phase composition of solidified coatings, in addition to raw meal and clinker constituents, is as follows [5]:

- CaSO_4 (anhydrite),
- KCl (sylvite),
- K_2SO_4 (arcanite)
- $\text{K}_2\text{SO}_4 \cdot \text{CaSO}_4$ (calcium langbenite)
- $2\text{C}_2\text{S} \cdot \text{CaCO}_3$ (spurrite)
- $2\text{C}_2\text{S} \cdot \text{CaSO}_4$ (sulphate spurrite)

Chlorine is introduced as a constituent of chlorides into the cement kiln in limestone, clays and, in some cases, in both primary and secondary fuels. In limestone and clay, the predominant chloride is sodium chloride as well as some coals containing chlorides, mainly NaCl . In waste-derived fuels such as waste-oils contaminated with chlorine, chlorinated hydrocarbons and tires, the chlorine occurs in different compounds in the high concentrations. Volatile chlorine containing compounds

react readily with alkalis, causing serious operational problems even in kilns equipped with bypass [3].

Sulphur is frequently present in coals, some fuel oils, and in limestones. Clayey sediments, the so-called marls, sometimes contain also sulphur as sulphides and sulphates. Sulphur forms volatile compounds and its behaviour in a kiln is complex. There is some fundamental knowledge of the sulphate behaviour, stated that the sulphur, coming from raw materials and fuels under oxidizing burning conditions, forms to SO_2 , which further in the presence of oxygen tends to react with alkalis present in different oxide phases according to reactions [5]:



Sulphates combine preferably with alkalis, giving alkali sulphates. When there is an excess of sulphates it tends to react with CaO and form calcium potassium sulphate $2\text{CaSO}_4 \cdot \text{K}_2\text{SO}_4$ (langbeinite) or CaSO_4 (anhydrite). Major alkali sulphates formed with SO_2 and their melting temperatures on base of Bhatti report [3] are presented in table 1.4.

Table 1.4. Major alkali sulphates forming during clinker production and their melting temperatures, based on [3]

Alkali compounds	Chemical formulae	Melting temperature/ $^{\circ}\text{C}$
Potassium sulphate (arcanite)	K_2SO_4	1071 [7]
Sodium sulphate	Na_2SO_4	883 [7]
Calcium sulphate (anhydrite)	CaSO_4	1462 [8]
Sodium potassium sulphate (aphthiaticite)	$\text{K}_2\text{SO}_4 \cdot \text{Na}_2\text{SO}_4$	968 [3]
Calcium potassium sulphate (calcium langbenite)	$2\text{CaSO}_4 \cdot \text{K}_2\text{SO}_4$ ($\text{Ca}_2\text{K}_2(\text{SO}_4)_3$)	1011 [8] (incongruent melting)
Calcium potassium sulphate (syngenite)	$\text{K}_2\text{SO}_4 \cdot \text{CaSO}_4 \cdot \text{H}_2\text{O}$ ($\text{Ca}_2\text{K}_2(\text{SO}_4)_2 \cdot \text{H}_2\text{O}$)	1004[3]

The most frequent recirculation and condensation ranges of the constituents that occurred in the kiln system are presented in figure 1.3.

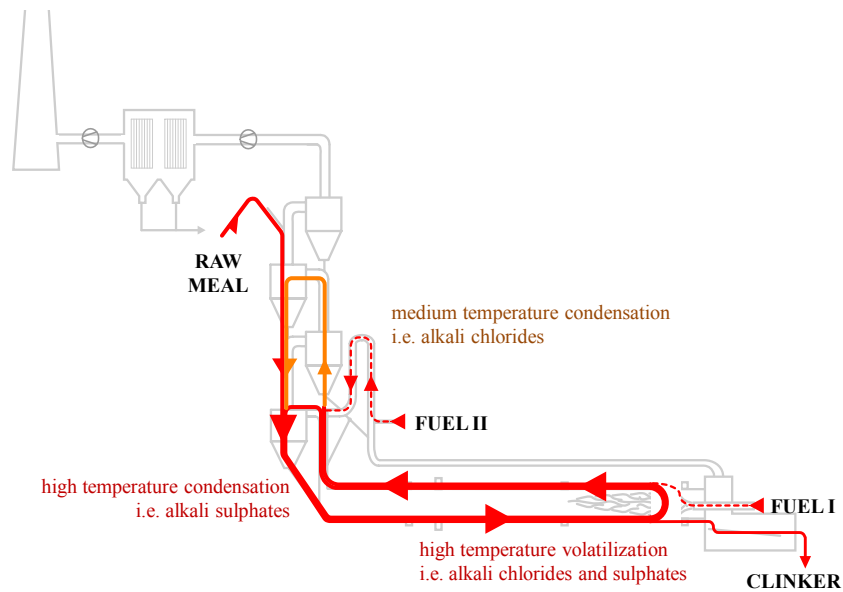


Figure 1.3. Vaporisation and condensation of alkali chlorides and sulphates in the cement kiln [9].

The recirculation of the constituents can be reduced by drawing off some of the gas by using bypass, but the volatilization mechanism is not known in accurate thermodynamic and kinetic terms.

2. Knudsen Effusion Mass Spectrometry

High temperature processes have nowadays become more common since the advent of new technologies. They have created a possibility of producing new materials, new efficient and ecological energy sources or to receive pure compounds in metallurgical processes based on chemical transport. Unfortunately, all high temperature processes also pose new problems and difficulties. For example, in the high temperature sections of the reactor only very small materials can be applied for its building since the utility of various materials decreases with the increasing temperature. Chemical and physical processes such as corrosion, diffusion and vaporisation, which do not occur at low temperatures, rise to an enormous challenge at high temperatures [10].

High temperature mass spectrometry, also known as Knudsen effusion mass spectrometry (KEMS), is the most powerful method to analyse vapour species in equilibrium with the condensed phases in spite of its rather rare applications for this purpose. It enables the identification of the major, minor and even traces of gaseous species and the determination of their partial pressures. This method offers the highest potential for equilibrium vaporisation studies. From the partial pressure one can obtain the thermodynamic data like activity, enthalpy ΔH or entropy ΔS . This method offers the highest potential for equilibrium vaporization studies.

Mass spectrometry combined with Knudsen effusion method was applied for the first time in 1948 by Ionov [11] for studying a vaporisation of alkali metal halides; later, the investigation of the free evaporation of carbon by Chupka and Inghram [12] and Honig [13] were carried out by applying KEMS method. Since that time, Knudsen effusion mass spectrometry, with its attractive features of high sensitivity and resolution under high vacuum conditions, has become a useful tool for the quantitative detection of gaseous species effusing from the Knudsen cell. Nowadays, the method is still a powerful tool for thermodynamic investigations of inorganic materials by the determination of the composition of the equilibrium gaseous phase. At present, around twenty six research groups work with this unique technique, showing still a large activity in this area [14].

2.1. Principle of the method

In past studies, in high temperature chemistry by studying the gas phase over the condensation phase, it was often assumed that the molecules in the gas phase should be simple and small, related to the chemical stoichiometry of the studied compound. In 1948, Ionov [11] showed in his first work, by means of the Knudsen effusion mass spectrometry, that the equilibrium vapour over the alkali halides $MX(c)$ consists of the monomer and dimer molecules $MX(g)$ and $(MX)_2(g)$, Chupka and Inghram [12] as well as Honig [13] showed that the main gas molecule over the carbon sample is $C_3(g)$. The identification of such molecules brought about some entirely new aspects to the usual concepts of chemical bonding and valence because in many cases complex molecules are the predominant species. Therefore, the subject of gas chemistry at high temperatures has grown to become a branch as distinct and varied as solution chemistry [15]. The molecular effusion method combined with mass spectrometry has become a standard thermodynamic tool applied to the characterization of vapour pressures of a variety of high-temperature materials and systems.

The Knudsen effusion mass spectrometry is the combination of two different experimental techniques. One technique is based on Knudsen effusion which was described by Martin Knudsen in the 1900 [16] and is based on the kinetic theory of dilute gases by which the molecular flux at a boundary can be calculated for a gas at equilibrium [17]; the other part is the mass spectrometry as a powerful complementary technique that enables a sensitive analysis of a gas phase.

The most important part of the spectrometer is the Knudsen cell. It is a small container made of inert material with an effusion orifice being small relatively to cell dimensions. The principle of the Knudsen effusion method is that the mass loss $dm(i)/dt$ of the sample effusing from Knudsen cell through the orifice with an area q in the unit of time in the form of different species or atoms i , is related to the partial pressures, $p(i)$ by the Knudsen equation (2.1).

$$\frac{dm(i)}{dt} = \frac{Cqp(i)\sqrt{M(i)}}{\sqrt{2\pi RT}} \quad (2.1)$$

where,

C – Clausig factor

M – molecular weight of the species i

T – absolute temperature

The loss of vapour which effuses from the cell does not disturb the equilibrium inside, therefore it can be considered quantitatively and qualitatively as a representative of the equilibrium gaseous phase being in equilibrium with condensed species present in the Knudsen cell. The Clausing factor C describes the probability of leaving the Knudsen cell by the gaseous species which reached the effusion orifice. It depends on the geometry and the size of the orifice [18].

The Knudsen effusion method is spoken, when the molecular flow takes place, that is the molecules of the gas passing through an orifice move nearly independently of one another and thereby have no appreciable effect on the equilibrium; these conditions are filled primarily in the medium and lower – pressure regions. The condition for the molecular flow was established by the equation [17]

$$\frac{\lambda}{D} > 10 \quad (2.2)$$

where

λ – mean free path for the gas

D – orifice diameter

Therefore, the disadvantage of the method is its limitation to comparatively low pressures up to about 10 Pa, which is a typical limit for the molecular flow. When the molecular flow is preserved, there are no gas collisions and molecules arriving at the orifice come directly from the area of the vaporizing material or from the walls of the enclosure. [17] The mathematical description of the probability of the molecule leaving the Knudsen cell according to limitation of the method was described by Motzfeldt [19], Whitman [20], et al. [21-25].

2.2. Hardware aspects

The Knudsen mass spectrometer consists of the ion source, the separation part and the detector system connected with the Knudsen cell assembly. The high vacuum is obtained in the mass spectrometer and in the Knudsen cell chambers by using a cascade of vacuum pumps. In figure 2.1, a scheme of a magnetic-type sector field mass spectrometer coupled with the Knudsen cell is presented.

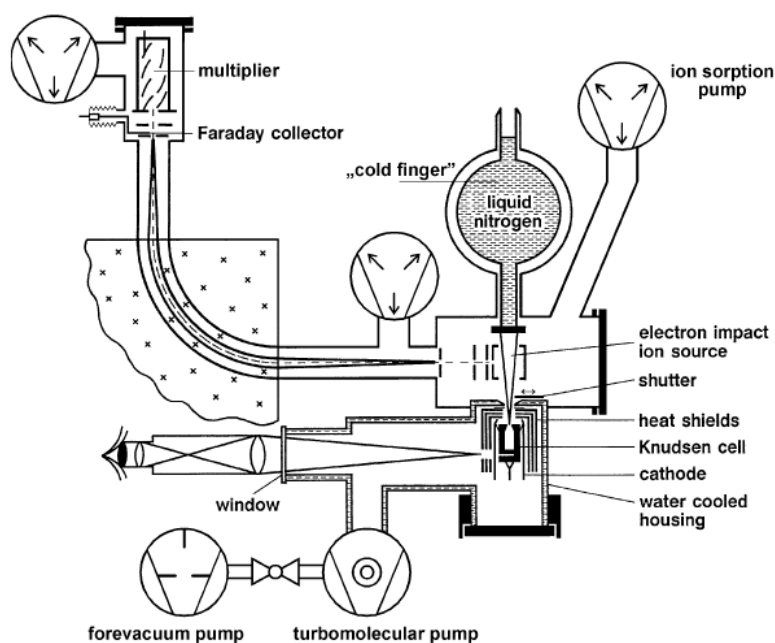


Figure 2.1. The scheme of mass spectrometer with the Knudsen cell [10]

Another scheme of the Knudsen effusion mass spectrometry is presented in figure 2.2.

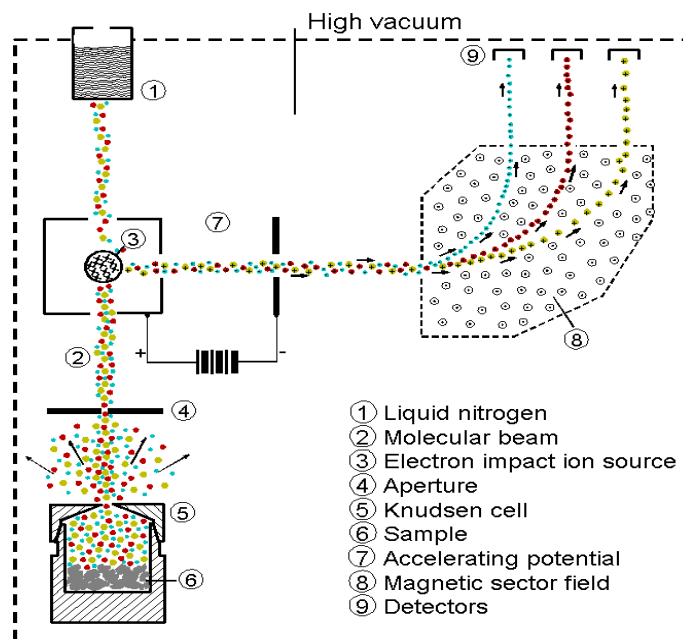


Figure 2.2. Schematic representation of the Knudsen effusion mass spectrometry [26].

The Knudsen cell (5) with the substance under investigation (6) is placed inside the mass spectrometer near the ionisation chamber (3). The sample effuses as molecular beam that goes through the ionisation chamber (3) where ions and molecular fragments are formed by electron impact. Molecules that do not undergo ionization are frozen in a cold trap (1). The ions are accelerated in the electric field (7) and then separated in the magnetic field (8) by their mass-to-charge ratio. For the ion detection Faraday cup and/or electron multiplier is used (9). Ions are identified by their mass, isotopic distribution and by interrupting the molecular beam with the shutter, which is placed near the aperture 4 as shown in figure 2.2.1. By the interruption of the beam by a shutter, the distinguishing of the ions from the sample vapours from those existing continuously in the background is possible.

Knudsen cell can be heated in the ambient temperature up to the 2500 K and more by heat radiation, by electron bombardment with energy of 1 to 2 keV or by a high voltage frequency. The temperature of the sample (or – rather – Knudsen cell) is measured by thermocouple or/and by optical pyrometer sighted on the black body cavity which is laterally positioned, close and below the bottom of the cell. [26]. Many authors described the principles of Knudsen effusion mass spectrometry [14, 15, 27-32]. The newest work of Copland [31] describes Knudsen effusion mass spectrometry and the relevant measurements in detail and presents solutions of the main difficulties during the measurement processes. Drowart et al.[32] in their recent report present an overview of the thermodynamic and technical aspects of the KEMS method.

Knudsen effusion mass spectrometry is a unique, and yet universal, method of gas analysis in the vapour over the condensed phase in equilibrium. Almost all groups of inorganic materials were investigated so far, which include: borides, carbides, fullerenes, nitrates, sulphates, halides, metals, alloys, oxides, glasses, and ceramics. An overview of these studies is summarized in the recent issue of The Open Journal of Thermodynamics [14].

2.3. Partial pressures

An understanding of the vaporisation process requires knowledge of both the condensed and the gaseous phases. The first step is the characterization of the vapour phase and the identification of the vapour species. There are several ways of measuring the vapour pressures of substances. The most common are: the static, boiling point, transpiration, Knudsen effusion and Langmuir free-evaporation methods. The Knudsen and the Langmuir methods are the most suitable because the experiment is carried out in the vacuum and the material transported away from the investigated sample [17].

The identification of the species allows then for the determination of other related aspects such as the thermodynamics of the various equilibria, mechanism of vaporisation, or even the molecular structures of the gaseous species could be further explored with great facility since the various gaseous species existing are known.

The first step in the gas phase analysis is the identification of the gas species. Mass spectrometry is the most versatile method for this purpose, since it enables very a sensitive identification of the various species in the vapour. High temperature mass spectrometry technique could be connected with Knudsen effusion method as a source of vapour species. In this manner, the various species occurring in the vapour could be detected and their partial pressures determined. Mass spectrometry is most universal for gas analysis used for the wide spectrum of analytical inorganic and organic samples [10, 33, 34].

The relationship between ion intensity measured by the detection system of the Knudsen effusion mass spectrometer and the partial pressure of a neutral species i inside a cell at the temperature T is defined by equation (2.3).

$$p(i) = \frac{k \cdot T \cdot \sum I(j,i)}{\sigma(i)} \quad (2.3)$$

where:

$p(i)$ - partial pressure of a molecule i

$I(j,i)$ - measured ion current j originating from the molecule i ,

$\sigma(i)$ - the total ionization cross-section of the molecule i

k - sensitivity constant of the KEMS system

When an ion j has more isotopes, only the most intense ion is usually measured, while and others are re-calculated taking into consideration their well-established isotopic distributions. The most difficult part in these calculations is the assignment of the ions to their neutral precursors, because the fragmentation of gas molecules makes it complicated. If an ion has more than one precursor, the contribution of each neutral precursor to the intensity of a particular ion must be determined.

The total ionization cross-section of the complex gaseous species could be either calculated or determined. The ionisation cross sections of the atoms were calculated theoretically by Mann [35], and measured by Freund et al. [36, 37]. The results for most chemical elements have shown complicity between the theoretical and measured values. The experimental studies of the ionisation cross section of the molecules have only been undertaken by few authors [36, 38]. For that reason, the additivity rule:

$$\sigma(M_x N_y K_v) = \sum \sigma(x \sigma(M) + y \sigma(N) + v \sigma(K)) \quad (2.4)$$

was suggested by Otvos and Stevenson [39] to obtain ionisation cross sections of complex molecules. However, the recent studies do suggest some modifications of the additivity rule [32]. The extensive calculation description of ionisation cross section was summarized in the IUPAC Report, by Drowart et al. [32].

2.3.1. The calibration procedure

The calibration procedure used in the present work was developed by Miller [10]. The temperature is measured by means of a thermocouple or by pyrometer calibrated *in situ* at the melting point of pure metal (*Me*), for example gold, nickel, silver placed in the effusion cell. Calibration constant *k* is calculated according to equation 2.5:

$$k = \frac{p(Me)\sigma(Me)}{I(Me^+)T_{melt}} \quad (2.5)$$

where *Me* is a pure metal and T_{melt} the temperature of the melting point of this metal.

For cooling the sample from T_l to T_{melt} or heating from T_{melt} to T_l , the temperature dependence of the vapour pressure of *Me* is described by an equation:

$$\ln p(Me, liq / sol) / Pa = -\frac{\Delta H_{vap/sub,m}^o}{RT} + \frac{\Delta S_{vap/sub,m}^o}{R} = A/T + B \quad (2.6)$$

The vaporisation/ sublimation enthalpy and vaporisation/sublimation entropy near the melting point are well known from the literature, for example [40]. The above reaction can be rearranged for the partial pressure of *Me* at T_l and T_{melt} to the following equation:

$$A = \frac{\ln p(Me, T_l^o) - \ln p(Me, T_{melt})}{1/T_l^o - 1/T_{melt}} = \frac{\ln(I_l \cdot T_l^o) - \ln(I_{melt} \cdot T_{melt})}{1/T_l^o - 1/T_{melt}} \quad (2.7)$$

where *A* is a calculated constant, from known values of vaporisation/sublimation enthalpy and vaporisation/sublimation entropy near the melting point and T_l^o is the corrected temperature. The only unknown value in equation (2.7) is T_l^o , which can be easily calculated by iteration. If temperature (T_l of the pyrometer/thermocouple is measured, the temperature correction ΔT_{corr} can be obtained as a difference $T_l^o - T_l$, the schematic representation of the calibration procedure is shown in figure (2.3).

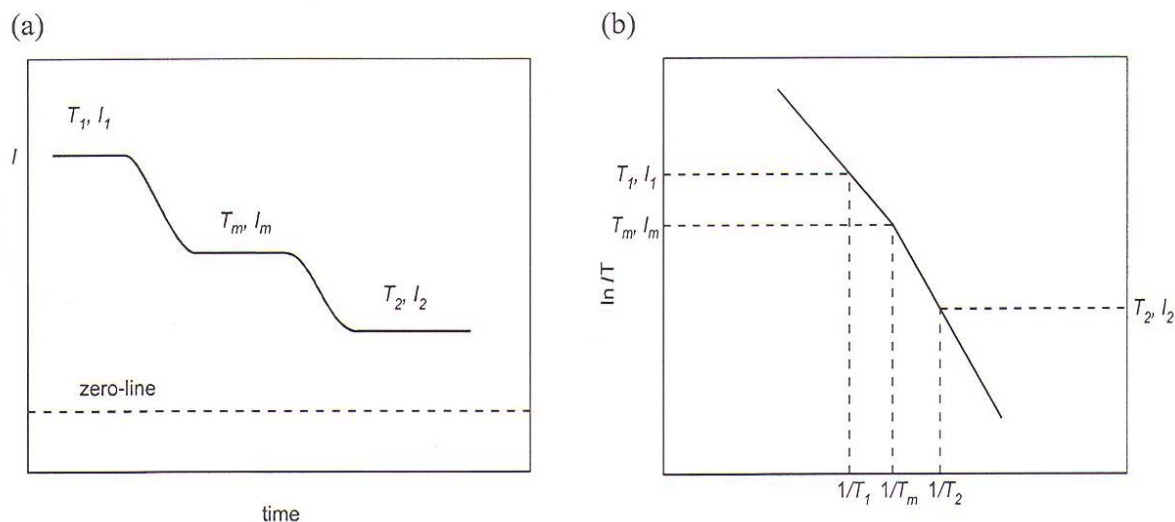


Figure 2.3. Schematic representation of calibration procedure, where T_m, I_m is $T_{\text{melt}}, I_{\text{melt}}$ – temperature and intensity in the melting point respectively.

From each cooling – heating measurement between T_1 and T_2 one obtains two corrections $T_1^o - T_1$ and $T_2^o - T_2$. The mean temperature correction ΔT_{corr} is calculated as the arithmetical mean of several values obtained in a series of cooling-heating measurements.

2.4. Thermodynamic properties of the condensed phase

Once the species have been identified and their pressures determined the thermodynamics of various equilibria involving the gaseous species and the mechanism of the vaporisation can be characterised, which enables the exhaustive characterisation of the gas phase in equilibrium with the condensed phase.

Knowledge of the partial pressures of the gas phase components in the system at the temperature T allows determining equilibrium constants K_p^o of the investigated reactions, according to the equation (2.8).

$$K_p^o = \prod \left(\frac{p(i)}{p^o} \right)^{\nu_i} \quad (2.8)$$

where ν_i is the stoichiometric coefficient of the reaction, and p^o denotes the standard pressure (10^5 Pa).

Temperature dependencies of the equilibrium constant are expressed by equation (2.9):

$$\ln K_p^\circ(T) = \frac{A}{T} + B \quad (2.9)$$

from which the value of enthalpy (2.10) and entropy (2.11) of the reaction are determined as follows

$$A = \frac{-\Delta_r H^\circ(T_m)}{R} \quad (2.10)$$

$$B = \frac{\Delta_r S^\circ(T_m)}{R} \quad (2.11)$$

The next step could be the determination of the Gibbs energy of the equilibrium process, as expressed by equation (2.12).

$$\Delta_r G^\circ(T) = \Delta_r H^\circ(T) - T\Delta_r S^\circ(T) = -RT \ln K_p^\circ(T) \quad (2.12)$$

Other thermodynamic values which can be determined by Knudsen effusion mass spectrometry are the thermodynamic activities of the component. The thermodynamic activity $a(i)$, of component i , at temperature T , in the condensed phase of the investigated system can be obtained from the partial pressure of the pure component, $p^\circ(i)$, and its partial pressures over the mixture, $p(i)$, determined at this temperature:

$$a(i) = \frac{p(i)}{p^\circ(i)} = \frac{k \cdot I(i) \cdot \sigma(i)}{k' \cdot I(i)^\circ \cdot \sigma(i)} \quad (2.13)$$

Providing thermodynamic activity of one component of binary system is known in the whole composition range, while the activities of the second component can be calculated by the Gibbs-Duhem method. At constant temperatures and pressure, the Gibbs-Duhem equation could be written as follows:

$$\sum_i x_i d \ln a_i = 0 \quad (2.14)$$

where:

x_i mole fraction of component i

a_i the activity of the component i .

The summation extends over all components. Adding $d \ln a_j$ to each side of the equation (2.14) and rearranging, one could obtain [41]:

$$d \ln a_j = - \sum_i x_i d \ln \frac{a_i}{a_j} \quad (2.15)$$

The rearranging of the eq. 2.15 lead to the equation 2.16 for activities calculation

$$d \ln a_j = - \frac{x_i}{x_j} \cdot d \ln a_i \quad (2.16)$$

Thermodynamic activities or activity coefficient and excess quantities can be obtained by the ion intensity ratio integration method developed by Belton and Fruehan [41]. The activity of a component is directly proportional to the partial pressure (assuming ideal gas behaviour) of the corresponding monomer gas species and in turn, is directly proportional to the measured ion current of an isotope of that species:

$$d \ln a_j = - \sum_i x_i d \ln \left(\frac{I_i^+}{I_j^+} \right) \quad (2.17)$$

For a binary system and with the pure component as standard state

$$\ln a_1 = - \int_{x_1=1}^{x_1=x_1} x_2 d \ln \left(\frac{I_2^+}{I_1^+} \right) \quad (2.18)$$

is obtained upon integration. For pure j component a_1 equals to zero; therefore, to avoid the neglecting of a certain integration area, instead of calculating activities directly, more suitable graphical integration of equation 2.18, that is

$$\ln \gamma_1 = - \int_{x_1=1}^{x_1=x_1} x_2 d \left[\ln \left(\frac{I_2^+}{I_1^+} \right) - \ln \left(\frac{x_2}{x_1} \right) \right] \quad (2.19)$$

can be evaluated, where γ_1 – is the activity coefficient, defined as

$$\gamma_1 = \frac{a_1}{x_1} \quad (2.20)$$

The activity coefficients are firstly calculated since γ_1 is not zero in pure j component but a finite value.

2.5. Congruent effusion

The applications of the molecular – effusion method require that the vaporisation process can be considered as a congruent one and the rate of vaporisation of the sample under investigation must be much greater than the rate of effusion. These conditions ensure that the vapour pressure is time invariant and the effusion rate is independent of the detailed mechanism of the vaporisation process [17]. The system must also be maintained at a constant temperature and there should be no reaction of the sample with the crucible material.

The distinction between the congruent and incongruent processes is that, as congruent vaporisation is concerned, when a gas has the same overall chemical composition as the condensed phase from which it arises, the same amount of the molecules turns up in the vapours and in the condensed phase. For example, alkali sulphate vaporisation, $M_2SO_4(c) = 2M_2(g) + O_2(g) + SO_2(g)$ is a congruent process. In the incongruent vaporisation process, the gas has a different composition from the condensed phase, for example vaporisation of water from the potassium chloride solution, $H_2O(KCl \text{ solution}) = H_2O(g)$ [17].

For a pressure measurement at a constant temperature in a two-component system to be meaningful, one of the following conditions must be applied:

- a) three phases must be present
- b) there must be two phases of the same composition
- c) there must be two phases that compositions are specified and fixed [17]

It is also possible to investigate a sample by means of the effusion method even though it vaporizes incongruently, but one of the cases (a) – (c) is fulfilled, for example reaction $CaSO_4(c) = CaO(c) + SO_2(g) + \frac{1}{2} O_2(g)$. There are three phases present and the vapour has a different composition from the condensed phase, but the composition of the phases is strictly specified. From one mole of $CaSO_4$ arise 1 mole CaO , 1 mole $SO_2(g)$ and 0.5 mole of oxygen, therefore the conditions a) and c) are fulfilled for pressure investigations. In the case of the water vaporisation from the potassium chloride/water system, the state of the water in the condensed phase is inadequately specified, the conditions a) – c) are not fulfilled, thus the congruent effusion method for this vaporisation cannot be applied.

According to the Knudsen effusion equation

$$\frac{dm(i)}{dt} = \frac{Cqp(i)\sqrt{M(i)}}{\sqrt{2\pi RT}} \quad (2.21)$$

Dividing both sides by molecular weight $M(i)$ of species (i) one obtain further

$$\frac{dn(i)}{dt} = \frac{Cqp(i)}{\sqrt{2\pi RT}\sqrt{M(i)}} \quad (2.22)$$

The vaporisation from the time when $t = 0$ to a particular time t will describe the total mass loss

$$\int_0^t \left(\frac{dn(i)}{dt} = \frac{Cqp(i)}{\sqrt{2\pi RT}\sqrt{M(i)}} \right) \quad (2.23)$$

therefore, for the constant temperature, the total mole number of species $M(i)$ effusing from the Knudsen cell can be expressed as a result of the previous integration and give the following equation (2.24) .

$$n(i) = B \frac{p(i)}{\sqrt{M(i)}} \quad (2.24)$$

where B is a constant.

3. The aims of the work

The present investigations were undertaken due to the serious problems of industry in obtaining clinker used for cement production. The aim of this work is a better understanding of the volatile cycles in cement production technology by studying the thermodynamics of gas-gas and gas-solid reactions between chemicals occurring in the cement kiln.

In order to study such chemically complex processes, investigations of pure compounds volatile at the cement production conditions: sulphates of sodium, potassium and calcium, are of particular importance. In the present work, mass spectra of the gaseous species over the samples of Na_2SO_4 , K_2SO_4 , CaSO_4 and their thermodynamic characteristics (vaporisation, thermal stability) were determined by the method of the Knudsen effusion mass spectrometry.

This work was focused on two aspects:

- the investigation of the quasi-binary systems $\text{Na}_2\text{SO}_4 - \text{CaSO}_4$ and $\text{K}_2\text{SO}_4 - \text{CaSO}_4$ and the determination of the chemical activities of components in both binaries
- the determination of the volatiles over the samples taken directly from the cement kiln to characterise the species that vaporise from such samples and the interaction of alkali chlorides and sulphates occurring during clinker burning.

By an innovative combination of the investigation of pure substances, the binary systems, and thermodynamic data determined for the industrial samples, the characterisation of vaporisation and processes occurring in the cement kiln could be performed in the current study. Such an innovative approach to the combination of the different data (model and real samples) also reinforces the applications of the Knudsen effusion mass spectrometry for the industrial purposes.

EXPERIMENTAL SECTION

4. Investigation procedure, apparatus

4.1 KEMS

The mass spectrometric investigation of the samples was carried out with single-focusing mass spectrometer (type CH5) equipped with a Knudsen cell.

For alkali sulphates investigation, the Knudsen cell made of platinum with drilling effusion orifice of 0.3 mm diameter was used. The outside crucible (a block) was made of tantalum, figure 4.1.



Figure 4.1. Platinum Knudsen cell (A) and outside tantalum crucibles (block) used in the experiment.

In the case of industrial samples investigation, the Knudsen cell was made of iridium with laser made effusion orifice of 0.26 mm diameter; the outside crucible was made of tantalum; it is presented in figure 4.2.

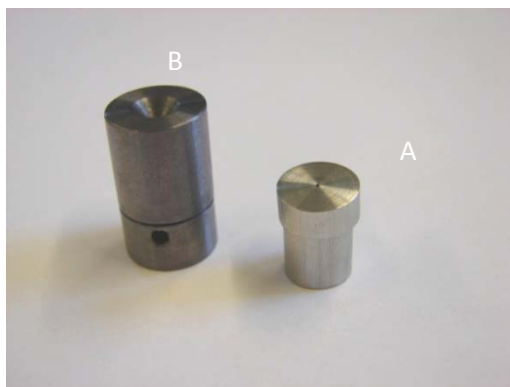


Figure 4.2 The Knudsen cell, made of iridium (A) and outside crucible made of tantalum (B) used for industrial samples investigations

The Knudsen cell was heated by heat radiation from a tungsten filament (diameter 0.25 mm, purity 99.95%) up to the temperatures 870 °C and then an automatic switch allows higher temperature to be achieved by high voltage electron bombardment heating. The gas species were ionized with energy 70 eV, emission current 0.5 mA. Between the effusion cell and the ion source region a moveable shutter was placed, that enabled to distinguish between species vaporising from the cell and those occurring as residual gases in the apparatus. A secondary electron multiplier (SEM) and Faraday cup was used for ion current (intensity) detection.

For sulphates samples investigation, the stability of the ion intensities with time was treated as an evidence for the achievement of equilibrium between gaseous and condensed phases inside the cell. Temperature was raised stepwise by 20°C and the mass spectra were scanned after the temperature of the Knudsen cell is stabilized.

For industrial samples investigation a special measurement procedure was thought, that will be given in section 6.3.1.

4.1.1 Calibration of the mass spectrometer

The calibration of the Knudsen effusion mass spectrometer was carried out over the period of two years and therefore is discussed separately. The temperature was measured with Pt-Pt10Rh thermocouple (type S) and pyrometer (ISQ 5, Impac Infratherm GmbH, Germany), calibrated *in situ* at the melting point of silver, purity 99,99%. The calibration constant k and the corrected temperature was calculated according to the calibration procedure from Miller [10], see Section 2.3.1 with the cross section σ_i value of 5.35 adopted from [37].

The sensitivity of the mass spectrometer was measured over the period of 2 years, which is presented in figure 4.3.

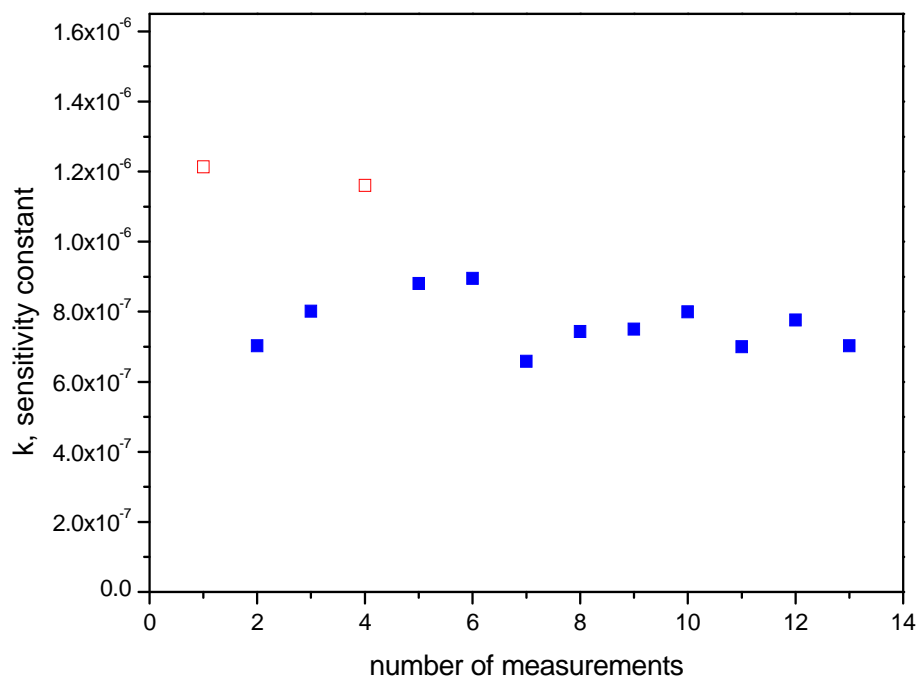


Figure 4.3. Sensitivity constant k , calibrated at the melting point of silver and its standard deviation.

Two points, red colour in figure 4.1 were not in accordance with others although there was no real change in the mass spectrometer. Therefore the statistic calculations were applied to calculate whether those two points come from the normal distribution. The results are presented in figure 4.4.

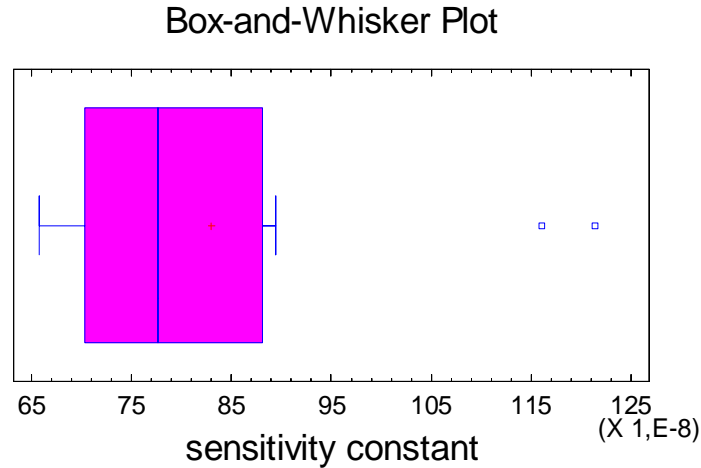


Figure 4.4. Box and Whisker plot of the sensitivity constant value indicating whether the points come from normal distribution.

As it is presented in figure 4.4 two values of calibration constant are not within the range expected for data from a normal distribution, therefore the sensitivity constant from this measurements were not taken into account (red points in figure 4.1). . Most probable deviation of these two data was the incorrect adjustment of the furnace in KEMS set what resulted in lower sensitivity and thereby higher calibration constant k . Finally, the statistical calculation was applied again. The results are presented in table 4.1.

Table 4.1. Summary of the statistic calculation for sensitivity constant values measured for the period over 3 years.

Statistic calculation	Value
Average	7.65 E-7
Standard deviation	7.54 E-8
Minimum	6.58 E-7
Maximum	8.95 E-7
Range	2.36 E-7
Std. skewness	0.742
Std. kurtosis	-0.338

In table 4.1 is presented the summaries of the statistics for sensitivity constant values without two omitted measurements. The statistic calculations include central tendency, variability, and shape. The standardized skewness and standardized kurtosis are use for determining whether the sample comes from a normal distribution, the values of these statistics should be in the range of -2 to +2 expected for data from a normal distribution. As it is presented in table 4.1 all the values are in

accordance with the ranges expected for data from normal distribution, the results are presented in figure 4.5.

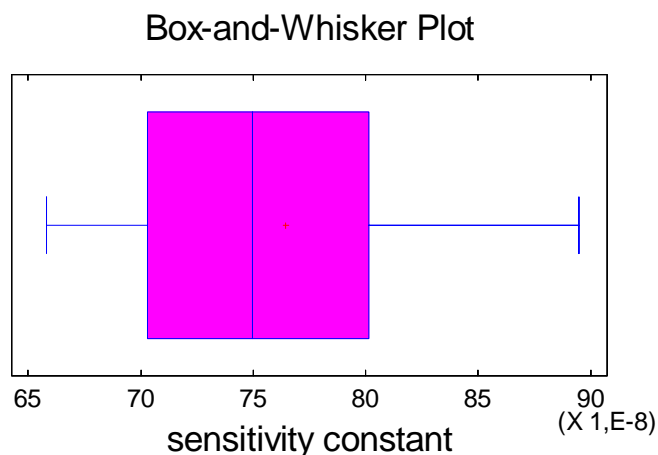


Figure 4.5. Box and Whisker plot of the sensitivity constant value indicating whether the points come from normal distribution.

The deviation from the average sensitivity constant equals only to 10%, therefore the average of 3 years calibration constant measurement was used for further calculation.

4.2. Additional methods

4.2.1 X-ray diffraction

Samples were analysed also with the powder X-ray diffraction method in order to identify the existing phases. The devices used in the measurements were Siemens D5000 Kristalloflex with soll-X-detector (Bruker-AXS) scintillation counter with second monochromator (Siemens) and with Cu-K α radiation ($\lambda=1,5406 \text{ \AA}$). Samples were powdered and deposited on silica sample holder. For the phase identification DiffracPlus XRD- Commander Ver.2.3 (Bruker-AXS, Karlsruhe) and Crystallographica Search-Match ver. 2.1.1.1 (Oxford Cryosystems) were used.

4.2.2 X-ray fluorescence

The industrial samples were analysed with X-ray fluorescence. The devices used in the measurements were S4 Pioneer, 4kW (WDXRF) Brucker, Rh – tube.

5. Alkali sulphates

5.1 Fundamentals

One of the more important elements influencing chemical transport via the gas phase in the rotary kiln is sulphur, which can be introduced into the kiln by the raw meal and fuel. Alkali containing compounds are also present in the kiln gas atmosphere and these have a high affinity for sulphur. Reactions between SO_2 and the alkali oxides (for instance solved in silicate and/or aluminasilicate phases) to form alkali sulphates take place during oxidation. Alkali sulphates evaporate and then condense in the colder parts of the reactor thereby contributing to a clogging formation [42]. Calcium sulphate is also being formed in the cement kiln as a reaction product between CaO and SO_2 . Calcium sulphate (CaSO_4) can, in turn, build liquid and solid phases with alkali sulphates and so it can moderate their chemical activity and vaporisation behaviour. The explanation of the chemical transport of the sulphur and alkalis in the kiln on the thermodynamic base is therefore needed.

The first step was to determine the vaporisation of different systems containing alkali sulphates. First, pure salts K_2SO_4 , Na_2SO_4 , CaSO_4 were determined as a pattern for binary systems, which are

- a) $\text{Na}_2\text{SO}_4 - \text{CaSO}_4$
- b) $\text{K}_2\text{SO}_4 - \text{CaSO}_4$

At the sintering temperature of clinker about 1450°C , the resulting sulphate systems are present as a melt, the alkali sulphates K_2SO_4 , Na_2SO_4 , $(\text{Na}, \text{K})_2\text{SO}_4$, a mixed crystal phase with variable $\text{Na}_2\text{O}/\text{K}_2\text{O}$ molar ratio are formed by crystallization of the sulphate melt, also a compound with formula $\text{K}_2\text{Ca}_2(\text{SO}_4)_3$ or $\text{K}_2\text{SO}_4 \cdot 2\text{CaSO}_4$ is found [5]. Therefore the systems of sodium or potassium sulphate together with CaSO_4 were chosen to characterize the influence of the existence of CaO and CaSO_4 , on the alkali sulphate vaporisation. Moreover another aim of choosing this system was the investigation of interaction of SO_2 liberating from CaSO_4 decomposition at higher temperature range on the alkali sulphates vaporisation. Such influences can be important for the description of the overall mechanism of the alkalis vaporisation in the clinker kiln.

In this work, the system $\text{Na}_2\text{SO}_4\text{-K}_2\text{SO}_4$ previous determined by the Author [43] will be summarised briefly, as these results have great importance in further understanding of the technical samples vaporisation.

The vaporisation of metal sulphates was subject of the many previous determinations; table 5.1 summarizes most of the original works about vaporisation of pure metal sulphates and the metal sulphate systems, performed by effusion methods, incl. KEMS.

The main unit of temperature used in Knudsen effusion mass spectrometry and thermodynamic evaluations is Kelvin, therefore in this chapter the K will be used mostly for the temperature description.

Table 5.1. The summary of the previous investigations of the metal sulphates vaporisation

Sample	ΔT / K	Vapour	Condensed phase	Investigation method	Cell	Ref.
Na_2SO_4	907 - 1473	Na, O_2 , SO_2 , Na_2SO_4	Na_2SO_4	Thermogravimetry + mass spectrometry	Pt-10%Rh	[44]
$M_2\text{SO}_4$, $M = \text{Li, Na, Rb, Cs}$	983-1274	M , SO_2 , O_2 , $M_2\text{SO}_4$	$M_2\text{SO}_4$	Torsion effusion + mass spectrometry	Pt	[45]
K_2SO_4	1180-1280	K, O_2 , SO_2 , K_2SO_4	K_2SO_4	Torsion effusion + mass spectrometry	Pt-30Rh	[46]
K_2SO_4	1180-1668	K, O_2 , SO_2 , K_2SO_4	K_2SO_4	Knudsen effusion + transpiration technique	$\text{Al}_2\text{O}_3 + \text{MgO}$	[47]
Na_2SO_4 $\text{Na}_2\text{SO}_4 + \text{SO}_2$, O_2	1400-1625	Na, O_2 , SO_2 , Na_2SO_4	Na_2SO_4	Transpiration method	Pt-10%Rh	[48]
$M_2\text{SO}_4$, $M = \text{Li, Na, K, Rb, Cs}$	833-1273	$M_2\text{SO}_4$	$M_2\text{SO}_4$	Knudsen weigh loss	Pt	[49]
$M_2\text{SO}_4$, $M = \text{Li, Na, K, Rb, Cs}$	<1250	M, O_2 , SO_2 , $M_2\text{SO}_4$	$M_2\text{SO}_4$	Mass spectrometry	Al lined Ta	[50]
Na_2SO_4	<1673			furnace	Pt	[51]
K_2SO_4 , K_2CO_3	900-1700	K_2O , SO_2 , O_2 , CO_2	K_2SO_4 , K_2CO_3	KEMS	Pt-5%Rh	[52]
Na_2SO_4	1173-1473			Continuous weight change measurements	Pt	[53]
$M_2\text{SO}_4$, $M = \text{Na, Rb, Cs}$ ad. Ref. 11	833-1273			Knudsen weigh loss	Pt	[54]
MgSO_4 , CaSO_4	<1155	SO_2 , O_2		Knudsen weigh loss	Pt	[55]
K_2SO_4 , Na_2SO_4 , CaSO_4 , $\text{K}_2\text{SO}_4 + \text{Na}_2\text{SO}_4$, $\text{K}_2\text{SO}_4 + \text{CaSO}_4$, $\text{KCl} + \text{K}_2\text{SO}_4$	< 1450 K	K, O_2 , SO_2 , K_2SO_4 , Na, O_2 , SO_2 , Na_2SO_4		KEMS	Pt	[1]

According to literature the vaporisation of the M_2SO_4 can be described by two reactions:

a) with dissociation



b) without dissociation



where $M = K, Na$.

The vaporisation processes in both cases are congruently ones, what means that both vapour and condensed phases present still M_2SO_4 stoichiometry. In contrary, $CaSO_4$ vaporises (decomposes) incongruently according to reaction



As the vaporisation of pure sulphates was deeply investigated, this work was mostly concentrated on binary systems K_2SO_4 - $CaSO_4$ and Na_2SO_4 - $CaSO_4$, not investigated before. The aim of renewed pure alkali sulphate vaporisation study was the division of the M^+ ion among $M_2SO_4(g)$ and $M(g)$ gas species, which was not solved in the previous work [1, 43]. The vaporisation of the pure sulphates will be therefore only briefly presented.

The partial pressures of the species were calculated by using the equation 2.3. The total ionisation cross sections $\sigma(i)$ of gaseous species were taken from the literature, according to the previous researcher [1] and are presented in table 5.2. Modified additive rule was adopted in references [55] and [29] for estimation of molecular cross sections.

Table 5.2. Ionisation cross-section for the gaseous species

Gas species (<i>i</i>)	σ_i	Reference
K	5.90	[30]
Na	4.10	[30]
O ₂	1.25	[56]
SO ₂	6.93	[57]
K ₂ SO ₄	16.1	[30]
Na ₂ SO ₄	13.4	[30]

5.2. Vaporisation of Na₂SO₄

For the measurement, sodium sulphate (Fluka, for analysis 99%) was used. The sample was firstly heated in the Knudsen cell in the mass spectrometer at the temp 873 K over the night before the measurement started. Mass spectrometric study of the vaporisation of pure Na₂SO₄ was carried out by heating up or cooling down in the range 1137 – 1377 K. Table 5.3 show the details of the Na₂SO₄ measurements.

Table 5.3. Details of the Na₂SO₄ vaporisation measurements

Sample	Runs	Number of measurement points	Temp. Range/K
Na ₂ SO ₄ (07)	4	70	1173-1375
Na ₂ SO ₄ (01)	2	44	1185-1348
Na ₂ SO ₄ (02)	1	20	1137-1367
Na ₂ SO ₄ (03)	2	40	1168-1377

Ions Na⁺, SO⁺, SO₂⁺, Na₂O⁺, and Na₂SO₄⁺ were observed in the mass spectrum. The ion $m/e = 32$ was observed in the mass spectrum, but not taken into account. This ion consists of two different parts, that is ³²S⁺ and ³²O₂⁺ and there was no possibility to distinguish those two ions in the current study.

Ions Na₂SO₄⁺, Na₂O⁺ were assumed to originate only from Na₂SO₄ species. Ions coming from the same molecule precursor typically show the same temperature dependencies what means, that the relative ion intensity ratio of such ions is independent on temperature. Therefore, in order to check molecular precursors of SO⁺ and SO₂⁺ ions, the spectral abundance of the intensities SO⁺/SO₂⁺ was plotted vs. temperature, what is presented in figure 5.1.

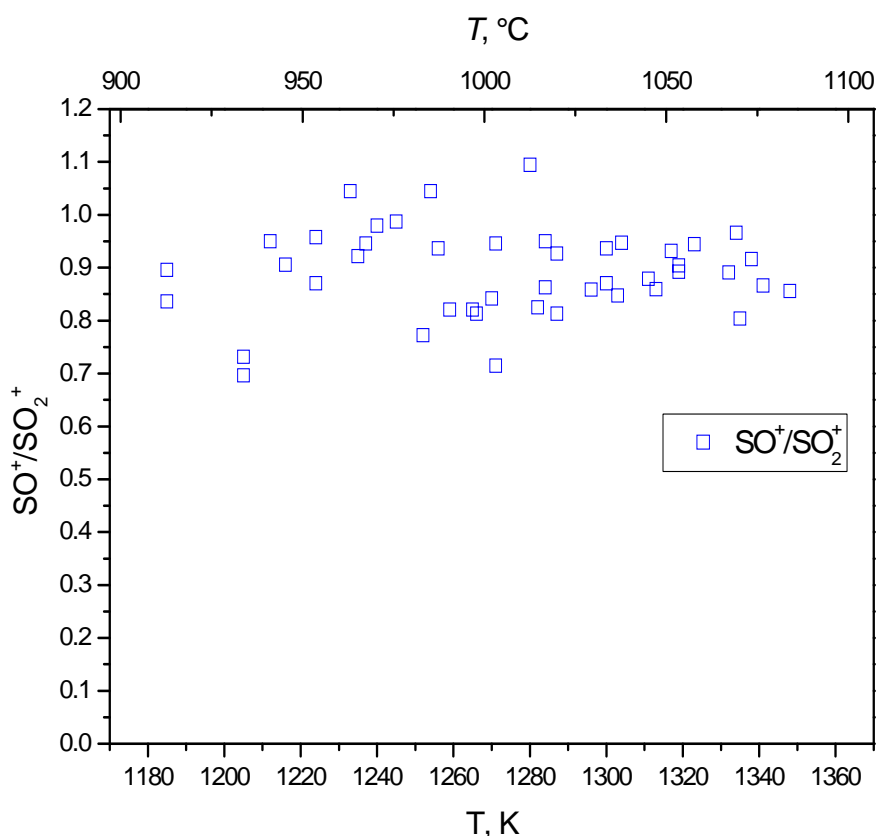


Figure 5.1. Temperature dependence of the intensity ratio $\text{SO}^+/\text{SO}_2^+$ from the measurement of $\text{Na}_2\text{SO}_4(01)$ sample

The spectral abundance of the intensities $\text{SO}^+/\text{SO}_2^+$ shows no temperature dependencies, therefore the ion SO^+ was assumed as coming only from $\text{SO}_2(\text{g})$ species. Final assignments of the ions to their neutral precursors are given in figure 5.2.

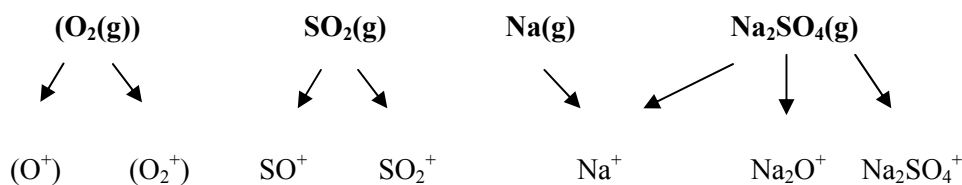


Figure 5.2. The assignment of the ions to their neutral precursors in the sample Na_2SO_4

Because the species were ionized by electron energy of 70 eV resulting in significant fragments, it was needed to apportion Na^+ ion between $\text{Na}_2\text{SO}_4(\text{g})$ and $\text{Na}(\text{g})$ species quantitatively. In order to this, the calculation from the congruent effusion evaluation was applied (see Section 2.5). Sodium sulphate vaporizes congruently [44-46, 49]; therefore the vaporisation could be considered to be in

the form of the gaseous species such as Na, SO₂, O₂ and Na₂SO₄. Each of these species transports a certain amount of the elements Na, S, and O by vapour effusion according to their stoichiometry.

The element S was taken as reference, because the ion SO⁺ has only one vapour precursor which is SO₂(g), so those pressure could be considered as representative. According to equation (2.24), it could be written:

$$n(S) = \frac{p(SO_2)}{\sqrt{M(SO_2)}} \quad (5.4)$$

and

$$n(Na) = \frac{p(Na)}{\sqrt{M(Na)}} \quad (5.5)$$

and also

$$n(O) = \frac{2p(SO_2)}{\sqrt{M(SO_2)}} + \frac{2p(O_2)}{\sqrt{M(O_2)}} \quad (5.6)$$

According to reaction 5.1, sodium sulphate vaporizes congruently and the ratio $n(S)/n(Na)=1/2$. With these relations the pressure of Na can be calculated as follows:

$$p(Na) = \frac{2 \cdot \sqrt{M(Na)} \cdot p(SO_2)}{\sqrt{M(SO_2)}} \quad (5.7)$$

and the vapour pressure of oxygen

$$p(O_2) = \frac{p(SO_2) \cdot \sqrt{M(O_2)}}{\sqrt{M(SO_2)}} \quad (5.8)$$

The obtained value of the partial pressure of Na(g) calculated from the congruent effusion was taken for the apportion of the Na⁺ ion between Na(g) and Na₂SO₄(g) gas species. The intensity of the ion Na⁺, which should belong to Na(g), according to congruent effusion results was calculated backwards from its partial pressure, according to equation:

$$I(Na^+(Na(g))) = \frac{p(Na(g))_{congr. eff.} \cdot \sigma_{Na}}{k \cdot T} \quad (5.9)$$

Subtraction of the calculated value of $I(Na^+)$ given by equation (5.9) from the measured $I(Na^+)$ signal

over condensed Na₂SO₄ remains in the part of $I(\text{Na}^+)$ fragment belonging to Na₂SO₄(g). Such calculation could be applied, because the ionization cross section of the atom Na is well known from the literature [30].

The apportion of the Na⁺ ion intensity between Na(g) and Na₂SO₄(g) allows the determination of the equilibrium constant K_p^0 (I) for reaction (5.1) and K_p^0 (II) for reaction (5.2) using the precursor assignment given in figure 5.1. The temperature dependence of the equilibrium constants was evaluated for each run by the last squares method, and compared with literature data [40] at the temperature of 1320 K. The results are presented in tables 5.4 – 5.5.

Table 5.4. Temperature dependencies of the K_p^0 (I) equilibrium constant for reaction $\text{Na}_2\text{SO}_4(\text{c}) = 2\text{Na}(\text{g}) + \text{SO}_2(\text{g}) + \text{O}_2(\text{g})$, and its value at the temperature 1320 K, compared with literature data [40]

Sample	$\ln K_p^0 \text{ (I)} = -A/(T/K) + B$ for reaction $\text{Na}_2\text{SO}_4(\text{c}) = 2\text{Na}(\text{g}) + \text{SO}_2(\text{g}) + \text{O}_2(\text{g})$		K_p^0 at 1320 K
	<i>A</i>	<i>B</i>	
Na ₂ SO ₄ (07)	154241	66.804	$1.84 \cdot 10^{-22}$
Na ₂ SO ₄ (01)	153723	61.795	$1.82 \cdot 10^{-24}$
Na ₂ SO ₄ (02)	153743	64.704	$3.29 \cdot 10^{-23}$
Na ₂ SO ₄ (03)	148514	61.247	$5.45 \cdot 10^{-23}$
Literature	145713	59.223	$6.01 \cdot 10^{-23}$

Table 5.5. Temperature dependencies of the K_p^0 (II) equilibrium constant for reaction $\text{Na}_2\text{SO}_4(\text{c}) = \text{Na}_2\text{SO}_4(\text{g})$, and its value at the temperature 1320 K, compared with literature data from Ivtanthermo [40].

Sample	$\ln K_p^0 \text{ (II)} = -A/(T/K) + B$ for reaction $\text{Na}_2\text{SO}_4(\text{c}) = \text{Na}_2\text{SO}_4(\text{g})$		K_p^0 at 1320 K
	<i>A</i>	<i>B</i>	
Na ₂ SO ₄ (07)	35159	13.497	$1.97 \cdot 10^{-6}$
Na ₂ SO ₄ (01)	40986	17.32	$1.09 \cdot 10^{-6}$
Na ₂ SO ₄ (02)	36941	14.097	$9.30 \cdot 10^{-7}$
Na ₂ SO ₄ (03)	40648	17.44	$1.59 \cdot 10^{-6}$
Literature	32222	11.361	$2.15 \cdot 10^{-6}$

The partial pressures of Na₂SO₄(g), Na(g), SO₂(g), O₂(g) for the all runs of the Na₂SO₄ measurements were calculated at 1320K and compared with literature [40]. The results are presents in table 5.6.

Table 5.6. Temperature dependencies of $\ln(p(\text{Na}_2\text{SO}_4))$ and the pressures of $\text{Na}_2\text{SO}_4(\text{g})$, $\text{Na}(\text{g})$, $\text{SO}_2(\text{g})$, $\text{O}_2(\text{g})$ at the temperature of 1320K compared with the literature data [40]

Sample	$\ln (p_{\text{Na}_2\text{SO}_4}/\text{Pa}) = -A/(T/\text{K}) + B$		$p_{\text{Na}_2\text{SO}_4}$ Pa	p_{Na} Pa	p_{SO_2} Pa	p_{O_2} Pa
	A	B	T = 1320K			
Na ₂ SO ₄ (07)	35159	25.010	0.197	0.440	0.367	0.260
Na ₂ SO ₄ (01)	40575	28.517	0.108	0.139	0.116	0.0818
Na ₂ SO ₄ (02)	37566	26.048	0.090	0.223	0.186	0.131
Na ₂ SO ₄ (03)	40648	28.953	0.159	0.325	0.271	0.192
Literature	35684	25.476	0.211	0.395	0.197	0.197

By means of Knudsen effusion mass spectrometry thermodynamic characteristic of sodium sulphate was determined. The gas species $\text{Na}(\text{g})$, $\text{Na}_2\text{SO}_4(\text{g})$, $\text{SO}_2(\text{g})$ and $\text{O}_2(\text{g})$ were detected in the vapour over the condensed phase. The ion Na^+ was apportioned between $\text{Na}(\text{g})$ and $\text{Na}_2\text{SO}_4(\text{g})$ species. The apportion of the ions to their neutral precursor caused that the equilibrium constants $K_p^\circ(\text{I})$ and $K_p^\circ(\text{II})$ of the reactions 5.1 and 5.2 agree now excellent with the literature data [40]. During the measurement of the sodium sulphate samples creeping occurs after sample was molten. Neither Pt wire, Pt powder added to the cell, nor additional lining of the cell with Al_2O_3 ceramic avoided the creeping. Measurements were interrupted in each case once increasing of ion intensities was observed at the constant temperature showing this phenomenon. Experimental points detected before creeping occurred were taken into the thermodynamic interpretation.

5.3. Vaporisation of K_2SO_4

For the measurement, potassium sulphate (Riedel-de Haen, anhydrous for analysis >99%) was used. The sample was initially heated in the Knudsen cell in the mass spectrometer at the temp 873 K over the night before the measurement started. Mass spectrometric study of the vaporisation of pure K_2SO_4 was carried out by heating up or cooling down in the range 1172 – 1361 K. Over the period of two days 39 measurement points were registered.

Ions K^+ , SO^+ , SO_2^+ , K_2O^+ , and $K_2SO_4^+$ were observed in the mass spectrum. The ion $m/e = 32$ was observed in the mass spectrum, but not taken into account, for the same reason as describe in chapter 5.2, in the case of the Na_2SO_4 . The assignment of the ions to their neutral precursors is given in figure 5.3.

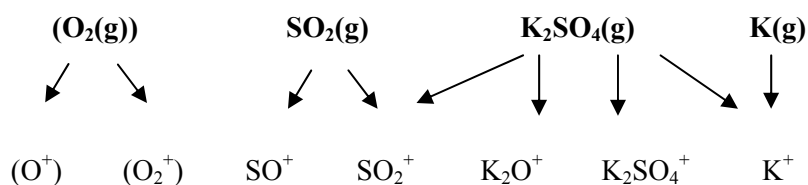


Figure 5.3. Assignments of the ions to their neutral precursors in the sample K_2SO_4

Ions $K_2SO_4^+$, K_2O^+ were assumed to be originating only from K_2SO_4 species since they have very close temperature dependencies. Ion SO^+ was assumed to be coming from $SO_2(g)$ species. In contrast to the Na_2SO_4 measurement, the intensity ratio of the ions SO^+/SO_2^+ shows a temperature dependencies as presented in figure 5.4; therefore, SO_2^+ has to be apportioned between the neutral precursors $SO_2(g)$ and $K_2SO_4(g)$.

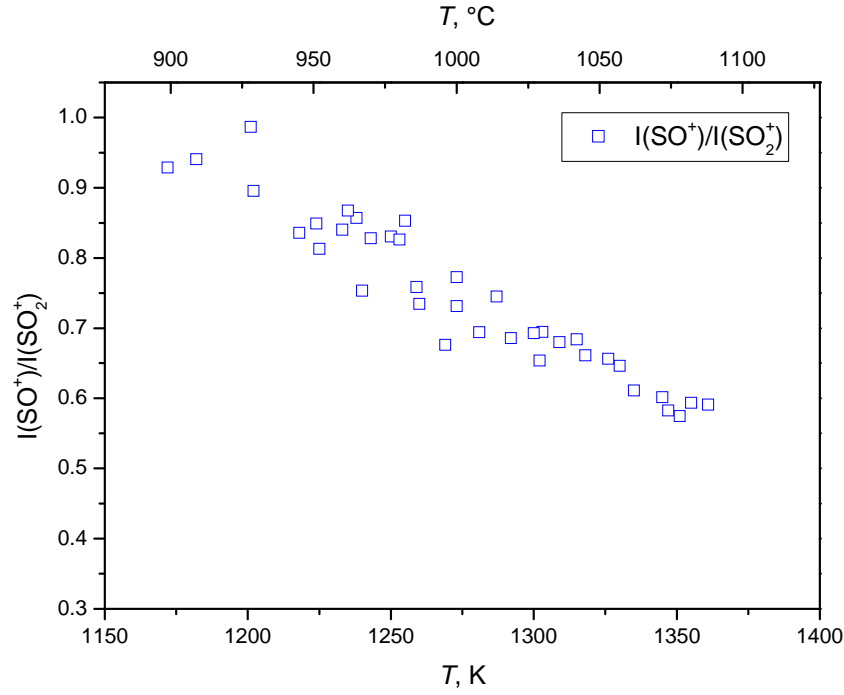


Figure 5.4. Temperature dependence of the intensity ratio SO^+/SO_2^+ by the measurement of K_2SO_4 sample.

The apportionment of the ion SO_2^+ between the two neutral precursors, $SO_2(g)$ and $K_2SO_4(g)$, was made by Miller's method [58]. The total intensity of SO_2^+ can be described as

$$I_{SO_2^+}^{tot} = I_{SO_2^+(SO_2(g))} + I_{SO_2^+(K_2SO_4(g))} \quad (5.10)$$

Dividing the equation by I_{SO^+} gives

$$\frac{I_{SO_2^+}^{tot}}{I_{SO^+}} = \frac{I_{SO_2^+(SO_2(g))}}{I_{SO^+}} + \frac{I_{SO_2^+(K_2SO_4(g))}}{I_{SO^+}} \quad (5.11)$$

The ratio $\frac{I_{SO_2^+(SO_2(g))}}{I_{SO^+}}$ is constant as SO^+ has the only one SO_2 precursor, and could be described as

constant value a , what gives:

$$\frac{I_{\text{SO}_2^+}^{\text{tot}}}{I_{\text{SO}^+}} = \frac{I_{\text{SO}_2^+(\text{SO}_2(\text{g}))}}{I_{\text{SO}^+}} + \frac{I_{\text{SO}_2^+(\text{K}_2\text{SO}_4(\text{g}))}}{I_{\text{SO}^+}} = a + \frac{I_{\text{SO}_2^+(\text{K}_2\text{SO}_4(\text{g}))}}{I_{\text{SO}^+}} \quad (5.12)$$

The fraction $\frac{I_{\text{SO}_2^+(\text{K}_2\text{SO}_4(\text{g}))}}{I_{\text{SO}^+}}$ is extended by $\frac{I_{\text{K}_2\text{SO}_4^+}}{I_{\text{K}_2\text{SO}_4^+}}$ and then split into two fractions

$$\frac{I_{\text{SO}_2^+}^{\text{tot}}}{I_{\text{SO}^+}} = a + \frac{I_{\text{SO}_2^+(\text{K}_2\text{SO}_4(\text{g}))}}{I_{\text{K}_2\text{SO}_4^+}} \frac{I_{\text{K}_2\text{SO}_4^+}}{I_{\text{SO}^+}} \quad (5.13)$$

The ratio $\frac{I_{\text{SO}_2^+(\text{K}_2\text{SO}_4(\text{g}))}}{I_{\text{K}_2\text{SO}_4^+}}$ is constant as ions come from the same neutral precursor, so it could be further

called constant value b and one obtain the final equation (5.14).

$$\frac{I_{\text{SO}_2^+}^{\text{tot}}}{I_{\text{SO}^+}} = a + b \frac{I_{\text{K}_2\text{SO}_4^+}}{I_{\text{SO}^+}} \quad (5.14)$$

where a and b are spectral ion intensity ratios in the specific mass spectrum of SO₂(g) and K₂SO₄(g), respectively and, therefore, do not depend on either the composition or the temperature [59]. The values of a and b constant ratio were determined by linear regression using the ion intensities vs. temperature data. The results of those calculations are presented in figure 5.5.

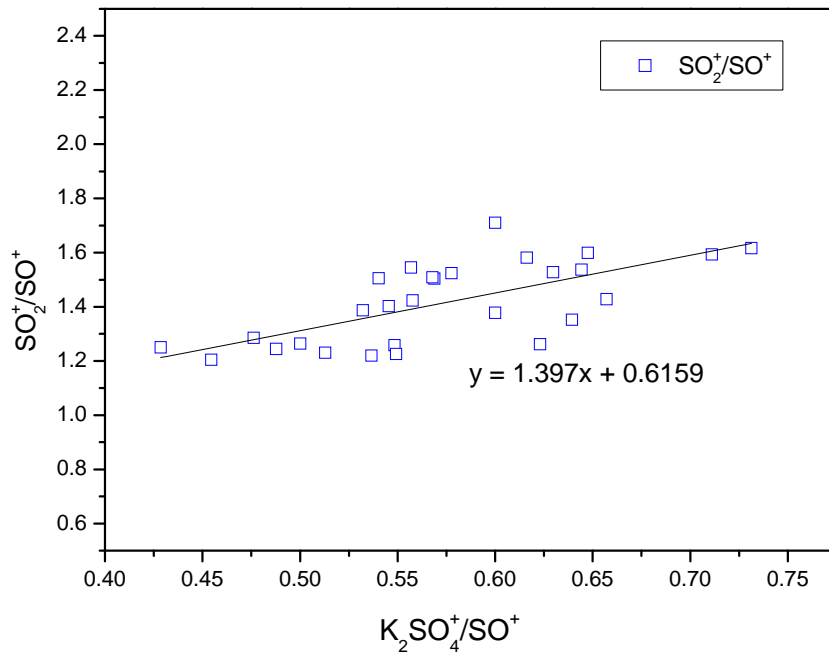


Figure 5.5. The apportionment of the SO_2^+ ion between $K_2SO_4(g)$ and $SO_2(g)$ species, where $a=0.616$, $b=1.40$.

Following equations (5.15), (5.16) will distribute the ion intensity of $I_{SO_2^+}^{tot}$ between the precursor molecules $SO_2(g)$ and $K_2SO_4(g)$.

$$I_{SO_2^+ (SO_2(g))} = 0.62 \cdot I_{SO^+} \quad (5.15)$$

$$I_{SO_2^+ (K_2SO_4(g))} = 1.40 \cdot I_{K_2SO_4^+} \quad (5.16)$$

For apportion of the ion K^+ between $K_2SO_4(g)$ and $K(g)$ species, similarly as by the Na_2SO_4 sample, the calculation from the congruent effusion was applied. Potassium sulphate vaporises congruently [46, 47, 49, 52], therefore the vaporisation of K_2SO_4 could be considered in the form of the gaseous species such as K , SO_2 , O_2 . Each of these species transports by vapour effusion certain amount of specific atoms (K , S , O) according to their stoichiometry. Atom of S was taken as reference, because the ion SO^+ and apportioned ion SO_2^+ has the only one source which is $SO_2(g)$, thus those pressure could be considered as reference, according to the equation 5.4. Potassium sulphate vaporizes congruently, and according to the reaction 5.1, therefore, similarly as in the case of Na_2SO_4 sample, the calculation of the congruent effusion from the appropriate equations 5.5 – 5.8 could be applied.

The obtained value of the partial pressure of K(g) was taken for the apportion of the K⁺ ion distribution between K(g) and K₂SO₄(g), as it was done by the Na₂SO₄ sample. The intensity of the ion K⁺, belonging to K(g), was calculated backwards from the partial pressure K(g) value, according to equation (5.17).

$$I(K^+) = \frac{p(K(g))_{\text{congr. eff.}} \cdot \sigma_K}{k \cdot T} \quad (5.17)$$

The obtained value of $I(K^+)$ calculated from equation (5.17) was subtracted from the whole measured intensity of K⁺, which yielded the intensities of K⁺ belonging to K₂SO₄(g). The ionization cross section of the atom K is well know, and reported before [30, 60], hence this calculation could be applied. The apportioning of the ion to their neutral precursor in per cent is presented in table 5.7.

Table 5.7. The fragmentation scheme of SO₂(g), K₂SO₄(g) and K(g).

Fragmentation of the species						
SO ₂ (g)		K ₂ SO ₄ (g)				K(g)
SO ⁺	SO ₂ ⁺	K ⁺	SO ₂ ⁺	K ₂ O ⁺	K ₂ SO ₄ ⁺	K ⁺
63%	37%	85%	6.0%	3.5%	5.5%	100%

After the apportioning of the ion SO₂⁺ between SO₂(g) and K₂SO₄(g) and the ion K⁺ between K(g) and K₂SO₄(g) species, the temperature dependence of the equilibrium constant K_p[°](I) for reaction (5.1) and K_p[°](II) for reaction (5.2) was evaluated for each run by the last squares method. The results are presented graphically in figure 5.6.

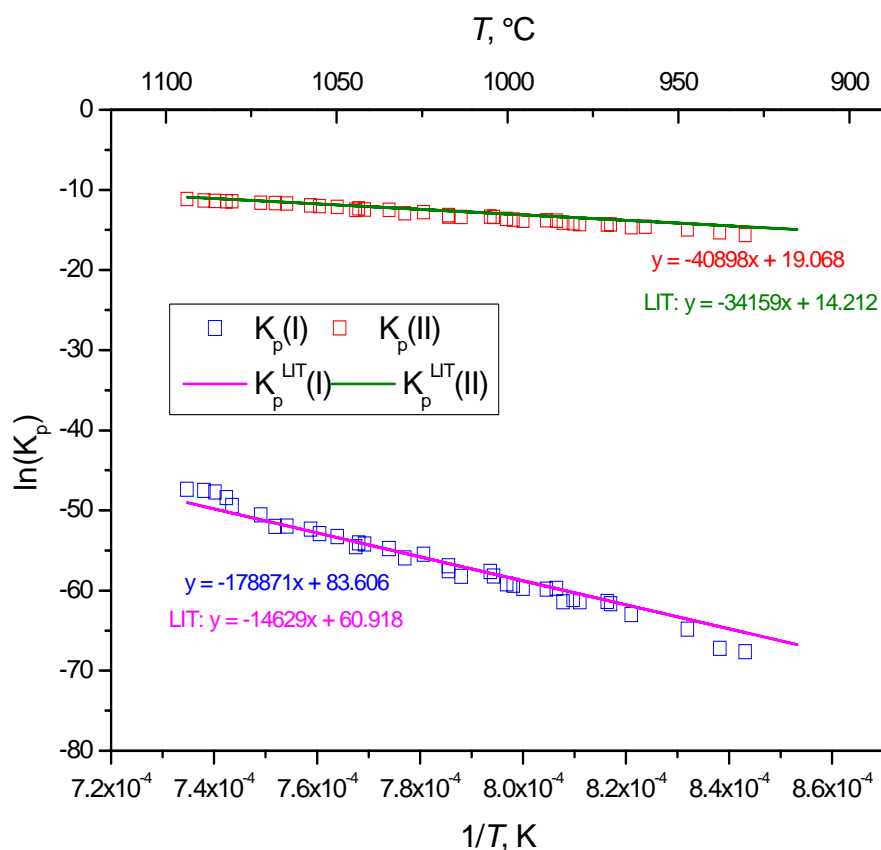


Figure 5.6. The temperature dependencies of the $K_p^\circ(I)$ for reaction (5.1) and $K_p^\circ(II)$ for reaction (5.2) for potassium sulphate compared with the literature data from Ivtanthermo [40].

The temperature dependencies of the $K_p^\circ(I)$ and $K_p^\circ(II)$ constants for all runs of K₂SO₄ measurements compared with the literature data [40] at the temperature of 1320 K are summarised in tables 5.8-5.9. The following table 5.10 presents $\ln p(K_2SO_4)$ as a function of temperature, compared also with literature data.

Table 5.8 Temperature dependencies of the $K_p^\circ(I)$ equilibrium constant for reaction $K_2SO_4(c) = 2K(g) + SO_2(g) + O_2(g)$, and its value at the temperature 1320 K, compared with literature data [40]

Sample	$\ln K_p^\circ(I) = -A/(T/K) + B$ for reaction $K_2SO_4(c) = 2K(g) + SO_2(g) + O_2(g)$		K_p° at 1320 K
	<i>A</i>	<i>B</i>	
K ₂ SO ₄	178871	83.606	$2.88 \cdot 10^{-23}$
Literature	149629	60.701	$1.35 \cdot 10^{-23}$

Table 5.9. Temperature dependencies of the $K_p^{\circ}(\text{II})$ equilibrium constant for reaction $\text{K}_2\text{SO}_4(\text{c}) = \text{K}_2\text{SO}_4(\text{g})$, and its value at the temperature 1320 K, compared with literature data [40].

Sample	$\ln K_p^{\circ}(\text{II}) = -A/(T/K) + B$ for reaction $\text{K}_2\text{SO}_4(\text{c})=\text{K}_2\text{SO}_4(\text{g})$		K_p° at 1320 K
	<i>A</i>	<i>B</i>	
K ₂ SO ₄	40989	19.068	$6.24 \cdot 10^{-6}$
Literature	34159	14.212	$8.58 \cdot 10^{-6}$

The partial pressures of K₂SO₄(g), K(g), SO₂(g), O₂(g) for the K₂SO₄ measurements were calculated at 1320K and compared with literature [40]. The results are presents in table 5.10.

Table 5.10. Temperature dependencies of $\ln p(\text{K}_2\text{SO}_4)$ and the pressures of K₂SO₄(g), K(g), SO₂(g), O₂(g) at the temperature 1320K with data from Ivtanthermo [40]

Sample	$\ln (p_{\text{K}_2\text{SO}_4}/\text{Pa}) = -A/(T/K) + B$		$p_{\text{K}_2\text{SO}_4}$ Pa	p_{K} Pa	p_{SO_2} Pa	p_{O_2} Pa
	<i>A</i>	<i>B</i>	T = 1320 K			
K ₂ SO ₄	40989	30.581	0.624	0.314	0.201	0.142
Literature	36941	27.995	0.592	0.187	0.0935	0.0934

By means of Knudsen effusion mass spectrometry thermodynamic characteristic of potassium sulphate was determined. The gas species K(g), K₂SO₄(g) SO₂(g) and O₂(g) were detected in the vapour over the condensed phase. The ion K^+ was apportioned between $K(\text{g})$ and $K_2\text{SO}_4(\text{g})$ species. The ion SO_2^+ was considered as a fragment of SO₂(g) and K₂SO₄(g) species and apportioned between them. The apportion of the ions to their neutral precursor caused that the equilibrium constants $K_p^{\circ}(\text{I})$ and $K_p^{\circ}(\text{II})$ of the reactions 5.1 and 5.2 agree well with the literature data [40].

5.4. Vaporisation of CaSO₄

For the measurement, calcium sulphate (Riedel-de Haen, dehydrate, for analysis >99%) was used. The sample was first heated in the Knudsen cell in the mass spectrometer at the temperature 873 K over the night before the measurement started in order to remove the moisture. Mass spectrometric study of the vaporisation of pure CaSO₄ was carried out by heating up or cooling down in the range 1143 – 1324 K. The details of the CaSO₄ measurements are presented in table 5.11.

Table 5.11. Details of the CaSO₄ vaporisation measurements

Sample	Runs	Number of measurements points	Temp. range, K
CaSO ₄ (01)	3	37	1153 - 1312
CaSO ₄ (02)	3	38	1143 - 1324

Only ions SO⁺, and SO₂⁺ were observed in the mass spectrum. The ion 32 was observed but not taken into account for the same reason as in the case of Na₂SO₄ and K₂SO₄.

In the case of the CaSO₄ sample, the ions SO⁺ and SO₂⁺ have only one precursor, that is SO₂(g), because CaSO₄ vaporizes incongruently according to reaction 5.3. Therefore, relative ion intensity ratio of SO⁺/SO₂⁺ ions must be independent of temperature, which was confirmed by plotting SO⁺/SO₂⁺ intensities ratio versus temperature, presented in figure 5.7.

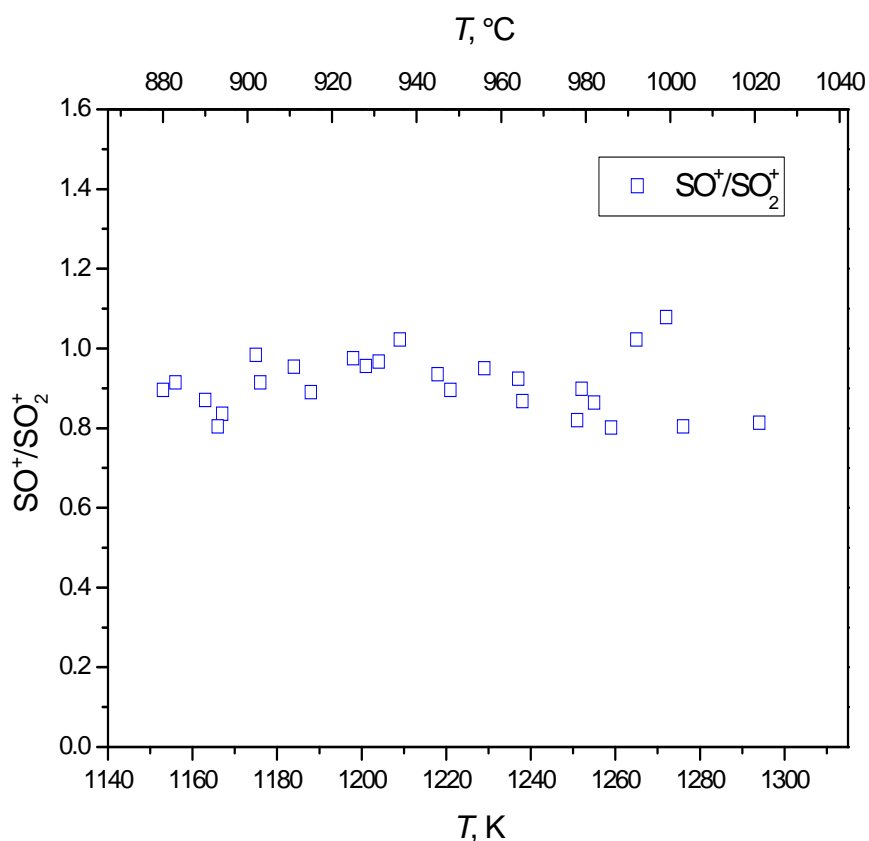


Figure 5.7. Temperature dependence of the intensity ratio $\text{SO}^+/\text{SO}_2^+$ by the measurement of $\text{CaSO}_4(01)$ sample.

For the calculation of O_2 partial pressures by CaSO_4 sample, congruent effusion was applied. CaSO_4 vaporizes incongruently, but the amounts of $\text{SO}_2(\text{g})$ and $\text{O}_2(\text{g})$ arise with the particular molar ratio, which is 2 to 1 (see reaction 5.3, Section 2.5). In this case, congruent effusion calculations for incongruent evaporation could be applied, section 2.5. The pressure of SO_2 was taken as a reference, according to eq. 5.4 and from this value the pressure of O_2 calculated, according to equation 5.6.

The temperature dependence of the equilibrium constant $K_p^\circ(\text{III})$ for the reaction (5.3) was evaluated for each run by the last squares method, and compared with literature data at the temperature 1320 K, summarised in table 5.12 and presented in figure 5.8.

Table 5.12. Temperature dependencies of the $K_p^{\circ}(\text{III})$ equilibrium constant for reaction $\text{CaSO}_4(\text{c}) = \text{CaO}(\text{c}) + \frac{1}{2} \text{O}_2(\text{g}) + \text{SO}_2(\text{g})$ and its value at the temperature 1320 K, compared with literature data [40].

Sample	$\ln K_p^{\circ}(\text{I}) = -A/(T/\text{K}) + B$ for reaction $\text{CaSO}_4(\text{c}) = \text{CaO}(\text{c}) + \text{SO}_2(\text{g}) + \frac{1}{2} \text{O}_2(\text{g})$		K_p° at 1320 K
	A	B	
CaSO ₄ (01)	70359	37.204	$1.02 \cdot 10^{-7}$
CaSO ₄ (02)	73102	39.299	$1.04 \cdot 10^{-7}$
literature	57613	30.275	$1.56 \cdot 10^{-6}$

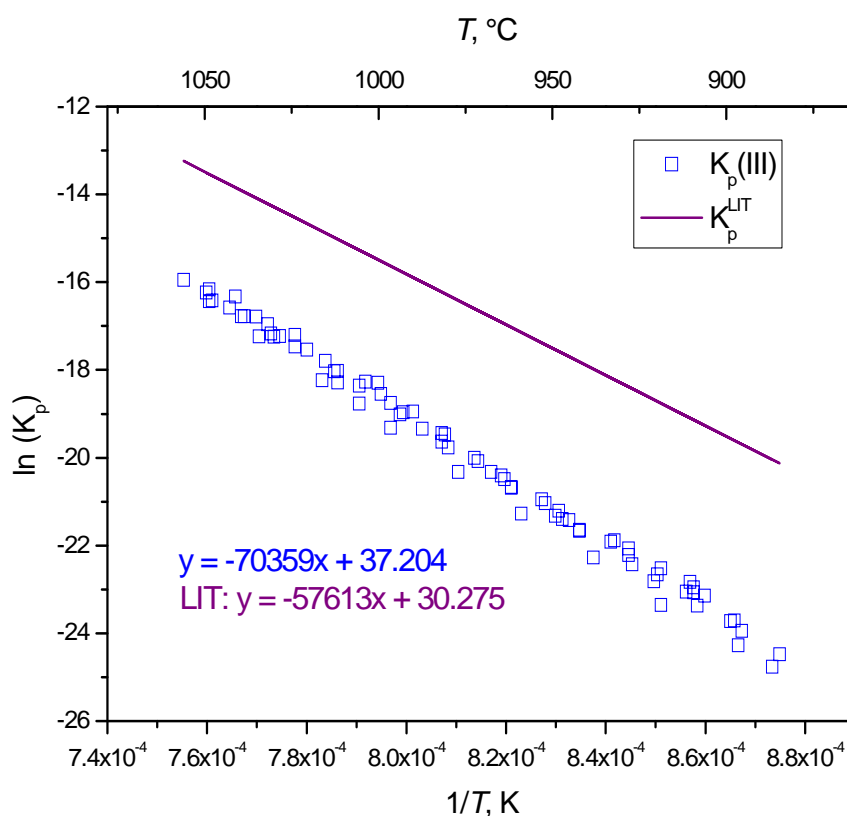


Figure 5.8. The temperature dependencies of the $K_p^{\circ}(\text{III})$ for reaction (5.3) compared with the literature data from Ivatanthermo [40].

The results obtained by the measurement of CaSO₄ dissociative vaporisation differ reasonably from the literature data. Possible reason for this discrepancy is a large background signal observed for ion currents coming from the SO₂(g) and O₂(g) fragmentation due to increasing of their pressure in mass spectrometer as of permanent non-condensing gases. The values of partial pressures obtained from the congruent effusion were too low as the results from the literature data [40, 61, 62]. The main reason for this, could be the background of O₂(g). The species SO₂(g) exists also in a background therefore it could have also the influence on the equilibrium constant of the reaction 5.3.

5.5. System $\text{Na}_2\text{SO}_4 - \text{CaSO}_4$

For preparing the samples, pure substances were first heated in Pt crucibles in oven for 3 hours at the temperature of 573 K to remove moisture. The compounds were weighted, ground in agate mortar together, pressed into pellets and then heated for 6.5 hour at 873 K in oven. After heat treatment the pellets were ground once again in an agate mortar. The details of the chemical composition of the investigated samples are presented in table 5.13.

Table 5.13. Chemical composition of the investigated samples

Sample	% mol		% mass	
	Na_2SO_4	Ca_2SO_4	Na_2SO_4	Ca_2SO_4
Na Ca 5 95	5	95	5.48	94.5
Na Ca 20 80	20	80	20.7	79.3
Na Ca 30 70	30	70	30.9	69.1
Na Ca 40 60	40	60	41.0	59.0
Na Ca 55 45	55	45	56.0	43.9
Na Ca 70 30	70	30	70.9	29.1
Na Ca 80 20	80	20	80.7	19.3
Na Ca 90 10	90	10	90.4	9.62

Mass spectrometric study of the vaporisation of the samples was carried out by heating up or cooling down in the various temperature ranges. The details of those measurements are presented in table 5.14.

Table 5.14. Measurement details for vaporisation study of the $\text{Na}_2\text{SO}_4 - \text{CaSO}_4$ system by Knudsen effusion mass spectrometry.

Sample	Runs (days of measurements of the same sample)	Number of measurement points	Temp. Range/K
Na Ca 5 95	1	23	1191-1334
Na Ca 20 80	1	23	1161-1342
Na Ca 30 70	2	34	1229-1338
Na Ca 40 60	6	81	1166-1320
Na Ca 55 45	4	45	1166-1329
Na Ca 70 30	2	30	1180-1353
Na Ca 80 20	3	53	1177-1367
Na Ca 90 10	2	45	1177-1361

The phase composition of the samples was checked by using XRD method before and after the vaporisation measurement. A phase diagram of Na_2SO_4 - CaSO_4 is presented in figure 5.9 [63], together with the temperature ranges of the vaporisation studies.

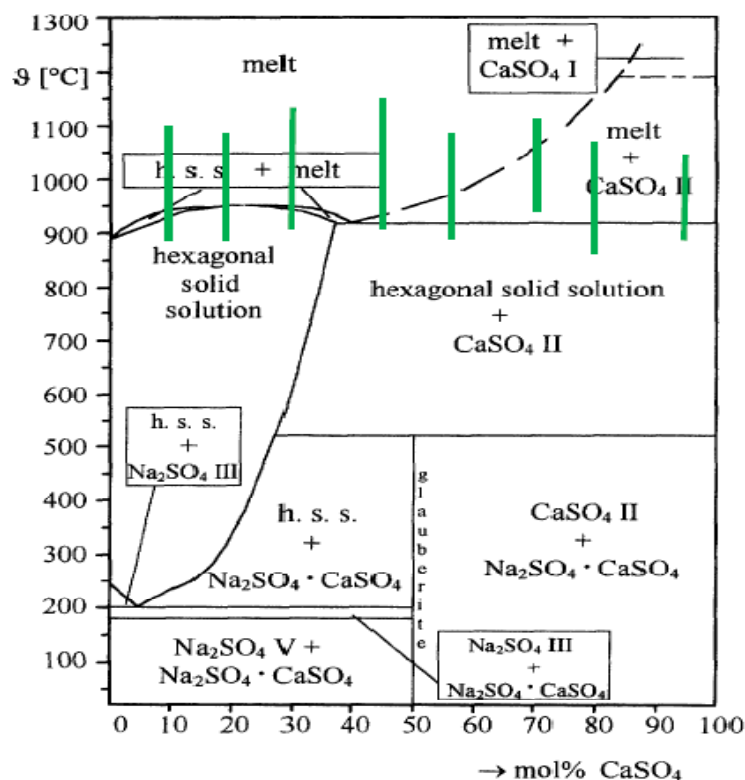


Figure 5.9. Phase diagram of the binary system Na_2SO_4 - CaSO_4 [63] and temperature ranges of the investigation of the samples by Knudsen effusion mass spectrometry in the present study.

The sodium sulphate has several polymorphic modifications. The temperatures for their stabilities were investigated by Eysel et al.[7]. Na_2SO_4 (II) appears sometimes upon the cooling of Na_2SO_4 (I) within narrow interval of temperature. The high temperature form of Na_2SO_4 (III) can exist as a metastable phase at room temperature for a long time. In the presence of humidity, the transformation into Na_2SO_4 (V) is accelerated. Pure Na_2SO_4 (I) cannot be quenched down to the room temperature. Table 5.15 presents the results of XRD study of the samples investigated after vaporisation process, this table contains also the numbers of the ICCD characteristic card for material description [64].

Table 5.15. The results of the XRD phase determination of the samples investigated before after investigation by Knudsen effusion mass spectrometry.

Sample	Phases		ICCD card [64]
	before KEMS	after KEMS	
Na-Ca_90-10	(Na _{0.8} Ca _{0.1}) ₂ SO ₄	- Na ₂ SO ₄ Na ₂ SO ₄ CaO	29-1196 24-1132 37-1465 37-1497
Na-Ca_80_20	Na ₆ Ca(SO ₄) ₄	- CaO (Na _{0.8} Ca _{0.1}) ₂ SO ₄	43-848 37-1497 29-1196
Na_Ca_70_30	CaSO ₄ (Na _{0.8} Ca _{0.1}) ₂ SO ₄	- (Na _{0.8} Ca _{0.1}) ₂ SO ₄ CaO	37-1496 29-1196 75-264
Na_Ca_55_45	CaSO ₄ (Na _{0.8} Ca _{0.1}) ₂ SO ₄	- - Na ₄ Ca(SO ₄) ₃	37-1496 29-1196 34-1238
Na_Ca_40_60	CaSO ₄ (Na _{0.8} Ca _{0.1}) ₂ SO ₄	CaSO ₄ (Na _{0.8} Ca _{0.1}) ₂ SO ₄	37-1496 29-1196
Na_Ca_30_70	CaSO ₄ (Na _{0.8} Ca _{0.1}) ₂ SO ₄	CaSO ₄ (Na _{0.8} Ca _{0.1}) ₂ SO ₄ CaO	37-1496 29-1196 37-1497
Na_Ca_20_80	CaSO ₄ (Na _{0.8} Ca _{0.1}) ₂ SO ₄	CaSO ₄ - CaO Na ₂ SO ₄	37-1496 29-1196 37-1497
Na_Ca_5_95	CaSO ₄ (Na _{0.8} Ca _{0.1}) ₂ SO ₄	CaSO ₄ - CaO Na ₂ SO ₄	37-1496 29-1196 37-1497

5.5.1. Thermodynamic activities for the system Na₂SO₄ – CaSO₄

There have been many difficulties with the calculation of activities in system Na₂SO₄ – CaSO₄, due to the creeping of molten samples, similarly as by measurements of pure Na₂SO₄. Therefore, the calculation of activities in that system could be considered only as estimated. The only one method of calculating the Na₂SO₄ activity was ion-to-ion method using Na₂SO₄⁺ ion intensities. Unfortunately, that ion was observed only in 3 samples, most common in the Na₂SO₄ component. The system Na₂SO₄ – CaSO₄ needs to be measured one more time, taking some means against creeping into consideration. In this work neither Pt wire, Pt powder put together with the sample into the cell, nor additional lining of the cell with Al₂O₃ ceramic avoided the creeping.

For three samples, where ion Na₂SO₄⁺ was detected, the activities of sodium sulphate were calculated. The reference Na₂SO₄⁺ ion intensity related to the pure Na₂SO₄ was taken from the Na₂SO₄(01) sample, which was measured in the lower temperature range; therefore the probability of creeping of the sample was the lowest.

The activities were calculated by using the ion-to-ion method. It is a direct comparison of the partial pressure over the binary samples and pure substances according to equation (2.13). All the measurements were carried out under the same conditions and the calibration constant, measured over the period of 2 years showing the statistical reproducibility of 10%; therefore, the average value of the calibration constant was taken for the calculation and thus k is equal to k' in the equation (2.13), which leads to the equation

$$a(i) = \frac{I(i)}{I(i)^o} \quad (5.18)$$

therefore

$$a(\text{Na}_2\text{SO}_4) = \frac{I(\text{Na}_2\text{SO}_4^+)_{\text{system}}}{I(\text{Na}_2\text{SO}_4^+)_{\text{pure}}} \quad (5.19)$$

The temperature dependencies of $\ln(I_{\text{Na}_2\text{SO}_4} \cdot T)$ and $\ln(a_{\text{Na}_2\text{SO}_4})$ are presented in table 5.16. Table 5.17 contains the results of the activities calculated by the ion-to-ion method.

Table 5.16. Temperature dependencies of $\ln(I_{\text{Na}_2\text{SO}_4} \cdot T)$ and of $\ln(a_{\text{Na}_2\text{SO}_4})$ interpolated at the temperature range of 1223 – 1323 K.

Sample	$\ln(I_{\text{Na}_2\text{SO}_4} \cdot T) = -$ $A/(T/K) + B$		$\ln a_{\text{Na}_2\text{SO}_4} =$ $A/(T/K) + B$	
	<i>A</i>	<i>B</i>	<i>A</i>	<i>B</i>
Na Ca 90 10	35555	38.876	1245	1.185
Na Ca 80 20	36818	38.625	- 18	- 0.255
Na Ca 70 30	35149	36.928	1651	1.948

Table 5.17. The activities of Na_2SO_4 in the system Na_2SO_4 - CaSO_4 received by ion-to-ion method

Sample	x Na_2SO_4	Activity at T =1273 K
		Na_2SO_4
Na Ca 90 10	90	0.813
Na Ca 80 20	80	0.767
Na Ca 70 30	70	0.521

In the Na_2SO_4 – CaSO_4 system investigation, the activities of Na_2SO_4 were estimated only in three samples where the ion Na_2SO_4^+ was observed. The serious difficulty in the investigation of this system was sample creeping, which enabled the investigation only in the selected, relative narrow temperature ranges. In the future a creeping should be firstly defeated to investigate that system at higher temperatures.

5.6. System K_2SO_4 – $CaSO_4$

For preparing of samples, pure substances were first heated in Pt crucibles in oven for 3 hours at temperature 573 K to remove moisture. The samples were prepared in particular rates of K_2SO_4 and $CaSO_4$ that are presented in table 5.18

Table 5.18. Chemical composition of the investigated K_2SO_4 - $CaSO_4$ samples

Sample	% mol		% mass	
	K_2SO_4	$CaSO_4$	K_2SO_4	$CaSO_4$
K $CaSO_4$ 5 95	5	95	6.31	93.69
K $CaSO_4$ 35 65	35	65	40.80	59.20
K $CaSO_4$ 50 50	50	50	56.14	43.86
K $CaSO_4$ 65 35	65	35	70.40	29.60
K $CaSO_4$ 80 20	80	20	83.66	16.34
K $CaSO_4$ 90 10	90	10	92.01	7.98

The components were weighed and ground in agate mortar together, than heated at 673 K in the Knudsen cell during the night before the measurement was started. The measurement details are presented in the following table 5.19.

Table 5.19. Measurement details for K_2SO_4 - $CaSO_4$ system investigated by Knudsen effusion mass spectrometry.

Sample	Runs (days of measurements of the same sample)	Number of measurement points	Temp. range (K)
K $CaSO_4$ 5 95	2	30	1156-1296
K $CaSO_4$ 35 65	1	22	1135-1307
K $CaSO_4$ 50 50	2	30	1152-1329
K $CaSO_4$ 65 35	2	30	1163-1331
K $CaSO_4$ 80 20	2	25	1139-1332
K $CaSO_4$ 90 10	2	25	1228-1346

In order to check the phase composition of the samples after vaporisation study, X-ray diffraction study was carried out. Phase diagram of the binary system K_2SO_4 - $CaSO_4$ [8], together with the temperature ranges of the KEMS investigation is presented in figure 5.10.

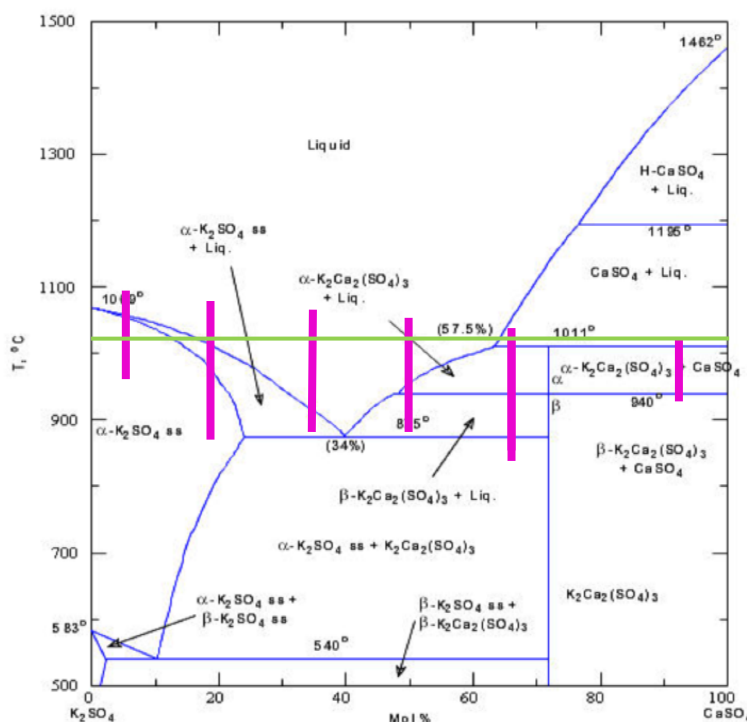


Figure 5.10. Phase diagram of the binary system $\text{K}_2\text{SO}_4 - \text{CaSO}_4$ [8] and temperature ranges of the investigation of the samples by Knudsen effusion mass spectrometry (marked temperature refers to figure 5.13).

The compound K_2SO_4 has two polymorphs, at the temperatures lower than 860 K crystallizes in α -form, which is orthorhombic, whereas at the high-temperature β -form is hexagonal. In the binary system $\text{K}_2\text{SO}_4 - \text{CaSO}_4$ a limited solution of CaSO_4 in K_2SO_4 exists. There is a eutectic at 1148 K and 34 % mass of CaSO_4 . Calcium langbenite melts incongruently at 1284 K, according to reaction $\text{K}_2\text{SO}_4 \cdot 2\text{CaSO}_4 = \text{Liquid} + \text{CaSO}_4(\text{c})$ with CaSO_4 as a solid phase. The melting point of CaSO_4 is 1765 K [8]. Table 5.20 shows the results of XRD determination of the samples investigated after vaporisation process, this table contains also the number of the ICCD characteristic card [64].

Table 5.20. The results of the XRD phase determination of the samples investigated after investigation by Knudsen effusion mass spectrometry.

Sample	Compound found in XRD after vaporisation process	ICCD card [64]
K_CaSO4_5_95	$CaSO_4$ $K_2Ca_2(SO_4)_3$ $Ca(OH)_2^*$	37-1496 20-867 44-1481
K_CaSO4_35_65	$K_2Ca_2(SO_4)_3$ K_2SO_4	20-867 5-613
K_CaSO4_50_50	K_2SO_4 $K_2Ca_2(SO_4)_3$ $CaSO_4$ $Ca(OH)_2^*$	72-354 20-867 37-1496 44-1481
K_CaSO4_65_35	K_2SO_4 $K_6Ca(SO_4)_4$ CaO $Ca(OH)_2^*$	4-7-2698 43-849 77-2376 72-156
K_CaSO4_80_20	K_2SO_4 $CaSO_4$ $K_2Ca_2(SO_4)_3$	72-354 72-503 20-867
K_CaSO4_90_10	K_2SO_4 $CaSO_4$ $K_2Ca_2(SO_4)_3$ $Ca(OH)_2^*$	72-354 72-503 17-741 44-1481
$CaSO_4$	$CaSO_4$ CaO $Ca(OH)_2^*$	37-1496 37-1497 44-1481
K_2SO_4	K_2SO_4	83-681

* comes from CaO hydration**5.6.1. Thermodynamic activities for the system K_2SO_4 – $CaSO_4$.**

Activities of K_2SO_4 and $CaSO_4$ in the K_2SO_4 - $CaSO_4$ system were calculated by using ion-to-ion method and Gibbs-Duhem method.

For the calculations of the activity of K_2SO_4 , ion-to-ion method was applied. The activities of K_2SO_4 were calculated similarly as in the case of Na_2SO_4 in the Na_2SO_4 – $CaSO_4$ system, section 5.5.1, by comparing the intensity of the ion $K_2SO_4^+$ in the binary system samples related to the $K_2SO_4^+$ ion from the pure K_2SO_4 measurement, according to the equation (5.20).

$$a(K_2SO_4) = \frac{I(K_2SO_4^+)_{system}}{I(K_2SO_4^+)_{pure}} \quad (5.20)$$

The ion intensities $\ln(I(K_2SO_4^+)T)$ obtained for different samples are plotted versus $1/T$, figure 5.11.

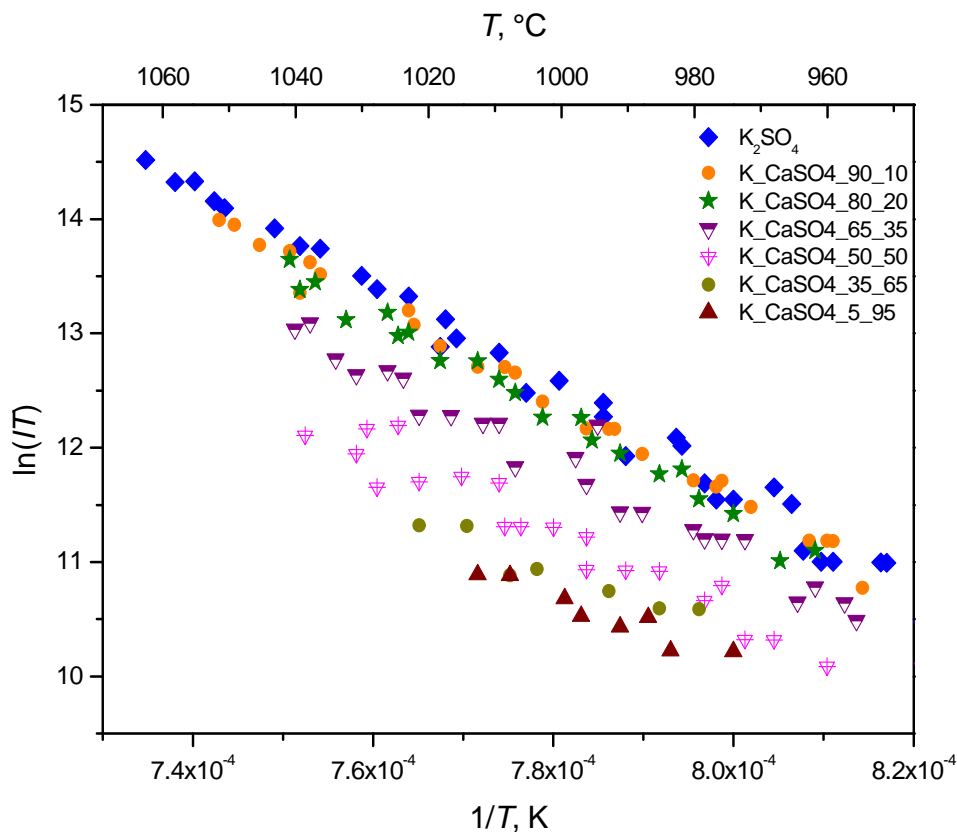


Figure 5.11. $\ln(I(K_2SO_4^+)T)$ vs. $1/T$ for all the samples from the binary system K_2SO_4 - $CaSO_4$ investigated by Knudsen effusion mass spectrometry.

The temperature dependencies of $\ln(I(K_2SO_4)T)$ and $\ln a(K_2SO_4)$ are summarised in table 5.21.

Table 5.21. Temperature dependencies of $\ln(I(K_2SO_4)T)$ and $\ln a(K_2SO_4)$ at the temperature range of 1223 – 1323 K.

Sample	$\ln(I_{K_2SO_4} \cdot T) = -A/(T/K) + B$		$\ln a_{K_2SO_4} = A/(T/K) + B$	
	<i>A</i>	<i>B</i>	<i>A</i>	<i>B</i>
K_CaSO4_5_95	26407	31.283	17530	-15.514
K_CaSO4_35_65	25582	30.878	14702	-13.103
K_CaSO4_50_50	35988	39.321	7949	-7.476
K_CaSO4_65_35	40099	43.163	3838	-3.64
K_CaSO4_80_20	43176	45.962	761	-0.835
K_CaSO4_90_10	42449	45.519	1488	-1.278

For the activity calculation, the highest common temperature of the all temperature ranges of the sample investigation was chosen, that is 1293 K. The activity of $CaSO_4$ at the temperature 1293 K was calculated by Gibbs-Duhem method, according to equation 2.14, which for the binary system K_2SO_4 – $CaSO_4$ could be written as follows:

$$d \ln a_{CaSO_4} = - \frac{x_{K_2SO_4}}{x_{CaSO_4}} \cdot d \ln a_{K_2SO_4} \quad (5.21)$$

The obtained values of $\ln a_{K_2SO_4}$ at the temperature 1293 K by the ion-to-ion method are plotted versus $\frac{x_{K_2SO_4}}{x_{CaSO_4}}$ in figure 5.12.

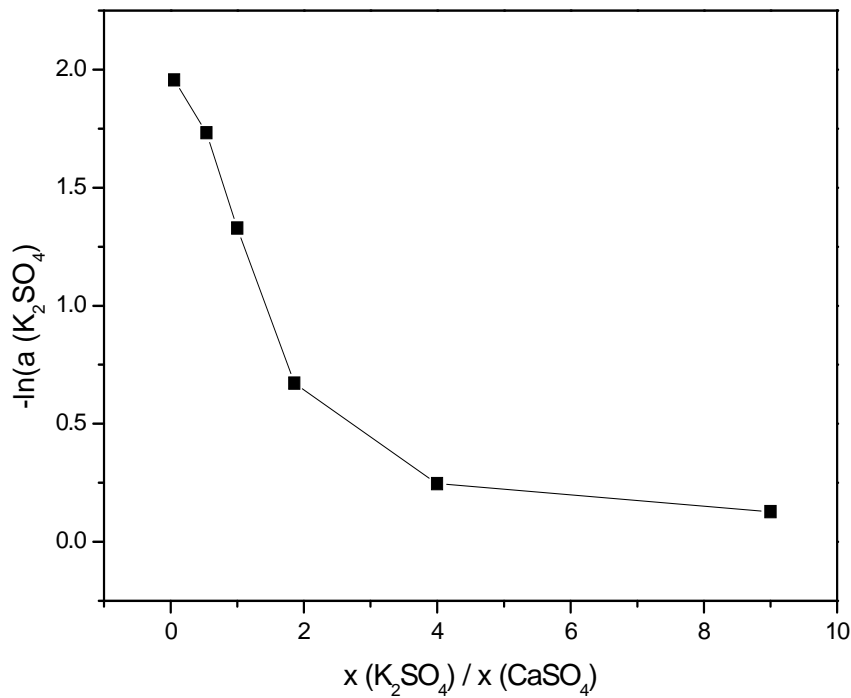


Figure 5.12. The obtained by ion-to-ion method values of $\ln a_{K_2SO_4}$ at 1293 K versus $\frac{x_{K_2SO_4}}{x_{CaSO_4}}$

Graphical integration of the function gives the activity of $CaSO_4$. The activities of K_2SO_4 received by ion-to-ion method and the activities of $CaSO_4$ obtained by Gibbs-Duhem method are presented in table 5.22 and graphically versus composition of the samples in figure 5.13.

Table 5.22. The activities of compounds in the system K_2SO_4 - $CaSO_4$ at the temperature 1293 K, received by ion-to-ion method and Gibbs- Duhem method

Sample	% mol	Activity at 1293 K	
	K_2SO_4	K_2SO_4	$CaSO_4$
K $CaSO_4$ 5 95	5	0.142	1.00
K $CaSO_4$ 35 65	35	0.174	0.963
K $CaSO_4$ 50 50	50	0.266	0.752
K $CaSO_4$ 65 35	65	0.517	0.316
K $CaSO_4$ 80 20	80	0.786	0.101
K $CaSO_4$ 90 10	90	0.886	0.044

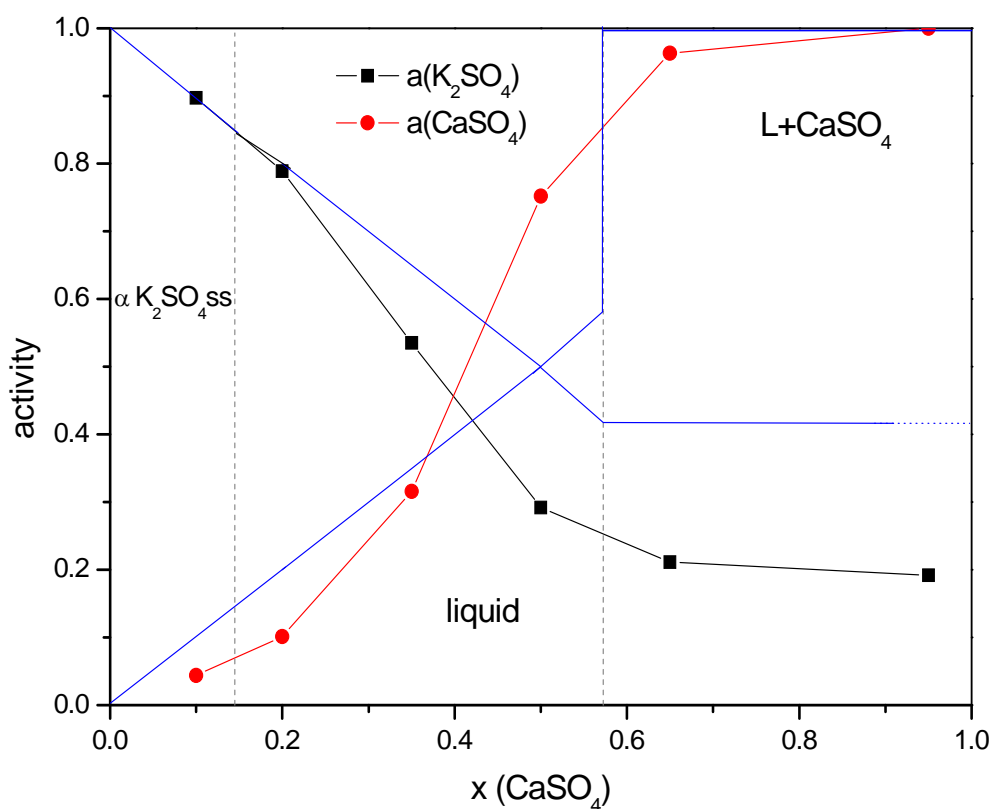


Figure 5.13. The activities of K_2SO_4 , $CaSO_4$ at 1293 K for all samples investigated, the blue lines indicate the activities expected without interaction.

In the K_2SO_4 – $CaSO_4$ system investigation, the activities of the components were determined by ion-to-ion method (for K_2SO_4) and Gibbs – Duhem method (for $CaSO_4$). The obtained values of K_2SO_4 activities show negative deviations, whereas the activities of $CaSO_4$ the positive deviations from the Raoult's rule. The further discussion of the results will be given in the Section 5.8.

5.7. System $\text{Na}_2\text{SO}_4 - \text{K}_2\text{SO}_4$

System $\text{Na}_2\text{SO}_4 - \text{K}_2\text{SO}_4$ was described before [1, 43]. In this work, it will be summarised only briefly, because it is needed for further evaluation by the investigation of the industrial samples. Eight samples of different chemical composition were prepared for vaporisation studies. The pure sodium and potassium sulphates were heated to remove humidity in Pt crucibles for 3 hours at 573 K before weighing, and then mixed in agate mortar, pressed into pellets and sintered for 6.5 hours at 873 K. The composition of the samples and measurement details are presented in table 5.23.

Table 5.23. The initial chemical composition of prepared samples and details to the vaporisation experiments in the $\text{Na}_2\text{SO}_4 - \text{K}_2\text{SO}_4$ system by Knudsen effusion mass spectrometry

Sample	% mol Na_2SO_4	Number of runs	Number of measurement points	Temperature range, K
$\text{Na}_{1.7}\text{K}_{0.3}\text{SO}_4$	85	4	55	1173 – 1375
$\text{Na}_{1.5}\text{K}_{0.5}\text{SO}_4$	75	3	65	1171 – 1385
$\text{Na}_{1.2}\text{K}_{0.8}\text{SO}_4$	60	3	62	1215 – 1368
$\text{Na}_{0.9}\text{K}_{1.1}\text{SO}_4$	45	3	67	1188 – 1381
$\text{Na}_{0.6}\text{K}_{1.4}\text{SO}_4$	30	4	64	1212 – 1375
$\text{Na}_{0.2}\text{K}_{1.8}\text{SO}_4$	10	2	49	1191 – 1385

Phase diagram of the binary system $\text{Na}_2\text{SO}_4 - \text{K}_2\text{SO}_4$ [7], together with the temperature ranges of the KEMS investigations is presented in figure 5.14. As it could be seen in figure 5.14, almost all the samples were liquid during KEMS measurement at the selected temperature ranges.

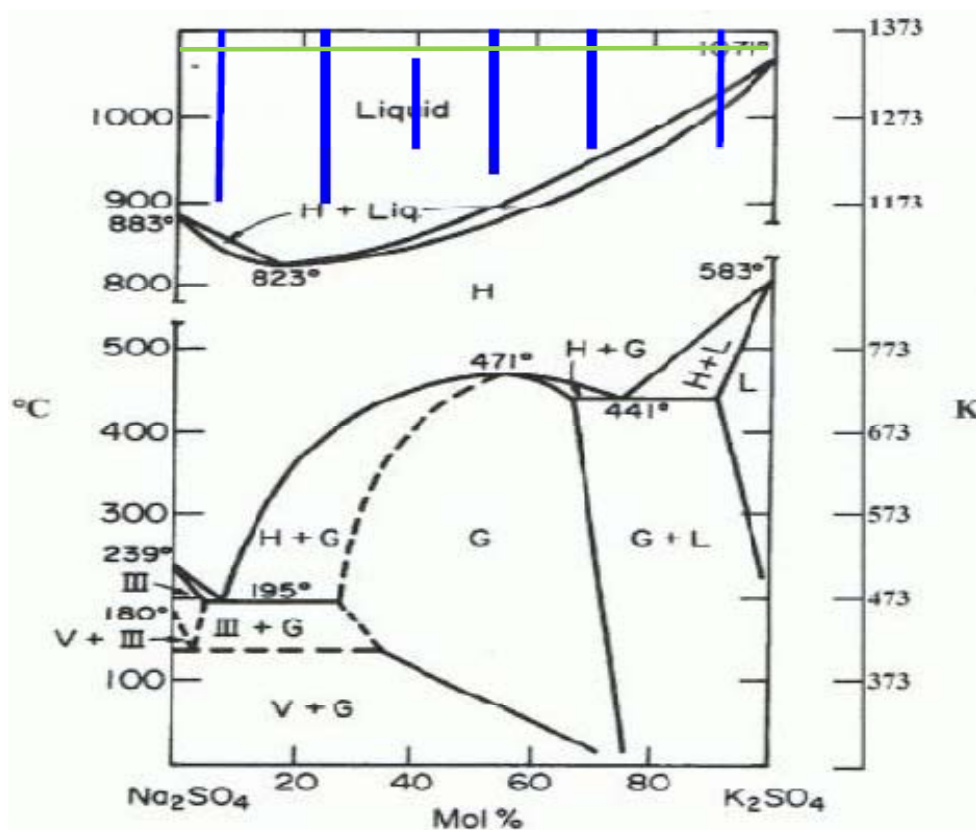


Figure 5.14. Phase diagram for binary – system $\text{Na}_2\text{SO}_4 - \text{K}_2\text{SO}_4$ [7] marked temperature refers to figure 5.15.

The partial pressures of a gas species over the system $\text{Na}_2\text{SO}_4 - \text{K}_2\text{SO}_4$ were evaluate by using eq. 2.3 for each measurement temperature. In this study the fragmentation path of M^+ as origin of $M_2\text{SO}_4(\text{g})$ or $\text{NaKSO}_4(\text{g})$ was neglected, therefore the partial pressures of the various species should be considered only as estimated values. The obtained partial pressures of different species at 1350 K are presented in table 5.24.

Table 5.24. The partial pressure values of volatile species over $\text{Na}_{2-x}\text{K}_x\text{SO}_4$ samples at 1350 K.

Sample	p / Pa						
	O_2	SO_2	Na	Na_2SO_4	K	K_2SO_4	NaKSO_4
$\text{Na}_{1.7}\text{K}_{0.3}\text{SO}_4$	0.48	0.18	2.6	$1.4 \cdot 10^{-3}$	0.77	-	$1.1 \cdot 10^{-3}$
$\text{Na}_{1.5}\text{K}_{0.5}\text{SO}_4$	0.64	0.23	1.9	$1.0 \cdot 10^{-3}$	1.0	$6.8 \cdot 10^{-3}$	$1.4 \cdot 10^{-3}$
$\text{Na}_{1.2}\text{K}_{0.8}\text{SO}_4$	0.84	0.47	1.3	$7.4 \cdot 10^{-3}$	1.7	$1.7 \cdot 10^{-3}$	$2.1 \cdot 10^{-3}$
$\text{Na}_{0.9}\text{K}_{1.1}\text{SO}_4$	0.92	0.77	1.3	$4.5 \cdot 10^{-3}$	2.5	$3.5 \cdot 10^{-3}$	$2.3 \cdot 10^{-3}$
$\text{Na}_{0.6}\text{K}_{1.4}\text{SO}_4$	1.2	0.45	0.69	-	3.0	$4.8 \cdot 10^{-3}$	$1.7 \cdot 10^{-3}$
$\text{Na}_{0.2}\text{K}_{1.8}\text{SO}_4$	1.2	1.0	0.30	-	5.4	0.10	$9.7 \cdot 10^{-3}$

The thermodynamic activity of each component was evaluated at 1350 K by using two different methods: by comparing of ion current values of Na_2SO_4^+ and K_2SO_4^+ , according the eq. 2.12 over binary samples and over pure substances (ion to ion method) and by ion intensity ratio integration Belton-Fruehan (B-F) method [41], the results are presented in table 5.25.

Table 5.25. The thermodynamic activities of the individual sulphates in the binary system $\text{Na}_2\text{SO}_4 - \text{K}_2\text{SO}_4$ at 1350 K obtained by the ion to ion method and by ion intensity ratio integration computation (B-F method) [41].

Sample	$a(\text{Na}_2\text{SO}_4)$			$a(\text{K}_2\text{SO}_4)$		
	Ion-to-ion	B-F method	Mean value	Ion-to-ion	B-F method	Mean value
$\text{Na}_{1.7}\text{K}_{0.3}\text{SO}_4$	0.718	0.792	0.755 ± 0.052	0.022	0.028	0.025 ± 0.004
$\text{Na}_{1.5}\text{K}_{0.5}\text{SO}_4$	0.551	0.629	0.590 ± 0.054	0.056	0.074	0.065 ± 0.013
$\text{Na}_{1.2}\text{K}_{0.8}\text{SO}_4$	0.394	0.420	0.407 ± 0.018	0.135	0.172	0.154 ± 0.026
$\text{Na}_{0.9}\text{K}_{1.1}\text{SO}_4$	0.241	0.230	0.236 ± 0.008	0.283	0.332	0.308 ± 0.035
$\text{Na}_{0.6}\text{K}_{1.4}\text{SO}_4$	0.107	0.114	0.110 ± 0.005	0.392	0.505	0.449 ± 0.080
$\text{Na}_{0.2}\text{K}_{1.8}\text{SO}_4$	0.016	0.014	0.015 ± 0.002	0.821	0.858	0.840 ± 0.026

The change of the chemical activity values of the investigated sulphates in the $\text{Na}_2\text{SO}_4 - \text{K}_2\text{SO}_4$ system is presented in figure 5.15.

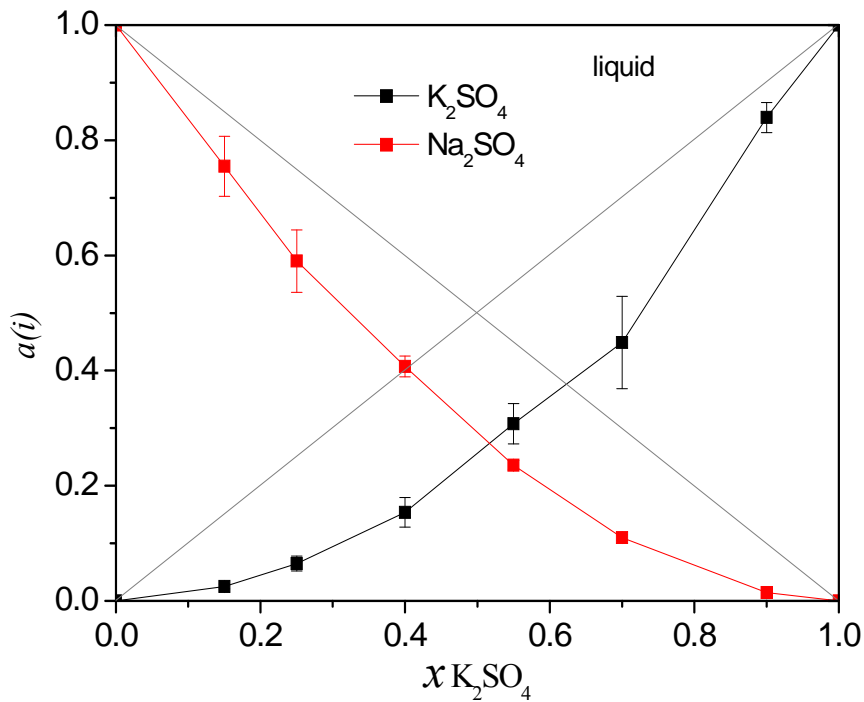


Figure 5.15. The dependence of the thermodynamic activities of the respective sulphates in the Na₂SO₄ – K₂SO₄ system at 1350 K on the molar fraction of K₂SO₄

In the Na₂SO₄ – K₂SO₄ system the gaseous species NaKSO₄(g) was described by gas reaction



The intensity equilibrium constant of reaction 5.19 was evaluated, equated to 0.838, according to equation 5.23.

$$K_p / D = \frac{p(\text{NaKSO}_4)^2}{p(\text{Na}_2\text{SO}_4) \cdot p(\text{K}_2\text{SO}_4) \cdot D} = \frac{I(\text{NaKSO}_4^+)^2}{I(\text{K}_2\text{SO}_4^+) \cdot I(\text{Na}_2\text{SO}_4^+)} \quad (5.23)$$

where D is a constant value.

Partial pressures of K₂SO₄(g), Na₂SO₄(g), NaKSO₄(g) were compared at the temperature 1350 K. Figure 5.16 summarized partial pressure of Na₂SO₄, K₂SO₄ and NaKSO₄ in all samples investigated at the temperature 1350 K.

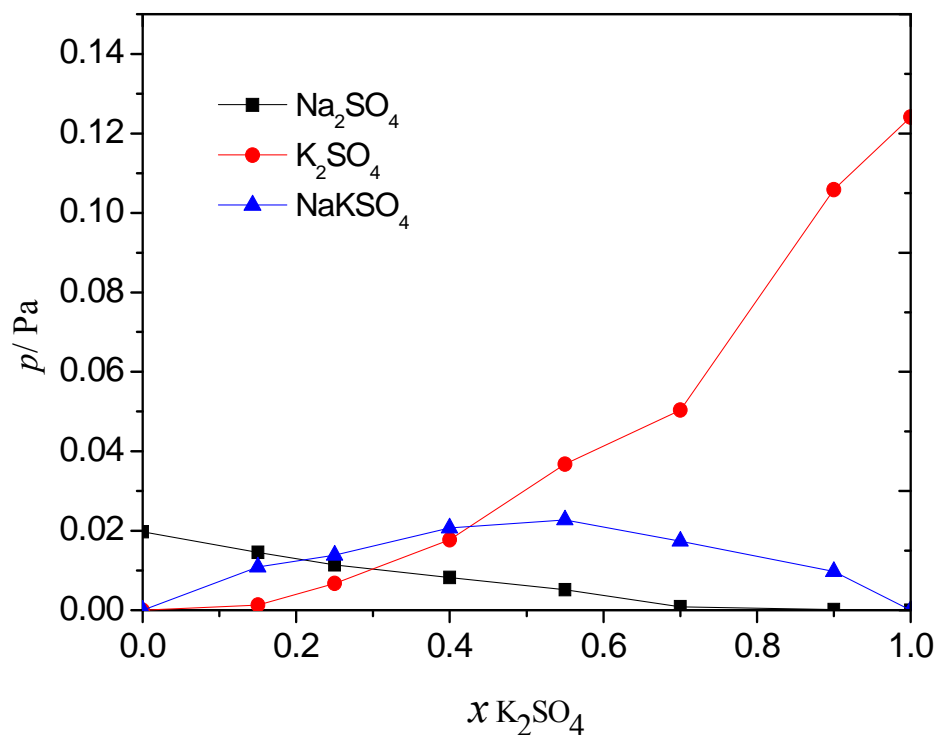


Figure 5.16. The average partial pressures of K_2SO_4 , Na_2SO_4 and NaKSO_4 at 1350 K for samples with different molar fraction of K_2SO_4

The $\text{Na}_2\text{SO}_4 - \text{K}_2\text{SO}_4$ system is known to build a continuous solid solution at temperature exceeding 856 K [7]. The change of the chemical activity of pure compounds in systems where the solubility of components is observed is usually accompanied by the negative deviations from the Raoult's law. During the study the vapour pressures of sodium and potassium sulphates have also shown such a kind of behaviour [43].

5.8. Discussion

During the Knudsen effusion mass spectrometry investigation of sodium sulphate, and potassium sulphate samples gas species Na(g), Na₂SO₄(g), K(g), K₂SO₄(g) SO₂(g) and O₂(g) were detected. Thermodynamic characteristic of pure sulphates was determined, the equilibrium constants K_p^o (I) and K_p^o (II) of the reactions 5.1 and 5.2 agree excellent with the literature data [40].

The determined value of the equilibrium constant at the defined temperature describes the relationship between the partial pressures of the components when the gases behave like ideal ones. This equilibrium constant expresses the equilibrium state and depends only on the temperature.

The equilibrium constants K_p^o (I) of the reaction 5.1 describe the correlation between the pressures in the equilibrium state at the defined temperature, according to equation:

$$K_p^o(I) = \frac{\left(\frac{pM}{p^o}\right)^2 \cdot \frac{pO_2}{p^o} \cdot \frac{pSO_2}{p^o}}{a(M_2SO_4)} \quad (5.24)$$

where $M = \text{Na or K}$

and p^o – is a standard pressure equals to 10^5 Pa

In the case of pure substances the activity of M_2SO_4 in above equation equals to 1, therefore at the defined temperature, equation (5.24) could be written as follows

$$K_p^o = \left(\frac{pM}{p^o}\right)^2 \cdot \frac{pO_2}{p^o} \cdot \frac{pSO_2}{p^o} = \text{const} \quad (5.25)$$

If there are solutions of various sulphates, the activity of the component $M_2SO_4(c)$, from the reaction 5.1 is not equal to 1, and therefore should be determined and considered for every sulphate system.

According to equation 5.25, at the defined temperature, when there is lower O₂(g) partial pressure, the partial pressures of $M(g)$ and SO₂(g) must be thus higher to balance it. Inversely, high partial pressure of O₂(g) causes the decreasing of the partial pressures of $M(g)$ and SO₂(g).

For the reaction 5.2 the equilibrium constants K_p° (II) expresses the correlation according to equation

$$K_p^\circ(II) = \frac{\left(\frac{p_{M_2SO_4}}{p^\circ}\right)}{a(M_2SO_4)} = \text{const} \quad (5.26)$$

The equilibrium constant $K_p^\circ(II)$ describes the equilibrium between $M_2SO_4(g)$ gas species and the condense phase and does not depend on $O_2(g)$ and $SO_2(g)$ pressure. In this case the higher or lower $O_2(g)/SO_2(g)$ pressure will not influence on the pressure of $M_2SO_4(g)$. In the case of the sulphate solutions, the activity of the M_2SO_4 is not equal to 1 and should be determined for appropriate sulphates systems.

By using the equilibrium constants of the various reactions, it is possible to model the transport of the alkalis in the gas phase in the clinker kiln, as it was presented in the previous work [43]. In that work, from the assumed O_2 and SO_2 partial pressures for the high temperature zone of the clinker kiln, the pressures of $Na(g)$, $K(g)$, $Na_2SO_4(g)$, $K_2SO_4(g)$, $NaKSO_4(g)$ were calculated. The obtained results lead to conclusions that in the clinker kiln [43]:

- the highest molar fraction of K_2SO_4 in the condensed phase favours the vaporisation of potassium sulphate as $K_2SO_4(g)$ species, which is independent of the $O_2(g)$ and $SO_2(g)$ in the atmosphere, therefore the whole SO_2 mass transport in gas is enhanced in form of K_2SO_4 increasing the sulphate circulation
- the partial pressure of $NaKSO_4(g)$ is in practise independent on the Na_2SO_4/K_2SO_4 molar ratio and on the O_2 and SO_2 atmospheres and is significantly responsible for alkali and sulphate transport in the cement kiln.

By the investigation of the binary sulphate systems the activities of the components were detected. According to Raoult's rule for solid and liquid solutions, the partial pressures of the components could be calculated according to equation (5.27).

$$p_a = x_a \cdot p_a^* \quad (5.27)$$

where

p – partial pressure of the component in the mixture

x_a – molar fraction of the component in the condensed phase

p_a^* – partial pressure of the pure component

According to Raoult's rule, the partial pressure of the gas in the mixture behaving like ideal one is proportional to the molar fraction of the component in the condensed phase. To describe the behaviour of the real gases the molar fraction of the equation (5.27) should be replaced by the activity of the component, equation (5.28).

$$p_a = a_a \cdot p_a^* \quad (5.28)$$

The activity of the component could show deviations of the Raoult's rule, what means that the partial pressures of real gases could be different from simply calculation of its molar fractions in the condensed phase. Therefore it is really important to investigate many systems and determine the appropriate activities.

In this work, two systems $\text{Na}_2\text{SO}_4\text{--CaSO}_4$ and $\text{K}_2\text{SO}_4\text{--CaSO}_4$ were investigated. In the case of the $\text{Na}_2\text{SO}_4\text{--CaSO}_4$ system, the activities were only estimated for three rich Na_2SO_4 samples because of the serious difficulty in the measurement caused by the creeping. By the $\text{K}_2\text{SO}_4\text{--CaSO}_4$ system, the activities were calculated for both components, by ion-to-ion method (for K_2SO_4) and Gibbs – Duhem method (for CaSO_4). The activities of the K_2SO_4 show negative deviations from the Raoult's rule, figure 5.13. The same could be considered by the results of the $\text{Na}_2\text{SO}_4\text{--K}_2\text{SO}_4$ activity determination [43], where the activities of the K_2SO_4 show also negative deviation from the Raoult's rule, figure 5.14.

The measurement of the $\text{Na}_2\text{SO}_4 - \text{K}_2\text{SO}_4 - \text{CaSO}_4$ system samples at the selected high temperature ranges was not possible in this work because of the enormous creeping; therefore the tendency of the activity deviations will be only estimated here. Considering the sample for which $x(\text{K}_2\text{SO}_4) = 0.5$, the activity coefficient, defined as

$$\gamma_a = a_a / x_a \quad (5.29)$$

could be calculated. In the case of the $\text{K}_2\text{SO}_4 - \text{CaSO}_4$ system, its value equals to 0.5, for $\text{Na}_2\text{SO}_4 - \text{K}_2\text{SO}_4$ system 0.46. It could be stated that the activity coefficient of K_2SO_4 is similar in both systems. The interactions of K_2SO_4 with CaSO_4 and K_2SO_4 with Na_2SO_4 could be considered as similar, therefore in the ternary system $\text{Na}_2\text{SO}_4 - \text{K}_2\text{SO}_4 - \text{CaSO}_4$ it is expected that the activities of K_2SO_4 will show also negative deviations from the Raoult's rule.

The obtained thermodynamical values and results could be important for the characterization of the alkali circulation in the cement kiln. The obtained activities and various equilibrium constants could be used in the thermodynamical modelling of the gas transport in the high temperature zone, like in the previous work [43]. The further determination of the activities in the various sulphate systems, especially $\text{Na}_2\text{SO}_4 - \text{K}_2\text{SO}_4 - \text{CaSO}_4$ will be suggested that allow for calculating the real pressures in the hot temperature zone.

6. Industrial samples

6.1. The fundamentals of the experiment

The second part of the project was the investigation of the vaporisation of alkali sulphates/chlorides and other volatile species from the industrial samples. For this purpose, the samples were collected directly from the clinker kiln. The samples were taken from 4 different cement plants, referred further as I, II, III, and IV. The points of kiln installation where samples were collected from are presented in the following figure 6.1. Kiln installation of the cement plant III does not include bypass, therefore only three samples were gathered in this case. All the materials were collected into alumina containers. The detailed description of sample materials is summarised in table 6.1.

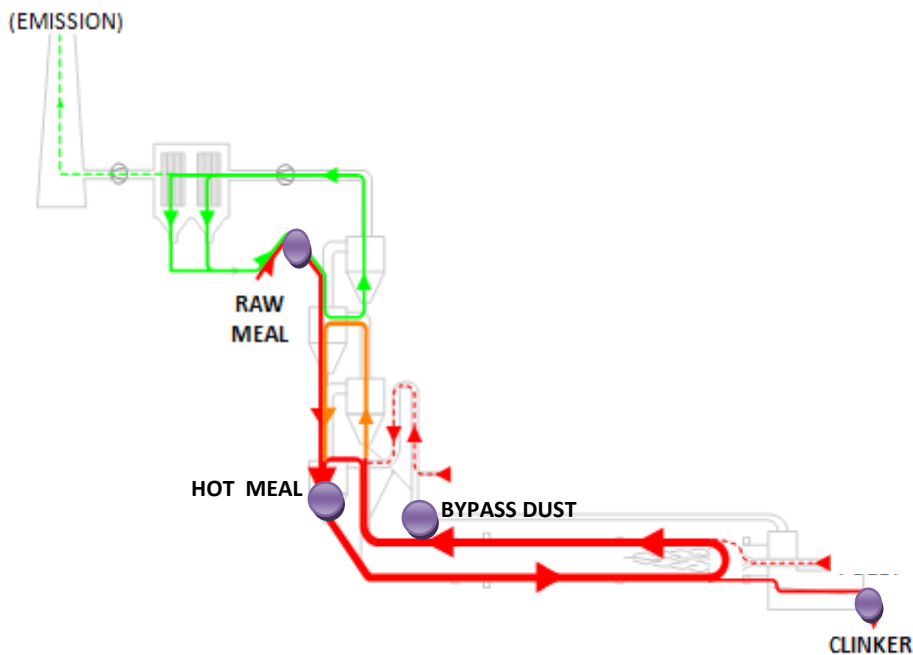


Figure 6.1. Kiln installation with the four points of samples collection

Table 6.1. The description of the collected material

Material	Materials description
Raw material (raw meal)	consist of the freshly grounded rock, used for the clinker production together with the filter dust with condensed salts traces
Hot meal	it is a raw material which was heated to 870 °C for ca. 2 min in the preheater
Bypass dust	A material arisen by drawing off some of the gases and dust from the kiln. The dust is a mixture of unreacted raw feed with partially calcined material, clinker dust and ash enriched with alkali sulphates, halides and other volatiles. These particulates are entrained by exhausted gases and captured in particulate matter control devices such as cyclones or electrostatic precipitators.[65]
Clinker	ready product

As mentioned before, different alternative fuels are used by clinker production plants. Global competition on the market and raising production costs demand effective solutions for reducing the cost of the energy, moreover using the substitute fuels has advantages not only for the cost reduction but also for climate protecting. The alternative fuels used in the selected cement plants are:

- Fluff – is a high calorific fraction of municipal wastes and commercial refuse
- Meat and bone meal (MBM) - is an animal meal, prepared by grinding and sterilizing the waste materials associated with slaughtering operations [66],
- Tires – old car tires, that material offer high heating value, comparable to coal or oil.

Fuels and their quantity used for clinker production in the selected cement plants are presented in table 6.2. Table contains also the daily clinker production of the each cement plant.

Table 6.2. Daily production of the cement plants and the type and quantity of fuels used

Cement plant	I	II	III	IV
Daily production t/day	2400	3400	546	2700
Fuels t/day				
Brown coal	187	86 - 105	56	307
Fluff	264	410	21	168
Meat and bone meat (MBM)	-	70 - 80	19	-
Tires	24	40	-	-

The recirculation processes depend on the raw material composition and fuels that are used in cement making. The fuels are one of the main sources of minor elements taking part in the recirculation process. The ash from fuels combine almost completely in the raw material, therefore, the chemical composition of the ash has to be considered. The sources of minor elements discussed in this work are presented in the following table 6.3

Table. 6.3. Sources of minor elements in cement manufacturing based on Bhatti [3]

Element	Source
Sulphur	Coal, slag, lubricating oil, petroleum coke, pyrite, tires, fluff, raw material, MBM
Chlorine	Coal, slag, fly ash, waste lubricating oil, chlorinated hydrocarbons (from tires, fluff), refuse derived fuels,
Alkalis (Na, K, Rb)	Raw materials
Lead	Raw material, tires, refuse derived fuel, waste derived fuel (fluff), fly ash

In order to characterize the vaporisation processes of the alkali sulphates/chlorides from the industrial materials, Knudsen effusion mass spectrometry was applied. The investigation of such processes is complex therefore also the additional methods were applied to characterize samples before the vaporisation investigations. The additional investigations were carried out by X-ray fluorescence and X-ray diffraction; moreover the humidity and the content of volatiles by heating to 1050 °C were determined by these materials. The samples were investigated after Knudsen effusion mass spectrometry measurement and also by XRD.

The temperature units mainly used in cement industry are in °C; therefore by industrial sample measurement it will be the main unit of the temperature.

6.2. Characterisation of the industrial materials

6.2.1 Humidity and volatiles matter

Firstly a humidity of the material and the content of the volatilities were determined. For humidity detection, the samples were heated up to 105 °C and then weighted. The percentage results of the humidity in the raw meal, hot meal and bypass dust samples are presented in the following table 6.4. It must be underlined, that only H₂O not chemically bound in the minerals (in contrast to hydrates) was determined in this experiment.

Table 6.4. The humidity per cent of the collected material

Material	Cement plant			
	I	II	III	IV
Raw meal	0.49	0.33	0.41	0.54
Hot meal	0.31	0.20	0.45	0.00
Bypass dust	0.76	0.70	-	0.44
Clinker	0.12	0.12	0.13	0.13

For determination of the volatiles in the materials, that is humidity, organic compounds, and other volatilities vaporising at the low temperatures, the samples were heated to the temperature 1050 °C and then weighted. The results are presented in table 6.5.

Table 6.5. The results of the mass loss (in mass %) during heating of the sample to the temperature of 1050 °C

Material	Cement plant			
	I	II	III	IV
Raw meal	35.8	34.8	33.5	35.2
Hot meal	18.0	7.36	19.5	3.39
Bypass dust	15.9	39.7	-	12.7
Clinker	0.38	0.32	0.55	0.42

The mass lost of the raw meal was the highest, over 30%, because this material consists mostly of a lime that includes high CaCO₃ content, which undergoes completely thermal dissociation, according to reaction



The vaporisation of CaCO_3 according to the reaction 6.1 caused high mass loss of the raw meal sample. Therefore, the raw meals were previously heated in Pt crucible in the oven at the temperature 850°C at 1 bar air for the time 1 hour 15 minutes in order to decompose calcium carbonate firstly.

The vaporisation processes of the other volatiles contained in the materials will be characterized further in this work.

6.2.2. XRF Results

The composition of raw materials, hot meals and bypass dusts was determined by means of x-ray fluorescence, taking into consideration the results of the mass lost from section 6.2.1. The results are presented in tables 6.6 – 6.9.

Table 6.6. The oxide composition (in mass %) of raw meal from the cement plant I, II, II, IV determined by x-ray fluorescence

Oxides	Raw meal			
	I	II	III	IV
CaO	43.8	42.7	43.9	43.5
SiO ₂	13.5	13,3	13.7	15.2
SO ₃	0.880	0.478	0.303	0.210
Al ₂ O ₃	3.19	3.33	3.36	2.74
K ₂ O	0.582	0.754	1.22	0.430
Fe ₂ O ₃	1.14	1.77	2.32	1.80
MgO	0.562	0.0244	1.20	0.573
Na ₂ O	0.170	0.0799	0.0831	0.115
TiO ₂	0.141	0.159	0.132	0.135
SrO	0.134	0.101	0.120	0.089
P ₂ O ₅	0.0969	0.0415	0.0381	0.097
MnO	0.0277	0.0244	0.0451	0.037
Cl	0.150	0.050	0.150	0.020
ZnO	< 0.01	< 0.01	0.040	0.040
Rb ₂ O	< 0.01	n.d.	< 0.01	n.d.
Br	n.d.	n.d.	n.d.	n.d.
PbO	n.d.	n.d.	< 0.01	n.d.
ZrO ₂	< 0.01	< 0.01	< 0.01	< 0.01

Table 6.7. The oxide composition of hot meal (in mass %) from the cement plant I, II, II, IV determined by x-ray fluorescence

Oxides	Hot meal			
	I	II	III	IV
CaO	52.3	61.4	51.8	67.0
SiO ₂	11.2	9.61	8.75	16.8
SO ₃	4.86	2.74	4.77	0.596
Al ₂ O ₃	3.10	3.43	3.06	3.77
K ₂ O	4.72	5.27	5.16	2.41
Fe ₂ O ₃	1.24	2.22	2.48	2.74
MgO	0.505	2.02	0.884	0.709
Na ₂ O	0.405	0.213	0.102	0.203
TiO ₂	0.167	0.226	0.148	0.248
SrO	0.164	0.150	0.148	0.148
P ₂ O ₅	0.0957	0.0496	0.0525	0.125
MnO	0.0326	0.0327	0.0544	0.0584
Cl	1.84	2.32	2.02	0.951
ZnO	0.0382	0.103	0.0846	0.0592
Rb ₂ O	0.0396	0.0292	0.0377	0.0234
Br	0.0428	0.0324	0.0170	0.0128
PbO	0.0465	0.0755	0.0225	0.0231
ZrO ₂	0.0021	0.0053	n.d.	0.0026

Table 6.8. The oxide composition of bypass dust (in mass %) from the cement plant I, II, II, IV determined by x-ray fluorescence

Oxides	Bypass dust		
	I	II	IV
CaO	30.1	16.5	50.9
SiO ₂	1.26	2.35	12.5
SO ₃	18.6	5.48	1.42
Al ₂ O ₃	0.329	0.846	2.68
K ₂ O	32.5	18.3	9.28
Fe ₂ O ₃	0.461	0.524	2.09
MgO	0.170	0.417	0.542
Na ₂ O	2.64	0.970	0.570
TiO ₂	0.0429	0.0460	0.176
SrO	0.0561	0.0409	0.109
P ₂ O ₅	0.0798	0.0559	0.0937
MnO	0.0342	0.0177	0.0464
Cl	16.4	12.5	5.41
ZnO	0.407	0.0837	0.0594
Rb ₂ O	0.239	0.100	0.0925
Br	0.236	0.135	0.0563
PbO	0.210	0.239	0.0628
ZrO ₂	0.000370	0.0026	0.0038

Table 6.9. The oxide composition of clinker (in mass %) from the cement plant I, II, II, IV determined by x-ray fluorescence

Oxides	Clinker			
	I	II	III	IV
CaO	67.8	63.7	64.1	66.8
SiO ₂	21.7	21.1	21.8	23.1
SO ₃	0.580	0.690	0.870	0.310
Al ₂ O ₃	5.18	5.28	5.33	4.49
K ₂ O	0.430	0.790	1.20	0.410
Fe ₂ O ₃	1.91	3.21	3.27	2.69
MgO	0.960	3.90	1.90	0.950
Na ₂ O	0.320	0.200	0.140	0.210
TiO ₂	0.260	0.280	0.20	0.230
SrO	0.210	0.150	0.17	0.140
P ₂ O ₅	0.160	0.260	0.310	0.150
MnO	0.050	0.040	0.07	0.060
Cl	n.d.	n.d.	n.d.	n.d.
ZnO	0.030	0.030	0.050	0.050
Rb ₂ O	< 0.01	< 0.01	n.d.	n.d.
Br	n.d.	n.d.	n.d.	n.d.
PbO	n.d.	n.d.	n.d.	n.d.
ZrO ₂	< 0.01	0.01	< 0.01	< 0.01

6.2.2.1 The degree of sulphatisation.

The degree of sulphatisation, that is the molar ratio of sulphate (SO₃) to alkalis, was calculated for raw meal and clinker samples, according to the equation 5.1 [5].

$$DS_{\text{in \% by mass}} = 74.41 \cdot \frac{\% \text{ by mass } SO_3}{\% \text{ by mass } Na_2O + 0.658 \% \text{ by mass } K_2O} \quad (6.1)$$

The degree of the sulphatisation shows the percentage of the alkalis which are present as alkali sulphate. For the other materials as hot meal and bypass dust, for calculation of degree of sulphatisation, equation (5.2) [67] was used. The alkalis combine first with chlorides, before reacting with the sulphur; therefore this phenomenon should be taken into consideration, by subtracting the potassium content, which is combined to chloride.

$$DS_{\text{in \% by mass}} = 100 \frac{\% \text{ by mass } SO_3}{1.29\% \text{ by mass } Na_2O + 0.85\% \text{ by mass } K_2O - 1.13\% \text{ by mass } Cl} \quad (6.2)$$

When the degree of sulphatisation equals 100% than theoretically all alkalis are combined as sulphates, the greater value shows that the sulphur is not fully combined as alkali sulphate, but its excess reacts with CaO and forms mixtures $K_2SO_4 \cdot 2CaSO_4$ or $CaSO_4$. [5]. By lower degree of sulphatisation the volatility of alkali oxides increases. The results of the degree of sulphatisation calculated for raw meal, hot meal and bypass dust are presented in table 6.10.

Table 6.10. The degree of sulphatisation of the raw meal in all cement plants, calculated according to eq. 6.1 for raw meal and 6.2 for hot meal and bypass dust

DS % by mass	Cement plant			
	I	II	III	IV
Raw meal	123	64.2	26.5	40.9
Hot meal	196	128	213	49.6
Bypass dust	149	204	-	56.4
Clinker	74.5	74.2	72.5	50.0

According to the degree of the sulphatisation calculated for the raw meal it could be stated that in raw material coming from cement plant (I) there is an excess of sulphur which will react with CaO. In the case of the other three cement plants all the sulphur should be combined as alkali sulphates.

By hot meal and bypass dust calculation results it could be stated that in the case of cement plant IV there is an access of alkali to the sulphur, in the other materials the degree of the sulphatisation is greater as 100%, which indicated an excess of the sulphur which reacts with CaO.

The value of the degree of the sulphatisation for the clinker is lower than 100% for all the samples that means that sulphur should be theoretically combined in clinker as alkali sulphates.

6.2.3. XRD Results

The results of the phase existing in the samples before and after the vaporisation process are presented in tables 6.11 – 6.14, where:

V – phases determined before KEMS investigation

A – phases determined after KEMS investigation

Tables contain also the number of the ICCD characteristic card for material description [64]. The content of the detected phases was estimated and described by means of /*/ symbols, where it indicates:

**** – dominative phase

*** – massive content of particular phase

** – high content

* – low content

(*) – traces

Table 6.11. XRD results for the samples, coming from cement plant I, investigated before (V) and after (A) vaporisation measurement by Knudsen effusion mass spectrometry.

ICCD card [64]	Phase	Cement plant I							
		Bypass dust		Hot meal		Raw meal*		Clinker	
		V	A	V	A	V	A	V	A
41-1476	KCl	****		****					
37-1497	CaO	*	***	*	*	****	*	(*)	
37-1496	CaSO ₄	*							
44-1481	Ca(OH) ₂	(*)	****	*	*	*	*		
5-586	CaCO ₃	****		*					
46-1045	SiO ₂	*				*			
49-442	Ca ₃ SiO ₅		**		****		****	****	****
33-302	Ca ₂ SiO ₄	***	*	*	**	***	**	**	**
72-2297	CaSiO ₃	(*)				(*)			
5-613	K ₂ SO ₄	*		*					
38-1429	Ca ₃ Al ₂ O ₆		*		**	*	**	**	**
30-226	Ca ₂ (Al,Fe) ₂ O ₅	(*)				*		*	

*phases after calcining

Table 6.12. XRD results for the samples, coming from cement plant II, investigated before (V) and after (A) vaporisation measurement by Knudsen effusion mass spectrometry

ICCD card [64]	Phase	Cement plant II							
		Bypass dust		Hot meal		Raw meal*		Clinker	
		V	A	V	A	V	A	V	A
41-1476	KCl	****		*					
37-1497	CaO	**	***	***	(*)	****	(*)		
45-946	MgO	*	*	*	*	*	(*)	(*)	(*)
37-1496	CaSO ₄	*							
44-1481	Ca(OH) ₂	(*)	(*)	**		*			
9-413	Ca ₁₂ Al ₁₄ O ₃₃	*				(*)			
5-586	CaCO ₃	(*)		(*)	**				
46-1045	SiO ₂	(*)		*		**			
49-442	Ca ₃ SiO ₅	*	****	*	****		****	****	****
33-302	Ca ₂ SiO ₄	**	**	***	**		**	***	***
47-1744	Ca ₂ Fe ₂ O ₅	*				(*)			
73-2041	Ca ₂ (Al(AlSi(O ₇))	*		*					
72-2297	CaSiO ₃	**							
5-613	K ₂ SO ₄	*							
38-1429	Ca ₃ Al ₂ O ₆		**	**	**		**	**	**
30-226	Ca ₂ (Al,Fe) ₂ O ₅			(*)	(*)		(*)	*	*

*phases after calcining

Table 6.13. XRD results for the samples, coming from cement plant III, investigated before (V) and after (A) vaporisation measurement by Knudsen effusion mass spectrometry

ICCD card [64]	Phase	Cement plant III					
		Hot meal		Raw meal*		Clinker	
		V	A	V	A	V	A
41-1476	KCl	*					
37-1497	CaO	***	*	****	*		
45-946	MgO			(*)		*	(*)
37-1496	CaSO ₄	*					
44-1481	Ca(OH) ₂	*	(*)	*			
5-586	CaCO ₃	****					
46-1045	SiO ₂	**		*			
49-442	Ca ₃ SiO ₅		***		****	****	****
33-302	Ca ₂ SiO ₄	***	****	***	**	**	**
47-1744	Ca ₂ Fe ₂ O ₅			(*)			
38-1429	Ca ₃ Al ₂ O ₆	*	*	*	**	*	*
30-226	Ca ₂ (Al,Fe) ₂ O ₅		*	(*)	*	*	*
20-867	K ₂ Ca ₂ (SO ₄) ₃	*					

*phases after calcining

Table 6.14. XRD results for the samples, coming from cement plant IV, investigated before (V) and after (A) vaporisation measurement by Knudsen effusion mass spectrometry

ICCD card [64]	Phase	Cement plant IV							
		Bypass dust		Hot meal		Raw meal*		Clinker	
		V	A	V	A	V	A	V	A
41-1476	KCl	**		*					
37-1497	CaO	***		****		***			
44-1481	Ca(OH) ₂	**		*		***			
5-586	CaCO ₃	(*)							
46-1045	SiO ₂	*		**		**			
49-442	Ca ₃ SiO ₅	**	****		****		****	****	****
33-302	Ca ₂ SiO ₄	***	*	***	**	***	**	***	* **
72-2297	CaSiO ₃	**				*			
38-1429	Ca ₃ Al ₂ O ₆	*	*	*	*	**	*	**	**
30-226	Ca ₂ (Al,Fe) ₂ O ₅	(*)	(*)	*	(*)	*	(*)	**	*
26-918	K _{0.2} Na _{0.8} Cl			(*)					

*phases after calcining

6.3. Analysis of the vaporisation of industrial samples by Knudsen effusion mass spectrometry

6.3.1. The investigation procedure

Knudsen effusion mass spectrometry was applied for the determination of vaporisation of industrial samples. The measurement procedure used for those samples was different from a typical measurement as used for sulphate investigations (Section 5.1). Because of the complex composition of the samples, the aim of the presented investigation was to characterize qualitatively the species that evaporate at the different stages of the clinker kiln. It was also important to compare the vaporisation of alkali sulphates/chlorides from different cement plants, where various sets of fuels and various compositions of raw materials are used.

The samples from cement plants (I), (II), (III) were investigated at the temperature range between 600 – 1400 °C, the samples from the cement plant (IV) at the temperature range 800 – 1400 °C. The temperature was raised with the rate of 10 °C/min stepwise by 100 °C. Five minutes after achieving appropriate temperature all the mass spectrum from $m/e = 20$ to 300 was detected, than a moveable shutter was applied for a background determination. The waiting time was adjusted in a manner allowing the detection of the vaporisation of traces and obtaining a parallel near equilibrium

condition. This procedure was applied for all the samples under investigation to achieve an overview of the vaporisation at all kiln zones, corresponding to the low, medium and high temperatures.

Because the “raw meal” material includes high CaCO_3 content, it was unfeasible to investigate that material directly by means of the Knudsen effusion mass spectrometry. The liberation of the high CO_2 contents disturbed proper high vacuum maintenance. Therefore, the materials “raw meal” was previously heated in Pt crucible in the oven at the temperature 850 °C at 1 bar air for the time 1 hour 15 minutes in order to decompose the calcium carbonate firstly.

A thermodynamic interpretation of the mass spectrometric results requires qualitative and quantitative assignment of the observed ions to their neutral precursors. The quantitative assignment of the ions to their neutral precursors was not possible here, due to the complex vapour composition, complexity of the samples under investigation and a difficult fragmentation. However, a qualitative and quasi-quantitative assignment of the ion currents to the specific vaporisation processes could be performed on the basis of the vaporisation studies of pure substances and of model melts studies in this work.

Therefore, in the case of the industrial samples investigation, the determination of the vaporisation quantitatively and partial pressure determination were omitted. For those samples, only qualitative and semi-quantitative analyses are presented and on that basis the vaporisation process of volatilities estimated. Resting upon the constancy of the sensitivity of mass spectrometer throughout this study, a comparison between these processes going on in four different kiln installations I-IV was possible. The ions presented in the mass spectrum originating from the vapour species were identified by the mass-to-charge ratio and the isotopic distribution by applying *isotope calculator* [68].

6.3.2. The assignment of the ions to their neutral precursors

An example of the ion spectrum from $m/e=20$ to $m/e=260$ registered during vaporisation of the bypass dust sample coming from cement plant II is presented in figure 6.2.

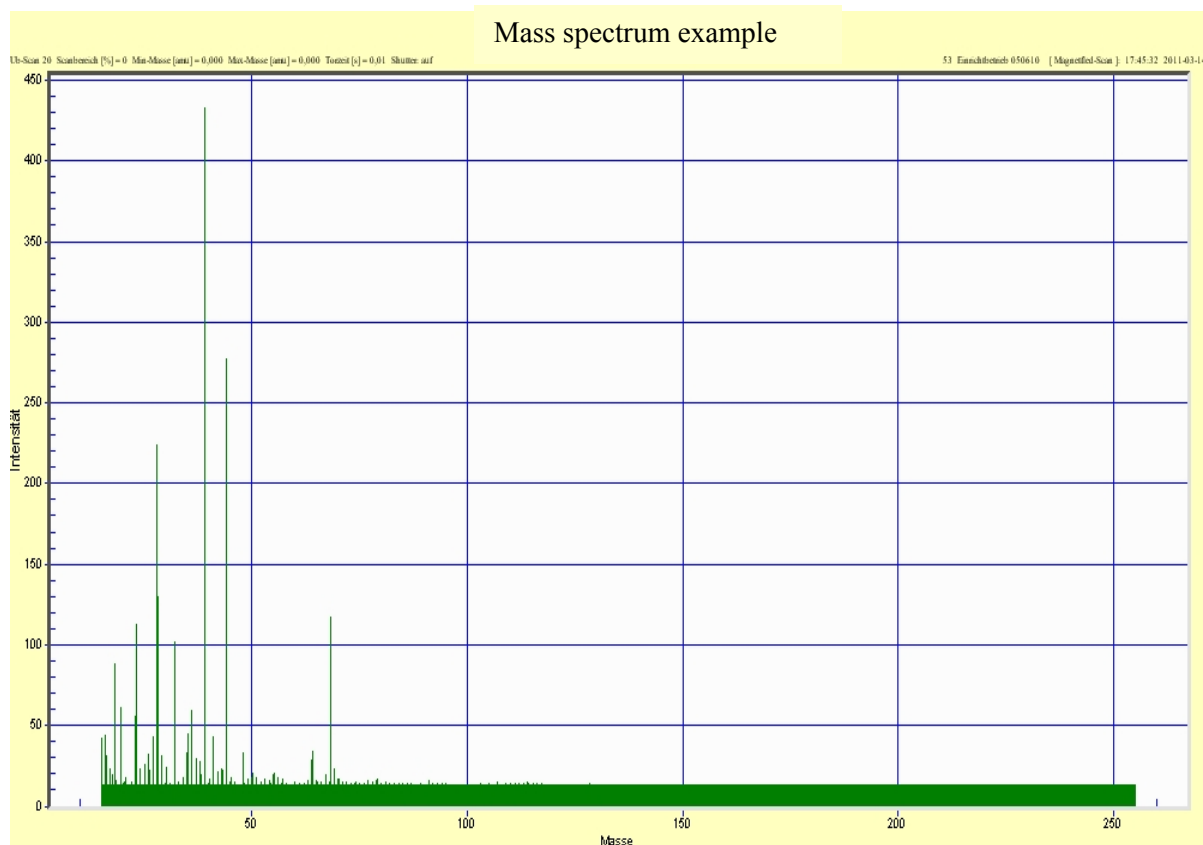


Figure 6.2. An example of the ion intensities in the mass spectrum from $m/e = 20$ to 300, registered during evaporation of bypass dust sample coming from cement plant II.

Various ions were registered during the vaporisation of the industrial samples. Table 6.15 presents briefly the main isotopes of the ions that have the highest intensities in the detected spectrum.

Table 6.15. Ions, and their main isotopes identified in the vapours over the samples investigated.

m/e of the main isotope of the ion	Ion identified
23	Na ⁺
32	O ₂ /S ⁺
35	Cl ⁺
39	K ⁺
48	SO ⁺
58	NaCl ⁺
64	SO ₂ ⁺
64	Zn ⁺
74	KCl ⁺
78	NaKO ⁺
85	Rb ⁺
94	NaKCl ⁺
94	K ₂ O ⁺
113	K ₂ Cl ⁺
142	Na ₂ SO ₄ ⁺
158	NaKSO ₄ ⁺
174	K ₂ SO ₄ ⁺
208	Pb ⁺

The assignment of the ions to their neutral precursor was difficult because of the complexity of the industrial samples under investigation. In many cases the molecular ions of the species were observed, that enabled their assignment to neutral precursors, according to isotope distributions by using *isotope calculator* [68]. The qualitative assignment of those ions to their neutral precursors is presented in the following table 6.16.

Table 6.16. The qualitative assignment of the molecular ions, measured in the vapours of the industrial samples, to their neutral precursors.

Ion	Neutral precursor
NaKCl ⁺	NaKCl ₂
K ₂ Cl ⁺	K ₂ Cl ₂
Na ₂ SO ₄ ⁺	Na ₂ SO ₄
K ₂ SO ₄ ⁺	K ₂ SO ₄
NaKSO ₄ ⁺	NaKSO ₄

The origin of the ions, which are fragments of the various species were qualitatively estimated on the basis of previous measurements of the pure sulphate systems (Section 5) and data coming from

literature [69], [70], [71]. The assignments of the ions that are fragments of various species established in this work are presented in table 6.17.

Table 6.17. The qualitative assignment of the ions that are fragments of a various species to their neutral precursors established in this work.

Ion	Neutral precursor
Na^+	NaCl , Na_2SO_4 , $(\text{Na}_2\text{O})_{\text{soluble in clinker phases.}}$
K^+	KCl , K_2SO_4 , $(\text{K}_2\text{O})_{\text{soluble in clinker phases.}}$
Cl^+	$M\text{Cl}$, $M=\text{Na}, \text{K}$
$\text{SO}^+/\text{SO}_2^+$	$M_2\text{SO}_4$, $M=\text{Na}, \text{K}$ SO_2
NaCl^+	NaCl
KCl^+	KCl

6.3.3 The comparison of the materials vaporisation

The most important recirculating substances which can affect the operation of a cement kiln system are alkali sulphates and alkali chlorides. The alkalis are also transported as alkali oxides in the gas phase, especially when the volatilization of alkali oxides increases by reducing degree of sulfatization.

In order to characterize qualitatively and semiquantitatively such complex process as alkali vaporisation from the industrial materials, intensities of the ions from table 6.16 and their temperature dependencies, registered in the vapours during industrial material vaporisation, were compared.

The results were discussed in two ways, by comparing:

- materials coming from different part of the kiln, but the same cement plant and
- materials coming from different cement plants, but from the same kiln stage.

Comparing the vaporisation of the materials coming from different part of the kiln was undertaken to characterize the vaporisation process at different stages of the cement kiln. The compared materials which are: raw meal, hot meal, bypass dust and clinker. They had previous contact with different atmospheres and temperatures, and went through the different stages of cement kiln. Those materials

underwent different physical and chemical conditions and reactions that could have an influence on the vaporisation process.

The second discussion is comparing the vaporisation of the samples coming from different cement plants but the same kiln stages. That was undertaken to determine the influence of the fuels, raw feed composition and differences by clinker production in various cement plants on the vaporisation process.

6.3.3.1. Materials coming from different parts of the kiln, but the same cement plant

Cement plant I

The temperature dependencies of the intensities of the ions Na^+ , K^+ , SO^+ , SO_2^+ , Cl^+ occurring in the vapour of the raw meal, hot meal, bypass dust and clinker samples from the cement plant I are presented in figures 6.3 – 6.7. As mentioned in Section 4, the sensitivity constant changes to 10% over the period of three years. Thus, the error of the intensity measurements equals to that sensitivity constant, and is also presented as a measurement error on the intensity curve. The values in figure 6.6 and following represent the average of two independent measurements.

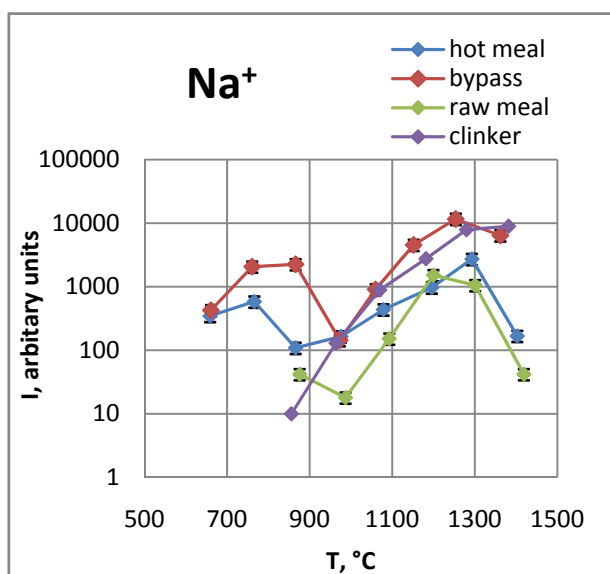


Figure 6.3. Temperature dependencies of the intensity of the ion Na^+ in raw meal, hot meal, bypass dust and clinker sample from cement plant I

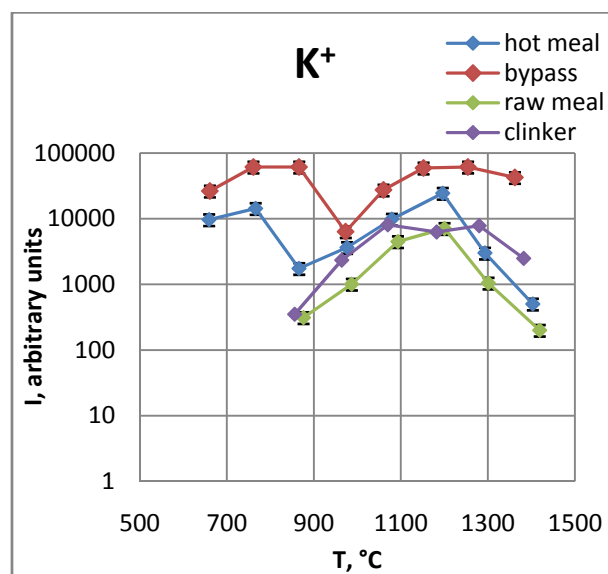


Figure 6.4. Temperature dependencies of the intensity of the ion K^+ in raw meal, hot meal, bypass dust and clinker sample from cement plant I

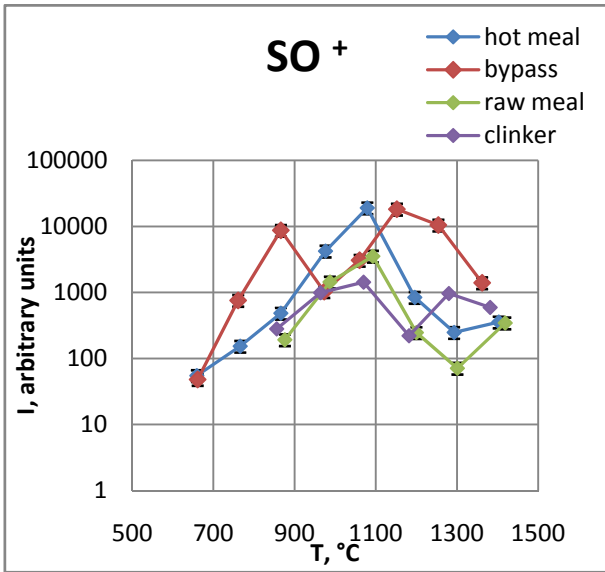


Figure 6.5. Temperature dependencies of the intensity of the ion SO^+ in raw meal, hot meal, bypass dust and clinker sample from cement plant I

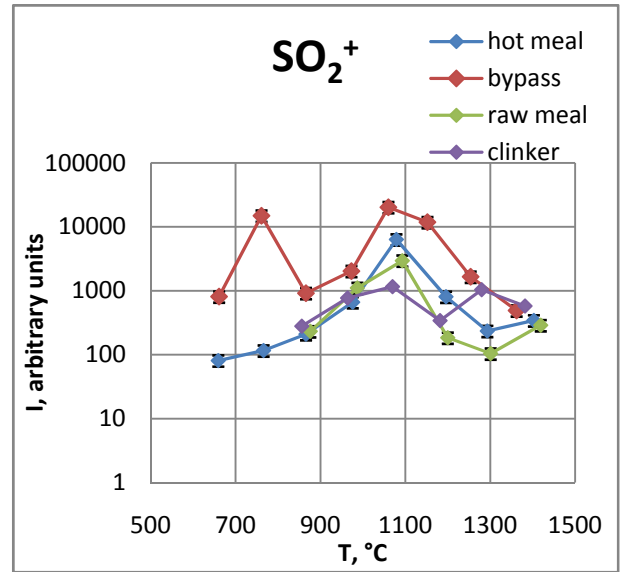


Figure 6.6. Temperature dependencies of the intensity of the ion SO_2^+ in raw meal, hot meal, bypass dust and clinker sample from cement plant I

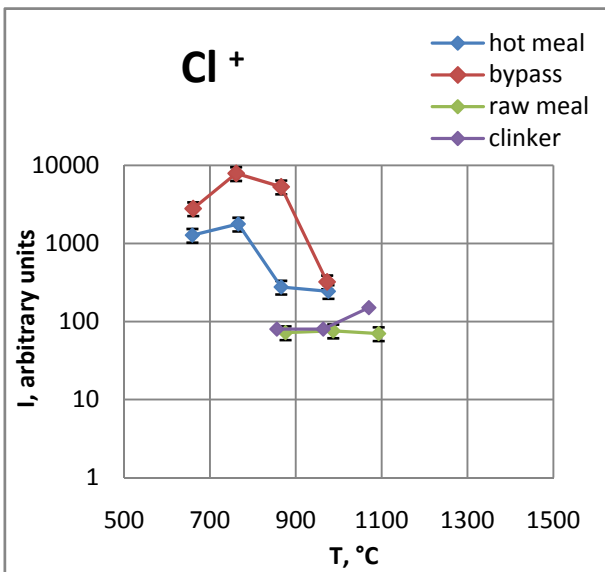


Figure 6.7. Temperature dependencies of the intensity of the ion Cl^+ in raw meal, hot meal, bypass dust and clinker sample from cement plant I.

As presented in figure 6.3 – 6.4, the intensity curves of alkalis (Na^+ , K^+) have two maxima. The first one occurs at the temperature range between 700 °C – 900 °C, the second at 1100 – 1300 °C temperature range. The intensity curves of SO^+ and SO_2^+ in figures 6.5 – 6. 6 also have two maxima – the first one at the temperature range 700 °C – 900 °C, and the second at 1100 – 1300 °C. The intensity curve of Cl^+ , in figure 6.7 has only one maximum at the temperature range between 700 °C – 900 °C. The listed temperature ranges of particular ions are the temperatures where the components which are the precursors of the ions vaporize at their higher content.

In Knudsen effusion mass spectrometry there is general rule, described by Hilpert [28], showing that the intensities of ions generated from the same neutral molecule should show the same temperature dependencies. Therefore the first maximum of the alkali intensity curve in figure 6.3 – 6.4 was assigned to alkali halide vaporisation. It reaches its maximum similarly as the intensity curve of ion Cl^+ in figure 6.7 what indicates that those ions have the same origin. Moreover the molecular ions KCl^+ and NaCl^+ , presented in figures 6.8 – 6.9, coming from gaseous species of alkali chlorides, that is KCl(g) and NaCl(g) , could be seen in the mass spectrum of hot meal and bypass dust samples.

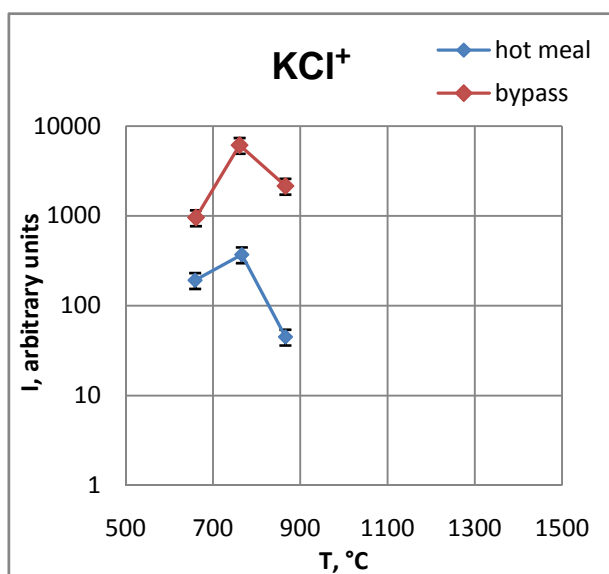


Figure 6.8. Temperature dependencies of the intensity of the ion KCl^+ in hot meal and bypass samples from cement plant I.

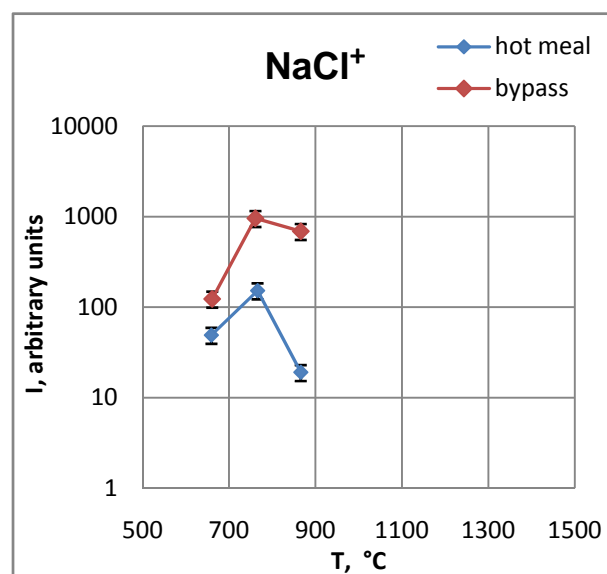


Figure 6.9. Temperature dependencies of the intensity of the ion NaCl^+ in hot meal and bypass dust sample from cement plant I.

Summarizing, the temperature dependencies of the ions KCl^+ , NaCl^+ together with the ion Cl^+ and first maximum of the intensity curves of the ions Na^+ and K^+ indicate the same alkali chloride origin,

which vaporise in the higher content at the temperature ranges 700 – 900 °C, and disappears completely from the vapour at the temperature 1100 °C.

Comparing intensity curves of SO^+ , SO_2^+ figures 6.5 – 6.6, with the intensity curve of the alkali (Na, K) vaporisation, figure 6.3 – 6.4, it could be realised that the maximum of the intensities of alkali vaporisation shows different temperature dependencies from the $\text{SO}^+/\text{SO}_2^+$ intensity curve. The maximum of the intensities of $\text{SO}^+/\text{SO}_2^+$ is at the temperatures 1000 – 1200 °C, but the maximum of alkalis intensity curve is at the higher temperature range 1100 – 1300 °C. To explain this phenomenon, the temperature dependencies of the molecular ion K_2SO_4^+ found in the vapour of the hot meal and bypass dust sample was taken into consideration, figure 6.10.

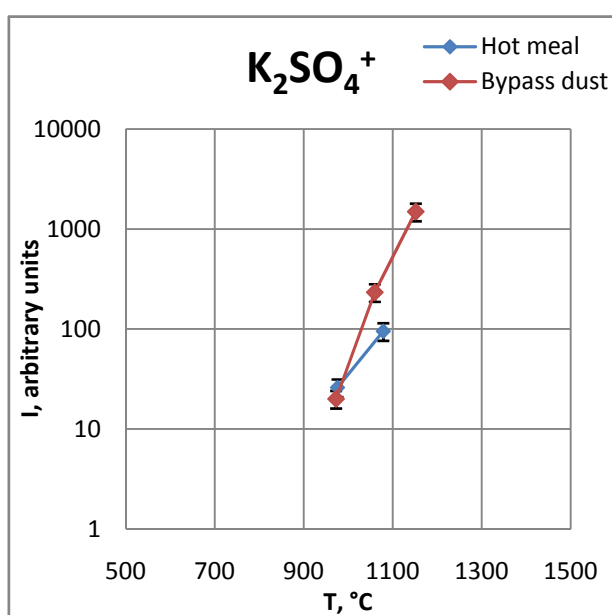


Figure 6.10. Temperature dependencies of the intensity of the ion K_2SO_4^+ in hot meal and bypass samples from cement plant I.

The ion K_2SO_4^+ has the only one precursor, that is $\text{K}_2\text{SO}_4(\text{g})$ and shows the same temperature dependencies as intensity curve of the ions $\text{SO}^+/\text{SO}_2^+$, vaporizing at the temperature range 1000 – 1200 °C at the higher content. Therefore these ions have the same neutral precursor that is alkali sulphate.

The intensity curves of alkalis shows different temperature dependencies from the intensity curves of the ions $\text{SO}^+/\text{SO}_2^+$ and K_2SO_4^+ , therefore the ion M^+ , where $M=\text{Na}, \text{K}$, must be a fragment of two different gaseous species vaporising in the similar temperature ranges 1100 – 1300 °C, where the

second intensity maximum occurs, in figures 6.3 – 6.4. First part of this intensity maximum is alkali sulphate vaporisation at the temperature range 900 – 1200 °C, what is with agreement with temperature dependencies of the molecular ion K_2SO_4^+ in figure 6.10. Second part of the intensity maximum is the vaporisation of alkali oxide from the clinker melt that occurs at higher temperature ranges as sulphates, that is at 1200 – 1300 °C.

Summarizing, the maximum on the alkali intensity curve, consists of the vaporisation of two neutral precursors, alkali sulphate and alkali oxide from the clinker melt. Because the vaporisation of alkali sulphates and alkali oxides from clinker melt occurs in the similar temperature range it could be seen as the only one maximum on the alkali intensity curve, but in fact there are two different vaporisation processes, by which the alkali are transported in the gas phase.

Moreover, in figures 6.5 – 6.6, in the case of bypass dust sample, there is an additional maximum of the intensity curve of SO^+ , SO_2^+ at the temperatures between 700 – 900 °C. This maximum comes from the incongruent vaporisation of CaSO_4 according to reaction 5.3. The reason for that is, that calcium sulphate vaporise incongruently at the lower temperature range as alkali sulphate, section 5. The low content of calcium sulphate phase was also detected by XRD analysis in a bypass dust sample, table 6.10.

If there is a CaSO_4 content in the sample under investigation, even not observable in XRD, its vaporisation causes a shift of the maxima of SO^+ and SO_2^+ intensity curves towards the lower temperatures. Calcium sulphate vaporises with decomposition according to the reaction 5.3 at the lower temperature ranges compared to alkali sulphates (see Section 5).

Cement plant II

The same analysing procedure was applied in the case of cement plant II. The temperature dependencies of the intensities of ions Na^+ , K^+ , SO^+ , SO_2^+ , Cl^+ together with an error, occurring in the vapour of raw meal, hot meal, bypass dust, clinker samples coming from the cement plant II are presented in figures 6.11- 6.15.

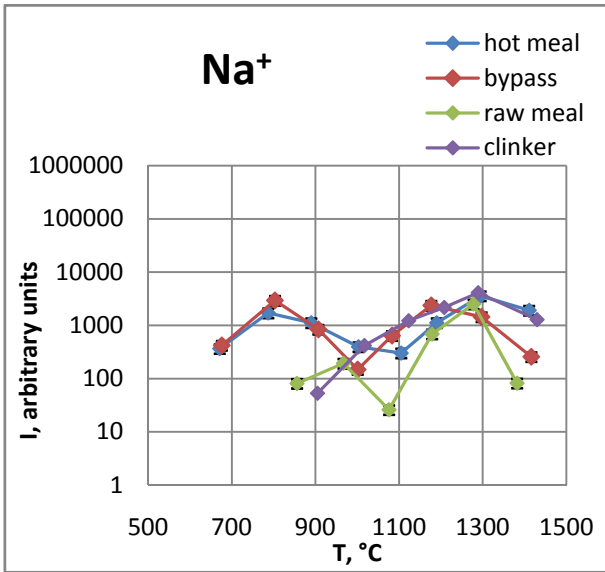


Figure 6.11. Temperature dependencies of the intensity of the ion Na^+ in raw meal, hot meal, bypass dust and clinker sample from cement plant II.

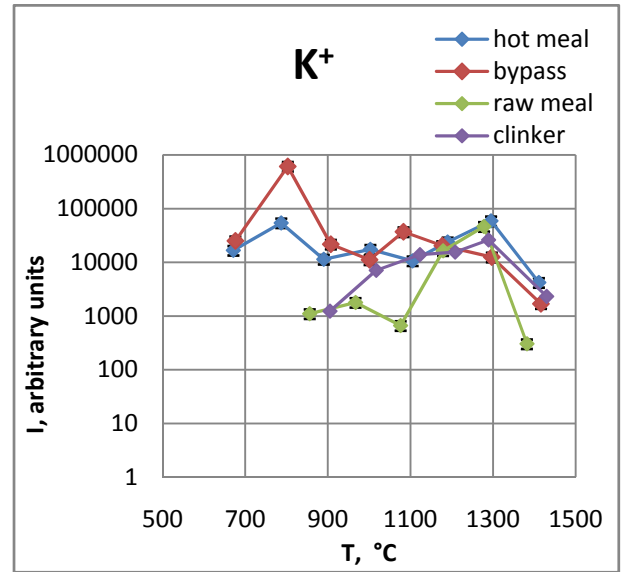


Figure 6.12. Temperature dependencies of the intensity of the ion K^+ in raw meal, hot meal, bypass dust and clinker sample from cement plant II.

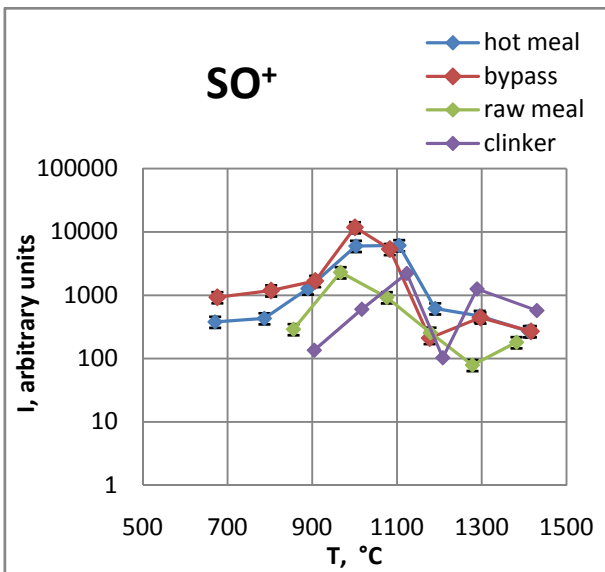


Figure 6.13. Temperature dependencies of the intensity of the ion SO^+ in raw meal, hot meal, bypass dust and clinker sample from cement plant II.

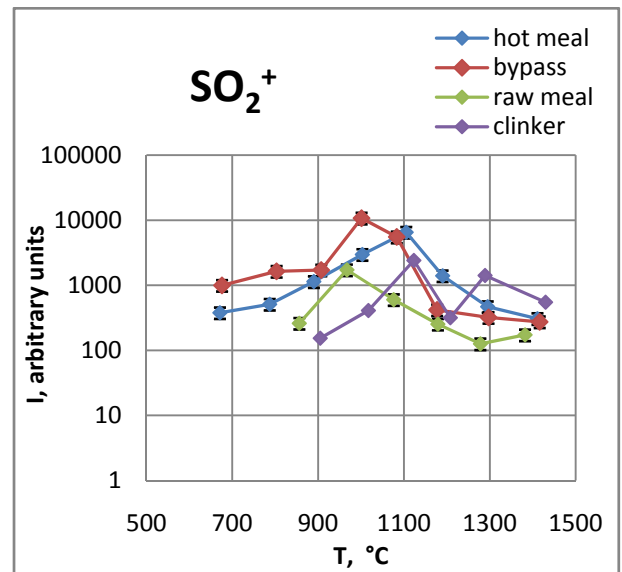


Figure 6.14. Temperature dependencies of the intensity of the ion SO_2^+ in raw meal, hot meal, bypass dust and clinker sample from cement plant II.

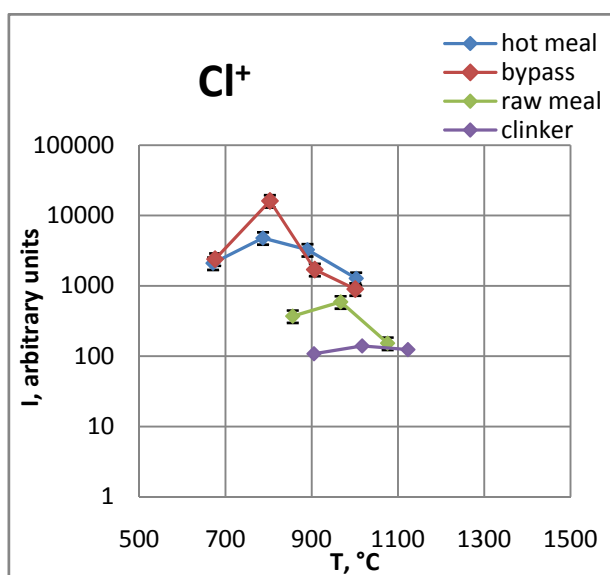


Figure 6.15. Temperature dependencies of the intensity of the ion Cl^+ in raw meal, hot meal, bypass dust and clinker sample from cement plant II.

Similarly to the materials coming from cement plant I, the intensity curves of alkalis (Na^+ , K^+) have two maxima, presented in figures 6.11– 6.12. The first one occurs at the temperature range between 700 °C – 900 °C, the second at 1100 – 1300 °C temperature range. The intensity curves of SO^+ and SO_2^+ in figures 6.13 – 6. 14 have a maximum at the temperature 900 °C – 1100 °C. The intensity curve of Cl^+ , in figure 6.15 has one maximum at the temperature range between 700 °C – 1000 °C.

According to the temperature dependencies of the intensity curves, the first maximum of the alkali intensity curve in figures 6.11 – 6.12 was assigned to alkali halide vaporisation. The temperature dependencies of the ion Cl^+ and first maximum of the alkali curve are analogous. Also in this case, the molecular ions KCl^+ and NaCl^+ coming from gaseous species of alkali chlorides, that is KCl(g) and NaCl(g) , could be seen in the mass spectrum of hot meal and bypass dust samples, figure 6.16 – 6.17, which indicate on the same origin of all those ions.

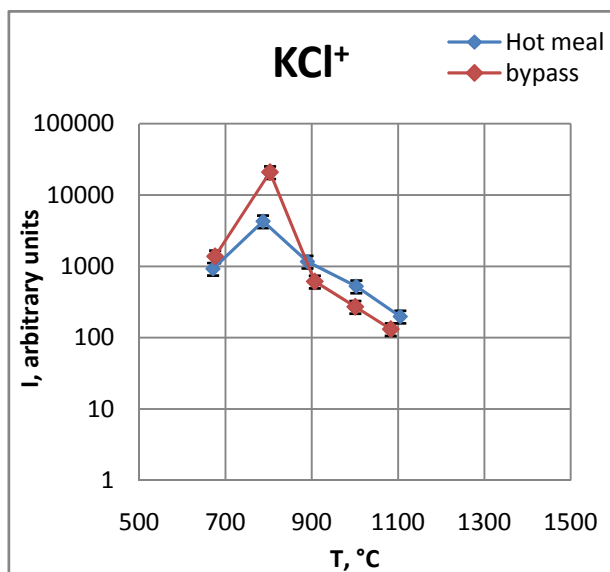


Figure 6.16. Temperature dependencies of the intensity of the ion KCl^+ in hot meal and bypass samples from cement plant II.

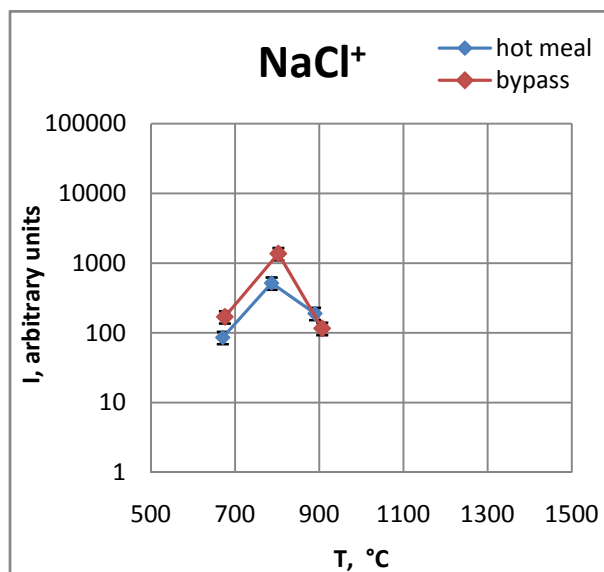


Figure 6.17. Temperature dependencies of the intensity of the ion NaCl^+ in hot meal and bypass dust sample from cement plant II

Similarly in the case of the materials coming from cement plant II, the same dependencies were found, showing that alkali chloride vaporizes at the temperature ranges 700 – 900 °C, and disappears completely from the vapour at the temperature 1100 °C.

Comparing intensity curves of SO^+ , SO_2^+ figures 6.13– 6.14, with the intensity curve of the alkali (Na, K) vaporisation, figure 6.11 – 6.12, it could be realised, similarly as by materials from cement plant I, that the maximum of the intensities of alkali vaporisation shows different temperature dependencies from the $\text{SO}^+/\text{SO}_2^+$ intensity curve. The maximum of the intensities of $\text{SO}^+/\text{SO}_2^+$ is at the temperatures 900 – 1100 °C, but the maximum of alkalis intensity curve is at the higher temperature range 1100 – 1300 °C. As was explained above, alkali sulphate vaporisation occurs at the temperature range 1000 – 1200 °C, what was also proved in this case, by comparing $\text{SO}^+/\text{SO}_2^+$ intensity curves with alkali intensity curves and the small signal of the molecular ion of $\text{K}_2\text{SO}_4(\text{g})$, presented in figure 6.18.

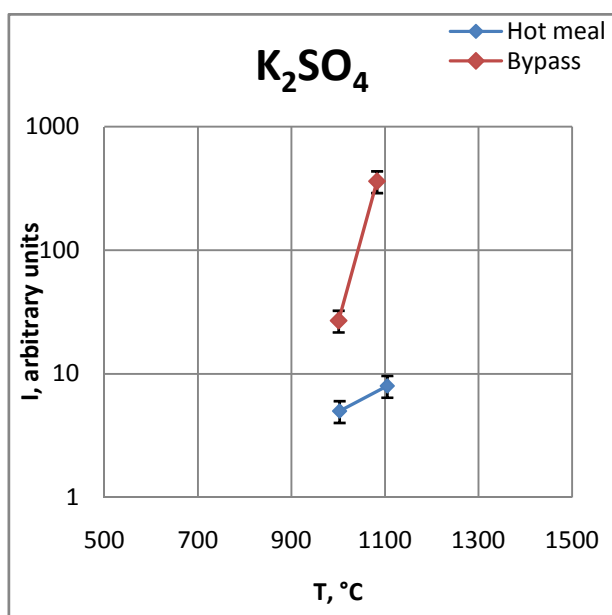


Figure 6.18. Temperature dependencies of the intensity of the ion K_2SO_4^+ in hot meal and bypass samples from cement plant II.

The high temperature maximum of the alkali intensity curves, fig 6.11 – 6.12, shows two different vaporisations: alkali sulphate, at the temperature ranges 1000 – 1200 °C, and alkali oxide from the clinker melt at the temperature ranges 1200 – 1300 °C. The vaporisation of alkali sulphates and alkali oxides from clinker melt occurs in similar temperature ranges and it could be seen as a unique maximum on the alkali intensity curve, but there are two different vaporisation processes. Where there is a high content of alkali sulphates and alkali oxides in the sample, the vaporisation of alkalis could be distinguished, as in the case of hot meal vaporisation curve in figure 6.26. The vaporisation curve of hot meal sample is presented additionally in figure 6.19.

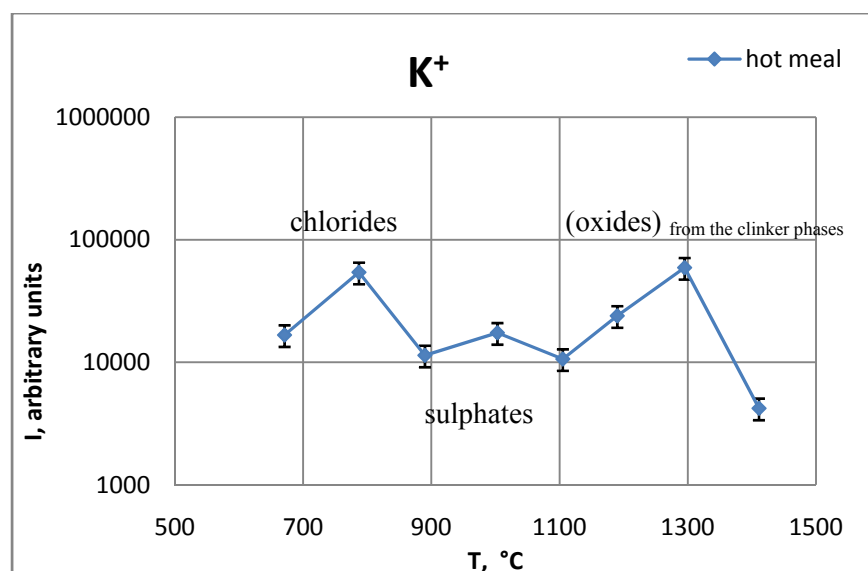


Figure 6.19. Temperature dependencies of the intensity of the ion K^+ in hot meal sample from cement plant II.

As presented in figure 6.19, three maxima on the intensity curves could be seen, which are responsible for three different vaporisation processes of alkalis. The first vaporisation is alkali chloride vaporisation at the temperatures 700 – 900 °C, while the second one, alkali sulphates vaporisation at the temperatures 900 – 1100 °C. The third one refers to the alkali oxide vaporisation at the temperature ranges 1200 – 1400 °C. These oxides are presumably solved in the clinker melt.

Summarizing, the maximum on the alkali intensity curve consists of the vaporisation of three neutral precursors, alkali chlorides, alkali sulphates and alkali oxide solved in the clinker melt. The vaporisation of chlorides is easy to distinguish because it occurs at lower temperature ranges and disappears from the vapour completely at 1100 °C. The vaporisation of alkali sulphates and alkali oxides from clinker melt occurs in similar temperature ranges; therefore, it could be seen as two maxima, where there is enough alkali sulphates and oxides in the sample, or by the only one maximum on the alkali intensity curve, where one component dominates.

Cement plant III and cement plant IV

The same discussion and conclusions as for cement plant I and II could be made in the case of the cement plants III and IV, because the intensity curves of alkalis, SO^+ , SO_2^+ and Cl^+ in all materials show the same vaporisation rules and principles, where at the appropriate temperature ranges, appropriate volatiles vaporize. Therefore same discussion as for cement plant I and II is valid. The intensity curves of Na^+ , K^+ , SO^+ , SO_2^+ , Cl^+ together with an error, occurring in the vapour of raw meal, hot meal, bypass dust, clinker samples over the materials coming from cement plant III are presented in figures 6.20 – 6.24, and from cement plant IV in figures 6.25 - 6.29.

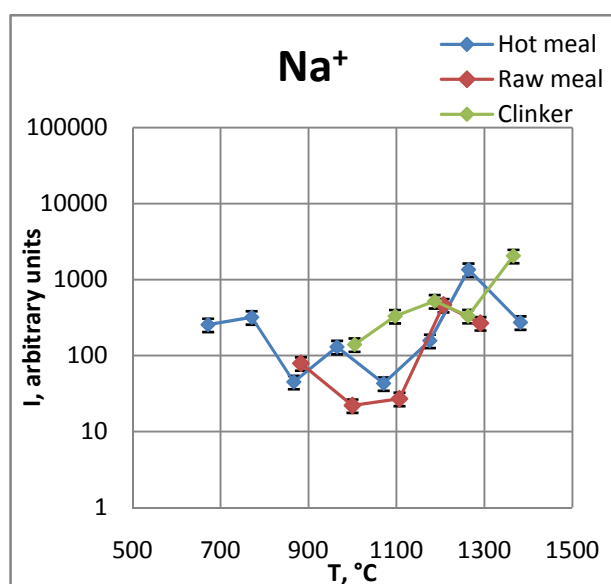


Figure 6.20. Temperature dependencies of the intensity of the ion Na^+ in raw meal, hot meal, bypass dust and clinker sample from cement plant III.

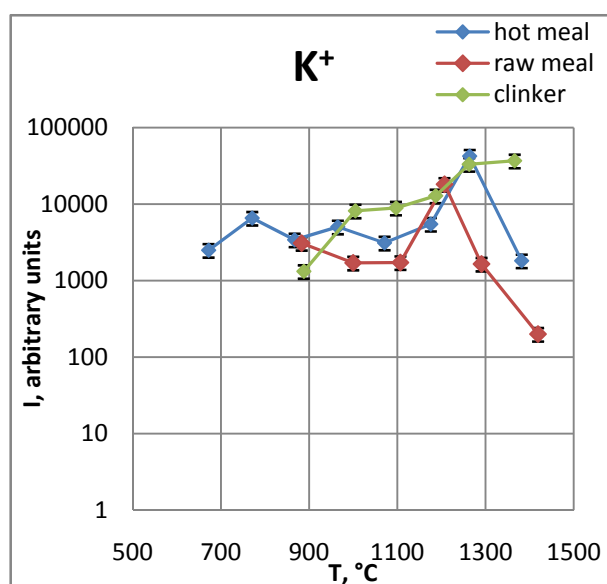


Figure 6.21. Temperature dependencies of the intensity of the ion K^+ in raw meal, hot meal, bypass dust and clinker sample from cement plant III

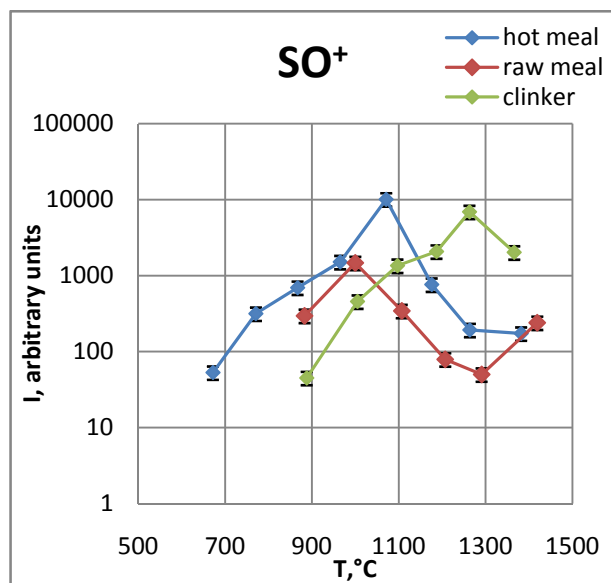


Figure 6.22. Temperature dependencies of the intensity of the ion SO^+ in raw meal, hot meal, bypass dust and clinker sample from cement plant III.

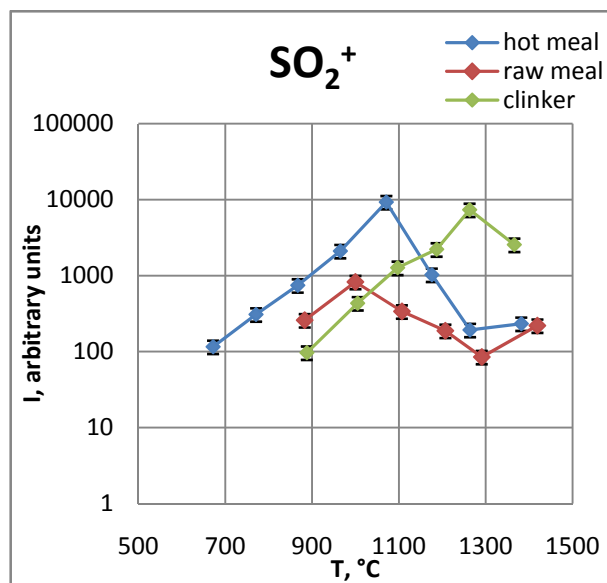


Figure 6.23. Temperature dependencies of the intensity of the ion SO_2^+ in raw meal, hot meal, bypass dust and clinker sample from cement plant III

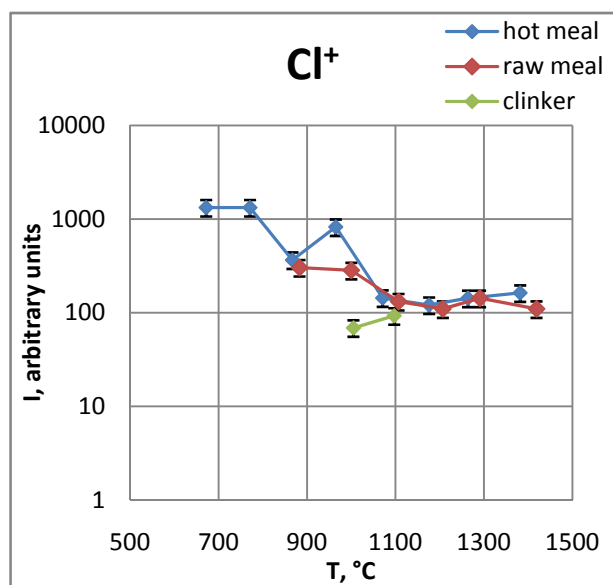


Figure 6.24. Temperature dependencies of the intensity of the ion Cl^+ in raw meal, hot meal, bypass dust and clinker sample from cement plant III

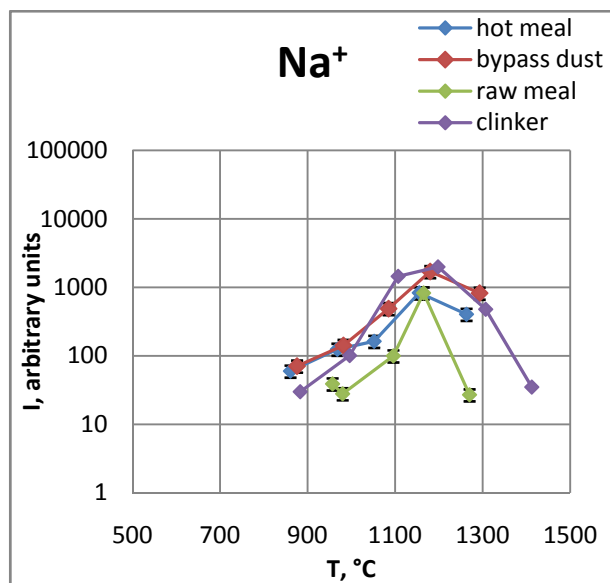


Figure 6.25. Temperature dependencies of the intensity of the ion Na^+ in raw meal, hot meal, bypass dust and clinker sample from cement plant IV.

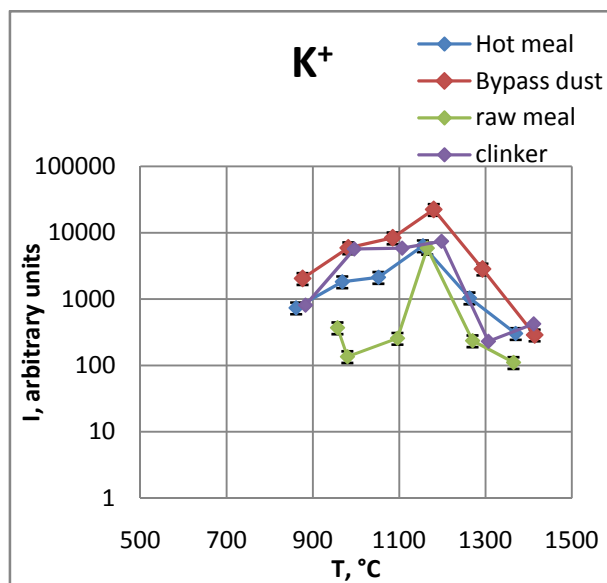


Figure 6.26. Temperature dependencies of the intensity of the ion K^+ in raw meal, hot meal, bypass dust and clinker sample from cement plant IV

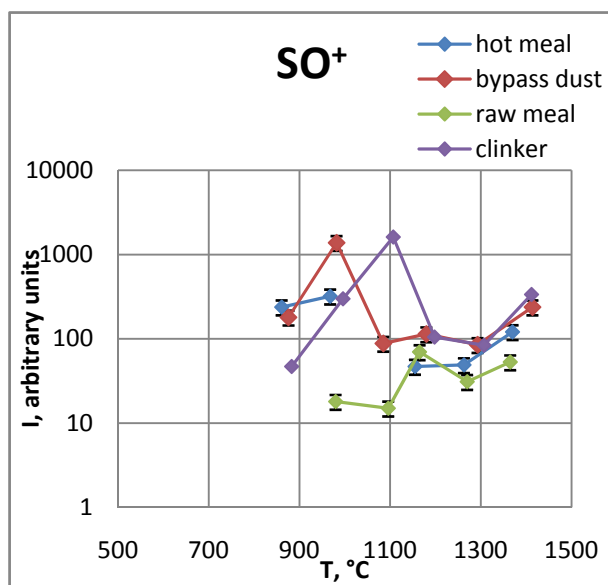


Figure 6.27. Temperature dependencies of the intensity of the ion SO^+ in raw meal, hot meal, bypass dust and clinker sample from cement plant IV.

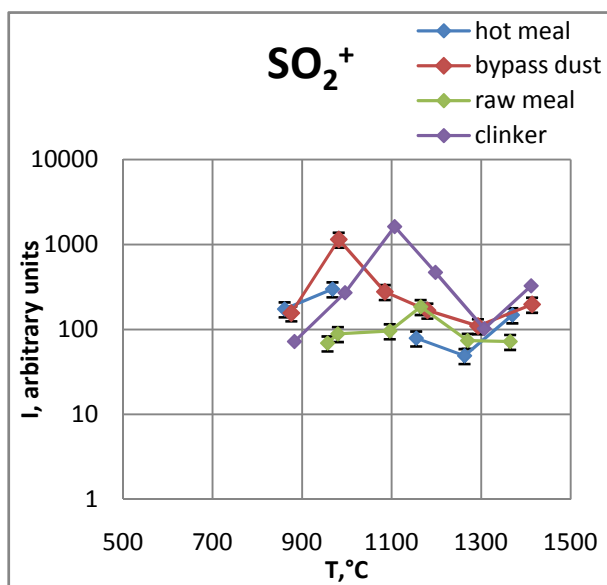


Figure 6.28. Temperature dependencies of the intensity of the ion SO_2^+ in raw meal, hot meal, bypass dust and clinker sample from cement plant IV

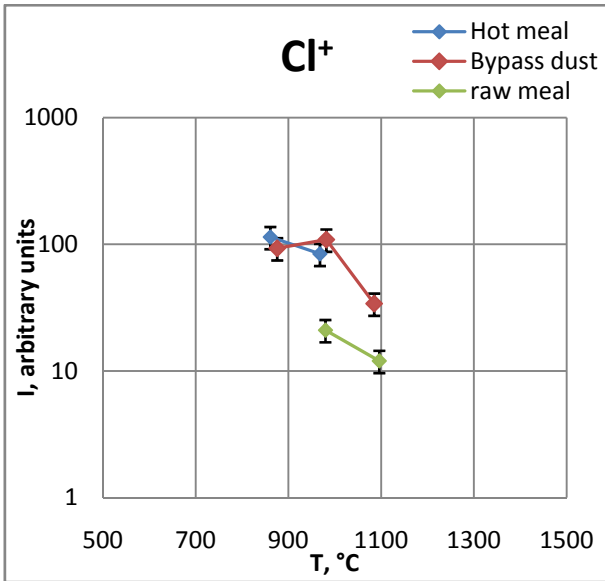


Figure 6.29. Temperature dependencies of the intensity of the ion Cl^+ in raw meal, hot meal, bypass dust and clinker sample from cement plant IV

6.3.3.2. Materials coming from different cement plants but the same kiln stage

According to discussion from section 6.3.3.1, the vaporisation process could be characterised as three processes occurring in different temperatures ranges, where appropriate maxima of volatile components occurs, that is:

- range 700 – 800 °C, vaporisation of halides
- range 900 – 1100 °C, sulphates vaporisation
- range 1200 – 1300 °C, vaporisation of the oxides solved in the clinker phases

For mentioned three temperature ranges, the maximum of the intensities of considered ions Na^+ , K^+ , SO^+ , SO_2^+ , Cl^+ were summarized in tables 6.17 – 6.25. Materials were called with numbers I, II, III and IV, according to the names of the cement plant from they were collected.

Raw meal

The ion intensities of the Na^+ , Cl^+ , K^+ , SO^+ , SO_2^+ , detected in the vapours over the all raw meal samples at temperatures around 1000 °C and 1200°C are presented in tables 6.18 – 6.19.

Table 6.18. The intensities of the ions Na^+ , Cl^+ , SO^+ , SO_2^+ , K^+ detected in the vapour of the raw meal sample from all cement plants at the 1000 °C.

Ion	Ion intensities/counts			
	I	II	III	IV
Na^+	18	193	22	28
Cl^+	76	591	284	21
K^+	1008	1786	1708	136
SO^+	3532	2299	1470	18
SO_2^+	2963	1731	826	89

Table 6.19. The intensities of the ions Na^+ , Cl^+ , SO^+ , SO_2^+ , K^+ , detected in the vapour of the raw meal sample from all cement plants at the 1200 °C.

Ion	Ion intensities/counts			
	I	II	III	IV
Na^+	1517	687	463	829
Cl^+	n.d.	n.d.	n.d.	n.d.
K^+	7104	16397	18231	5854
SO^+	246	256	79	70
SO_2^+	184	253	188	185

The raw meal sample was heated in the oven at the temperature 850 °C for 1 hour 15 minutes, before measurement by Knudsen effusion mass spectrometry; therefore most of the chlorides contained in the sample had been liberated in the oven, before the measurement started. The intensities of chlorides at the temperature 1000 °C are the traces of the chlorides; therefore the discussion of the vaporisation of chlorides in the case of these samples will be omitted.

The intensities of SO^+ and SO_2^+ at the temperature of sulphates vaporisation, table 6.18, are the highest in the case of the raw meal I. Also the XRF results of SO_3 (tab. 6.6) shows the highest content of sulphur in material I that is 0.880 per cent by mass. In the raw meal II the content of SO_3 equalled to 0.478 and by material III, 0.303 per cent by mass that could be also seen in the similar sequence in the vaporisation content. The highest intensity of $\text{SO}^+/\text{SO}_2^+$ coming from alkali sulphates are in the case of raw meal I, further raw meal II than raw meal III, accordingly with XRF results. In the case of

material IV, there is the lowest content of sulphur detected by XRF, that is 0.210, and also the lowest alkali sulphate content in the vapour.

Considering the temperature of sulphate vaporisation, the highest Na^+ intensities are in the case of raw meal II, where the Na content found by XRF equals to 0.0799, whereas the highest Na content, that is 0.170 per cent by mass, is in the raw meal I. The explanation of that is following; in the raw meal II sample sodium is mostly combined as a sulphate, where the highest Na^+ signal at the sulphate temperature range appears. In the raw meal I sample, sodium is combined mostly as oxide, what could be also seen on the intensities of the Na^+ at the temperature range of oxide vaporisation, table 6.19. The highest intensity of Na^+ is by raw meal I, what is in accordance with XRF results. The intensities of Na^+ are also high in the case of material IV, where the content of Na found by XRF was also high, that is 0.115 per cent by mass.

Summarizing, in the vapour of raw material II there is the highest content of sodium sulphate, by other raw materials, sodium vaporizes mostly as oxide soluble in clinker phases.

The highest content of potassium was found by XRF in the case of material III that is 1.22; further 0.754 by material II and 0.582 and 0.430 for raw materials I and IV respectively. Considering sulphate vaporisations, table 6.17, the highest intensities of K^+ are in the case of material II, where it is the highest content of potassium sulphate in the vapour. The intensities of K^+ by materials I and IV are also high, indicating high K_2SO_4 content in the vapour. Taking into account the oxide vaporisation range, table 6.18, it could be realised that the highest intensities of K^+ are in the case of material III, decreasing towards II, I and IV, the same sequence as the content of potassium, detected by XRF.

Hot meal

The ion intensities of the Na^+ , Cl^+ , K^+ , SO^+ , SO_2^+ , detected in the vapours over the all hot meal samples at temperatures 800 °C, 1100°C and 1300 °C are presented in tables 6.20– 6.22.

Table 6.20. The comparison of the intensities of the ions Na^+ , Cl^+ , SO^+ , SO_2^+ , K^+ , detected in the vapour of the hot meal samples from all cement plants at 800 °C .

Ion	Ion intensities/counts*		
	I	II	III
Na^+	583	1709	319
Cl^+	1772	4804	1330
K^+	14302	54156	6576
SO^+	153	432	316
SO_2^+	116	512	309

*hot meal (IV) was not detected at this temperature range

Table 6.21. The comparison of the intensities of the ions Na^+ , Cl^+ , SO^+ , SO_2^+ , K^+ detected in the vapour of the hot meal samples from all cement plants at the 1100 °C.

Ion	Ion intensities/counts			
	I	II	III	IV
Na^+	438	302	43	833
Cl^+	n.d.	n.d.	n.d.	n.d.
K^+	9814	10640	3119	6365
SO^+	19029	6139	10100	47
SO_2^+	6350	6533	9293	79

Table 6.22. The comparison of the intensities of the ions Na^+ , Cl^+ , SO^+ , SO_2^+ , K^+ , during evaporation of the hot meal samples coming from all cement plants at 1300 °C.

Ion	Ion intensities/counts			
	I	II	III	IV
Na^+	2723	3576	1353	405
Cl^+	n.d.	n.d.	n.d.	n.d.
K^+	3000	59088	42543	1045
SO^+	247	470	193	49
SO_2^+	235	470	193	49

Comparing the intensities of sodium, potassium and chlorine at the temperatures corresponding to chloride vaporisation, table 6.20, it could be stated that at 700 °C the highest intensities of Cl^+ , K^+ , Na^+ are in the case of hot meal II. It is in agreement with chloride content determined by XRF, which equals to 2.32 per cent by mass, table 6.7, being the largest within samples I-IV. The intensities of

Cl^+ , K^+ , Na^+ in the vapour over hot meal I and II are also high, showing high content of alkali chlorides. Comparing Na^+ and K^+ intensities it could be also observed that the intensities of potassium are two magnitudes higher as sodium, what indicates that KCl is in the vapour dominative.

Considering table 6.21, the highest intensities of $\text{SO}^+/\text{SO}_2^+$ in are in the vapour over the hot meal I and III what is with agreement with XRF data, showing similar sulphur content in those materials that is 4.86 and 4.77 per cent by mass for hot meal I and III respectively. The intensities of $\text{SO}^+/\text{SO}_2^+$ are one magnitude higher, as by hot meal II, what corresponds to XRF results, showing twice lower sulphur content that is 2.74 per cent by mass. The lowest intensities of sulphate in the vapour are in hot meal IV, where the intensities of $\text{SO}^+/\text{SO}_2^+$ are 3 magnitudes lower, what is also observable in the XRF results, where mass per cent of SO_3 equals to 0.596.

At the temperatures of oxide vaporisation from the clinker phases, table 6.22, the highest intensities of K^+ comes from the vapours over hot meal II and III. The highest content of potassium is soluble in the clinker melt by materials II and III. The sequence of the K^+ intensities correspond to the XRF results, where potassium content equals to over 5 mass per cent by materials II and III. The K^+ intensities by hot meal I are one magnitude lower, where XRD indicated potassium content of 4.7 mass per cent. The lowest K^+ intensities are by hot meal IV, also correspond with XRF data that is 2.4 mass per cent.

Comparing the intensities of Na^+ from table 6.22, it could be stated that the highest content of Na^+ is in the case of hot meal I and III, where the highest content of sodium is dissolved in the clinker melts. By sodium it is worth to consider hot meal II and IV in comparison. The sodium content, determined by XRF is similar and equal to 0.2 mass per cent. Analysing sodium intensities, it could be realised that in the case hot meal II, sodium evaporates mostly as chloride and oxide from clinker melts. In the case of material IV there is high intensity of Na^+ at the temperature of sulphate vaporisation, table 6.20, and smaller at the oxide vaporisation from clinker phases, table 6.22. That could suggest that Na^+ vaporize mostly as sulphates, therefore such alkali intensities cannot be consider separately. In the case of hot meal IV, there is only small signal of $\text{SO}^+/\text{SO}_2^+$, table 6.21 that exclude sulphate vaporisation as a dominative. The intensity of Na^+ from table 6.21 and 6.22 comes mostly from oxide vaporisation from clinker phases, what is also in accordance with the calculated DG for this material, that equals to 49.6 (table 6.9). This example shows that the temperature ranges of alkali sulphate and alkali oxides solved in clinker phases are really close, and difficult to distinguish by simple single ion analysing.

Bypass dust

The ion intensities of the Na^+ , Cl^+ , K^+ , SO^+ , SO_2^+ , detected in the vapours over the all bypass dust samples at temperatures 750 °C and 1200°C as representative for both sulphates and oxides vaporisation from the clinker phases are presented in tables 6.23 – 6.24.

Table 6.23. The intensities of the ions Na^+ , Cl^+ , SO^+ , SO_2^+ , K^+ , during evaporation of the bypass dust sample coming from all cement plants at the 750 °C

Ion	Ion intensities/counts [*]	
	I	II
Na^+	2068	2940
Cl^+	7866	16200
K^+	61108	612090
SO^+	8692	1190
SO_2^+	14969	1640

^{*} bypass dust (IV) was not detected at this temperature range

Table 6.24. The intensities of the ions Na^+ , Cl^+ , SO^+ , SO_2^+ , K^+ , during evaporation of the bypass dust sample coming from all cement plants at the 1200 °C

Ion	Ion intensities/counts		
	I	II	IV
Na^+	4550	2378	1701
Cl^+	n.d.	n.d.	n.d.
K^+	59122	20358	22482
SO^+	18216	11818	1381
SO_2^+	20332	10793	1148

The intensities of K^+ by bypass dust II sample at the chloride vaporisation temperature range, table 6.23, are one order of magnitude higher than by bypass dust I. Also the intensities of Cl^+ by the bypass dust II are twice higher than by bypass II. That indicates that from this sample vaporize enormous contents of potassium chloride. Moreover, KCl was a dominative phase found by XRD, table 6.11. That led to conclusions that in bypass dust II sample, potassium vaporizes mostly as chloride. The chloride content found by XRF in bypass dust sample I that is 16.4 was higher as by bypass dust sample II, where it equals to 12.8, which is not in accordance with the intensities of Cl^+ in the vapour. The reason for that will be discussed in section 6.4.

Considering the intensities of $\text{SO}^+/\text{SO}_2^+$, table 6.24, the highest intensities are by bypass dust I sample, further by bypass II and III. XRF results shows, that the highest content of sulphur is in bypass I, 18.6 mass per cent, what is in accordance with the intensities of $\text{SO}^+/\text{SO}_2^+$ responsible for vaporisation of alkali and calcium sulphates, that are twice higher as those from bypass dust II, where the content of sulphur found by XRF equals to 5.48 by mass (table 6.8). The intensities of ions $\text{SO}^+/\text{SO}_2^+$ by bypass dust IV are one magnitude lower than others what is also in accordance with XRF data, where there is only 1.42 mass per cent of sulphur in this material.

Those results are in accordance with the measurement of hot meal samples, where in the case of the cement plant I, table 6.21, the alkalis are transported mostly as sulphates and in the case of cement plant II, as chlorides, table 6.20, are two magnitudes higher than the others, what indicates that K vaporises mostly as sulphates. The higher Na^+ , K^+ intensities and low SO^+ and SO_2^+ intensities at the vapour of bypass dust (II) and (III) samples indicate that those ions come from oxide vapour from the clinker melt.

Clinker

Clinker is a material, which was sintered at the temperature to 1450 °C in the cement kiln, thus the most of the volatilities have already vaporised in the furnace. Some of those volatilities could get into clinker phases, or could be cooled with the clinker as separate phase. The ion intensities of Na^+ , Cl^+ , K^+ , SO^+ , SO_2^+ , detected in the vapours over the all clinker samples at temperatures 1100 °C and 1300°C are presented in tables 6.25 – 6.26.

Table 6.25. The comparison of the intensities of the ions Na^+ , Cl^+ , SO^+ , SO_2^+ , K^+ , during evaporation of the clinker sample coming from all cement plants at the 1100 °C

Ion	Ion intensities/counts			
	I	II	III	IV
Na^+	890	1223	331	1446
Cl^+	n.d	n.d	n.d.	n.d
K^+	8070	13905	8937	5866
SO^+	1430	2211	1352	1611
SO_2^+	1160	2417	1269	1628

Table 6.26. The comparison of the intensities of the ions Na^+ , Cl^+ , SO^+ , SO_2^+ , K^+ , during evaporation of the clinker sample coming from all cement plants at 1300 °C

Ion	Ion intensities/counts			
	I	II	III	IV
Na^+	7891	4098	332	479
Cl^+	n.d.	n.d.	n.d.	n.d.
K^+	7827	26172	33282	232
SO^+	959	1258	6912	84
SO_2^+	1040	1417	7362	102

As it could be realised in tables 6.25 – 6.26, chloride was not detected in the vapour. As it was stated before, the chlorides vaporize completely at lower temperature ranges, 700 to 900 °C.

Considering the intensities of $\text{SO}^+/\text{SO}_2^+$ from tables 6.25 – 6.26 it could be realised that some of the alkali sulphate got into the clinker, also the molecular ion of potassium sulphate was found in the vapour of the clinker, figure 6.30.

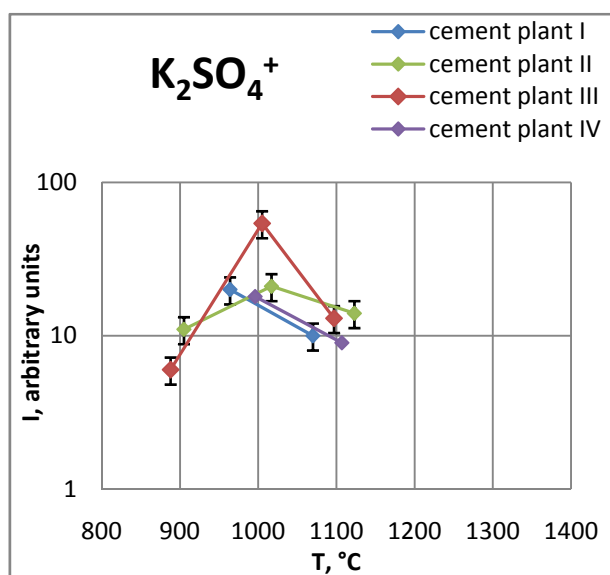


Figure 6.30. The temperature dependencies of the intensity of a molecular ion K_2SO_4^+ detected in the vapour over the clinker samples from all cement plants.

As it is presented in figure 6.30 the highest intensity of potassium sulphate that went into the clinker phases are from the clinker from cement plant III, where there was no bypass installation. Also by clinker III, the intensities of $\text{SO}^+/\text{SO}_2^+$ at 1300 °C (table 6.26) are six times higher than others. That

suggests, that the sulphur is caught by clinker and vaporises as other, more durable sulphates. Worth considering is also the high intensity of $\text{SO}^+/\text{SO}_2^+$ in the case of clinker IV. The sulphur did not vaporize before as alkali sulphate in such high content by the investigation of any of the materials coming from cement plant IV. That indicates that sulphur should be combined in some more durable phase that get into the clinker and later decompose during heating.

The highest sodium content that went into the clinker phases as oxide was in the case of cement plant I. The highest content of potassium sulphate was found in the vapour over the clinker III, where there was no bypass installation.

6.3.3. Lead vaporisation

In all samples under investigation lead was detected in the vapours. In many cases the intensities were too low therefore its vaporisation couldn't be considered together with alkalis. The highest content of lead was detected in hot meal and bypass dust coming from cement plant I and II, presented in figures 6.31 and 6.32 respectively.

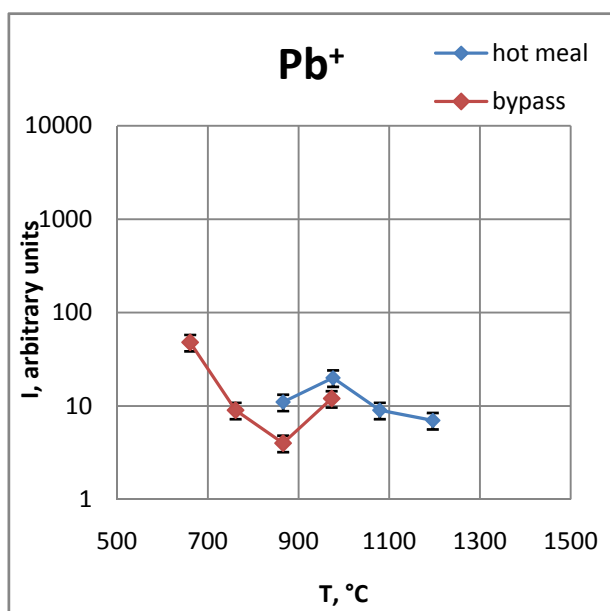


Figure 6.31. Temperature dependencies of the intensity curves of Pb^+ during vaporisation of the hot meal and bypass dust sample coming from the cement plant I.

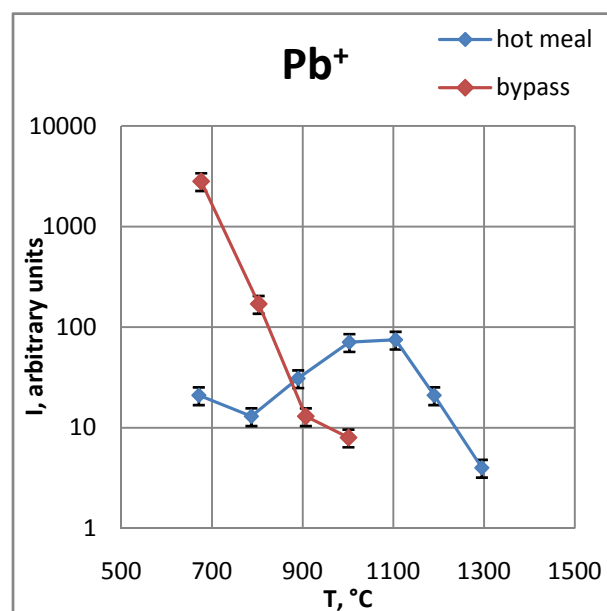


Figure 6.32. Temperature dependencies of the intensity curves of Pb^+ during vaporisation of the hot meal and bypass dust sample coming from the cement plant II

The molecular ion of the lead containing species was not detected; therefore, its vaporisation could only be estimated according to temperature dependencies of the ion intensities of Pb^+ .

The intensity curve of Pb^+ , determined in the vapours over the hot meal samples from both cement plants I and II, shows a maximum between 900 – 1100 °C. That is in accordance with temperature ranges of the vaporisation of sulphates. Therefore, the vaporisation of lead from hot meal sample could be considered as lead sulphates.

The maximum of the intensity curve of Pb^+ from the bypass dust vaporisation occurs at the low temperature ranges far below 900 °C suggesting halides vaporisation. Lead halides are known to be volatile compounds, being even more volatile than alkali halides [40, 72]. The vaporisation of lead could explain also the differences of XRF results and measured intensities of Cl^+ by bypass dust vaporisation, table 6.23. Although the Cl content by bypass I found by XRF equals to 16.4 and by bypass II, 12.5 by mass per cent, the intensities of Cl^+ are higher by vaporisation of bypass II. It could be explained by lead chloride vaporisation that is more volatile as alkali chloride and therefore the strong fragmentation of $\text{PbCl}_2(\text{g})$ species to the Cl^+ ion causes increasing of Cl^+ intensity detected by bypass dust II sample.

Different content of lead was detected in the vapours over bypass dust samples and over hot meal samples in all cement plants. Figures 6.33 – 6.34 present the temperature dependencies of the lead intensity in the gas phase over the bypass dust and hot meal samples coming from all cement plants.

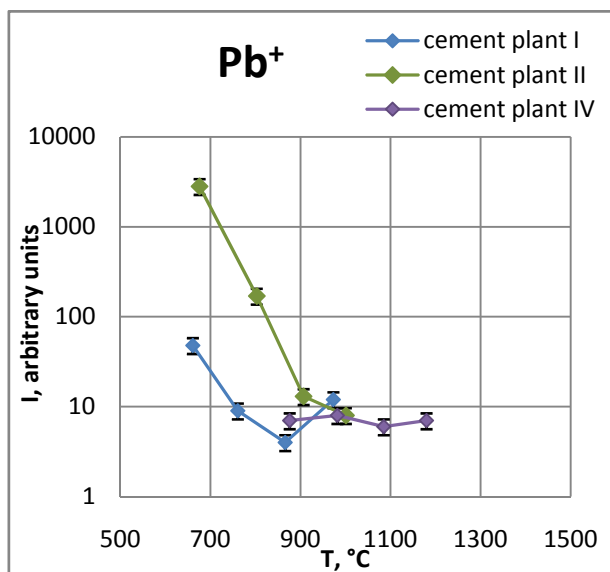


Figure 6.33. The temperature dependencies of lead vaporisation over the bypass dust samples coming from all the cement plants

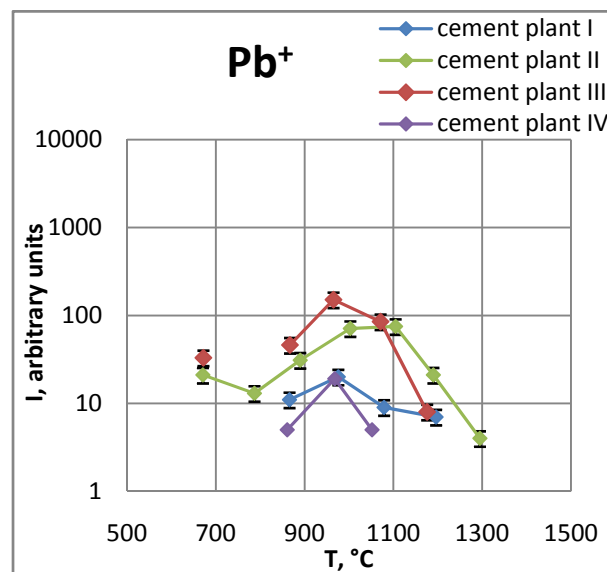


Figure 6.34. The temperature dependencies of lead vaporisation over the hot meal samples coming from all the cement plants

Considering bypass dust samples in figure 6.33, the highest intensity of the Pb^+ in the vapour occurs in the case of the cement plant II and I. The bypass material coming from the cement plant IV includes only traces of the lead in the vapour phase. In the case of the hot meal vaporisation, figure 6.34, the highest intensity of Pb^+ was found in the hot meal III, where there was no bypass installation. In hot meal lead is transported mostly as sulphates in the gas phase.

In the case of the cement plant II the enormous quantity of the fluff, refuse derived fuel and tires are used for clinker production, which are one of the main sources of lead. Similarly, it is in cement plant I, where also high quantity of fluff and tires are used for clinker production.

Lead is removed from the cycle mostly by bypass, as far as it could convert in advance by a cation exchange to the chlorides, and therefore vaporises from the bypass dust samples in the lower temperature ranges, adequate to chloride vaporisation as it is seen in figure 6.33.

In the case of the cement plant III, lead is transported in the gas phase as sulphate in the highest level. In this cement plant was no bypass installation therefore the part of gases contained much lead sulphate remained in the cycle. In this cement plant the main source of lead is fluff which is in use as an alternative fuel.

By hot meal from cement plant IV only traces of Pb^+ were detected, where the lowest quantity of fluff are used.

6.3.5. Mixed and polymeric species

Some other elements and mixed species were found in the vapours over the samples under investigation. In the vapour over the samples investigated, rubidium was found in the vapours. Its behaviour is similar to sodium and potassium vaporisation and it is transported through the gas phase as chlorides and sulphates. An example of the temperature dependencies of rubidium intensity over the all hot meal samples is presented in figure 6.35.

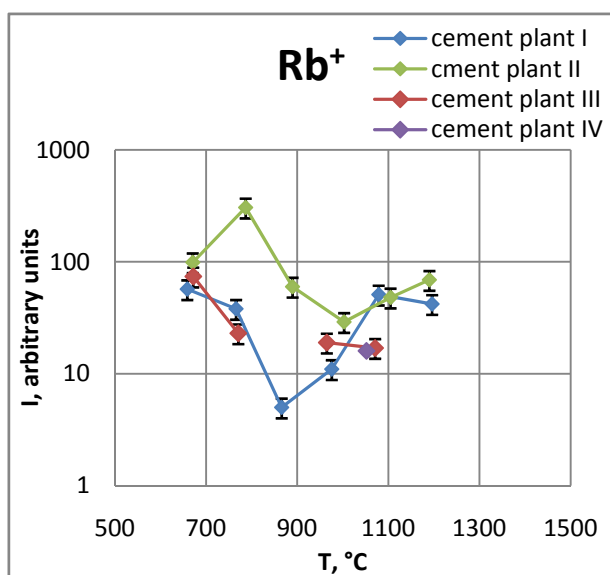


Figure 6.35. The temperature dependencies of the intensity of rubidium over the hot meal samples from all cement plants

The mixed species like NaKSO_4 detected by Eguia [1] and described by the Author [43] was found in the vapours over the hot meal and bypass dust samples. The example of the part of the mass spectrum, determined in the vapours over the bypass sample from cement plant I, is presented in figure 6.36.

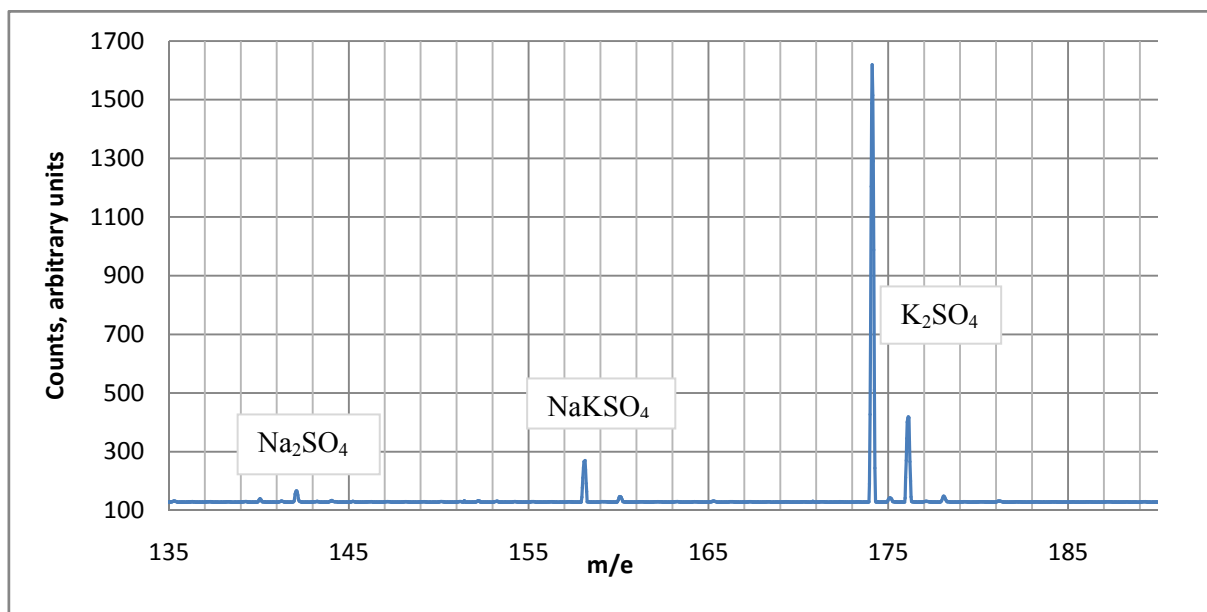


Figure 6.36. Part of the mass spectrum detected in the vapours over the bypass dust sample from the cement plant I at 1100 °C.

The intensity of mixed species is much higher as intensity of Na_2SO_4 . Assuming similar ion cross section of the molecules Na_2SO_4 and NaKSO_4 it could be stated, that the molecule NaKSO_4 would have higher vapour pressure as Na_2SO_4 and are easier transporting sodium as Na_2SO_4 itself.

The other species found in the vapour phase are those coming from chlorides vaporisation that is polymeric species as NaKCl_2 , and K_2Cl_2 .

6.4. Discussion

When the equilibrium is obtained, the vaporisation does not depend on quantity of the sample in the system and, specifically in Knudsen cell, what is used as the principle in the Knudsen effusion mass spectrometry. In the case of the measurement of the industrial samples, alkali chlorides and alkali sulphates were the traces of the materials. The content of volatiles (alkali chlorides, sulphates) was too low and obtaining the equilibrium was unfeasible because of kinetic barriers avoiding equilibrium processes (diffusion, gas flow). The content of the volatiles that vaporized effused immediately through the effusion orifice. The vaporisation was too low in comparison to the escape of the vapours from the cell. All gaseous species arising at the appropriate temperature ranges effused from the cell completely thus the intensities of the ions were proportional to the content of the volatiles in the sample but too low to obtain the equilibrium state. Therefore, in this case, the intensities of the ions measured by Knudsen effusion mass spectrometry could be compared as a representative for the vaporisation of the volatilities from the samples.

The volatilities vaporize completely from the materials at appropriate temperature ranges, specific for the chemical compounds they are, that is

- chlorides between 700 – 900 °C
- sulphates between 1000 – 1200 °C
- alkali oxides from clinker phases > 1200 °C,

schematically presented in figure 6.37.

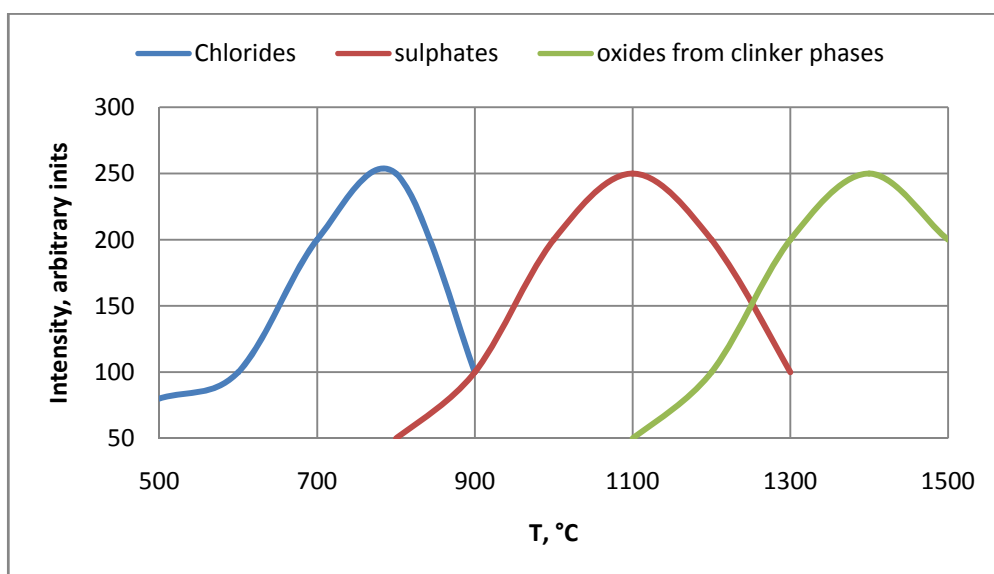


Figure 6.37. Schematic representation of the temperature ranges of the vaporisation of alkali chlorides, sulphates and oxides from the industrial samples.

That effect was reproducible for all the samples under investigation. In the case of some of the materials the three temperature ranges of vaporisation were easily to distinguish, by others only two maxima were observable. This phenomenon occurs when there is a higher content of one ingredient whereas the other is much lower; than instead of three peaks two peaks occur together by superposition as schematically presented in figure 6.38.

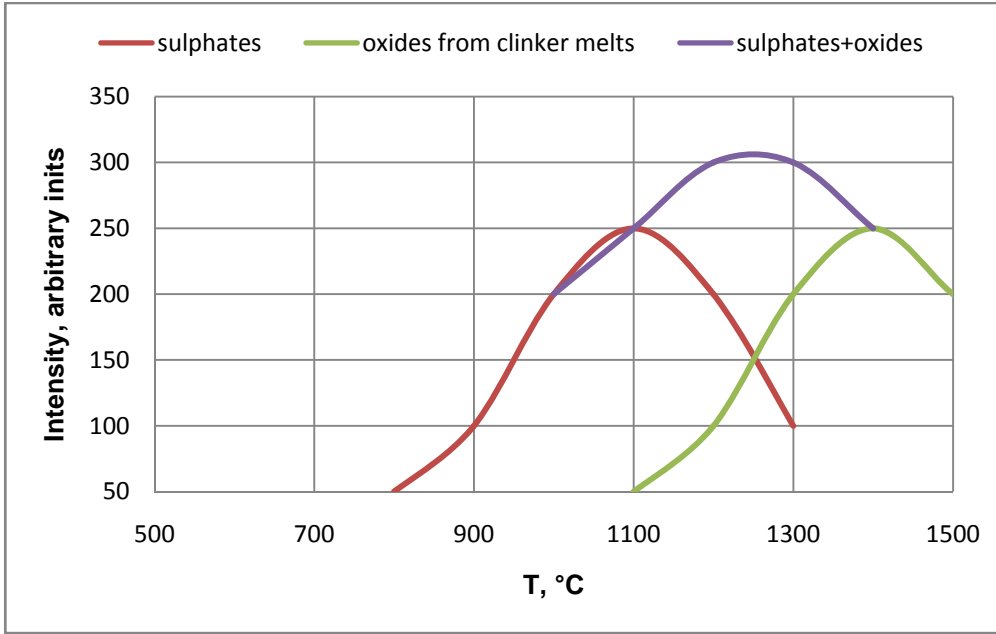


Figure 6.38. Schematic representation of the temperature ranges of vaporisation of alkali sulphates and oxides from the clinker phases; the effect when there is higher content of one component in the vapour and one maximum occurs is marked as violet curve.

In the literature, for example [5], one can find the diagram coming from Bucci data [2], figure 6.39.

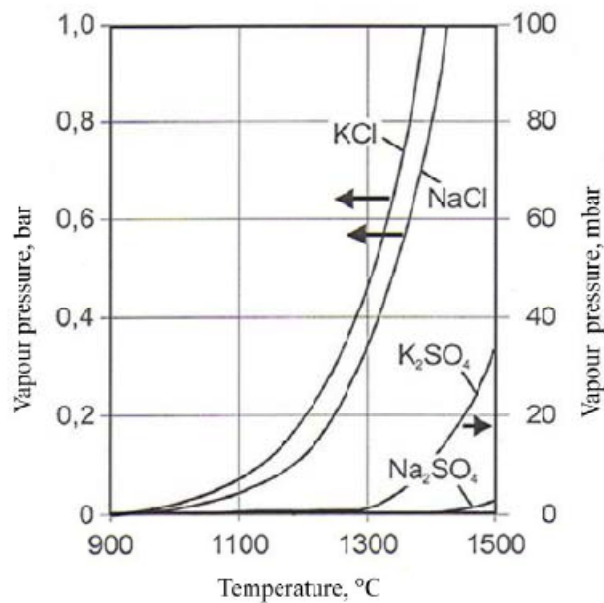


Figure 6.39. Vapour pressures of the chlorides and sulphates of sodium and potassium as function of temperature [5].

This diagram bases on the data from Halstead [47] and Cubicciotti [48] investigations of the pressures of alkali sulphates over the pure substances by effusion methods. The chlorides vaporisation data comes from Ritter [73]. The diagram, presented in figure 6.39 shows the pressures of pure alkali chlorides and sulphates, measured under equilibrium condition, extrapolated into the high temperatures. It was stated by many authors that in the sinter zone alkali chlorides pressures are some order of magnitude higher as sulphates and could reach even 1 bar [5]. That could be truth when there would be enough chlorides and sulphates content and the equilibrium state or near equilibrium state could be achieved in the system. The presented investigations, where the vaporisation of the real industrial samples taken from the cement kiln was carried out, showed that the content of chlorides is far not enough to achieve the equilibrium. By every sample metal chloride phase vaporizes and disappears from the vapour completely over 1000 °C, before sulphates start vaporizing at its high content. Therefore the vaporisation of alkali chlorides and sulphates should be considered separately. According to presented investigations it is not possible, that at the sintering zone, the pressures of chlorides could reach 1 bar, the same pressure as pure alkali chloride at equilibrium state at those temperatures. The vaporisation of alkali sulphates and sulphates of other metals from clinker melts should be considered together, as they could vaporise at the same temperature ranges.

The vaporisation of alkalis increases according to Ivtanthermo database as follows presented in figure 6.40.

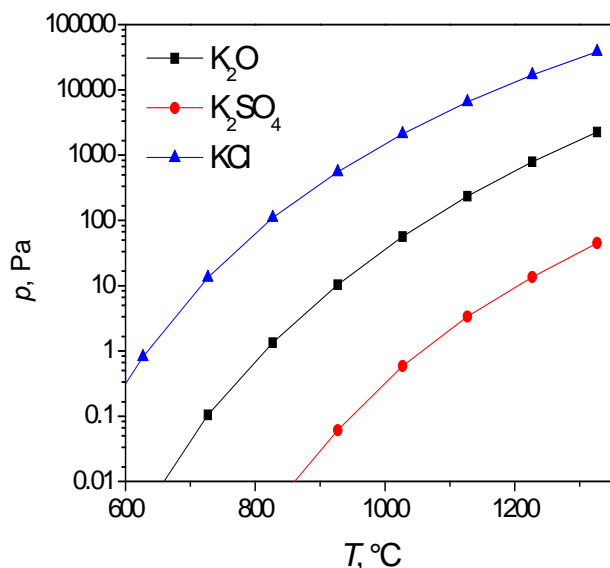


Figure 6.40. Partial pressure of potassium oxide, sulphate and chloride from Ivtanthermo database [40]

Alkali oxides are very volatile, but in the case of industrial samples, the alkali oxides are solved in the clinker phases what decreases their pressures by few orders of magnitude because of its lower activity. The alkali sulphates exist as separate phase or as alkali sulphate – calcium sulphate melts, that could be seen in XRD data table 6.10 – 6.11. Therefore the alkali sulphates are more volatile as alkali oxides soluble in the clinker melt.

In the industrial process of the clinker burning, it is worth to consider the retention time in the sintering zone and the agglomeration of the kiln feed. In the real process the material has a contact with the high temperatures only around 10 minutes, differently as in the KEMS experiment. In the real process, the material is flowing through the cyclones and rotary kiln in the counter-current towards the flame what enables faster reaction and also the vaporisation of volatiles. In the burning process, the important influence on the course of the chemical reactions originates from the material agglomeration. In the normal state, due to the rotation of the tube, the kiln feed in rotary kiln forms a roll of loose material which moves slowly towards the lower end of the tube as a result of the inclination of the kiln. The rolling motion of the kiln feed contributes substantially to the formation of dense clinker granules [5]. However, when the

granules are formed too early or grow too big the vaporisation process of volatiles can be inhibited, what results in remaining of a part of volatiles inside the granules. The vaporisations of such granules resemble the hot meal vaporisation that means inside the granules remains nonreacted material. The example of the vaporisation of such granules is presented in figure 6.41.

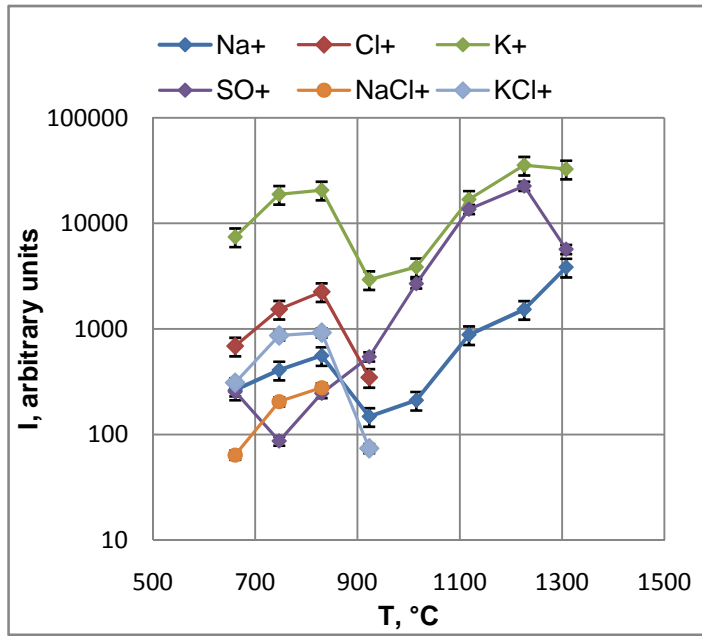


Figure 6.41. The example of the vaporisation of not reacted clinker granules where the wrong burning conditions occur.

The degree of sulphatisation described by eq. 6.2, 6.3 (section 6.2.2.1) that show the percentage of the alkalis which are presents as alkali sulphate was taken into account in the case of materials under investigation. According to table 6.9 the degree of sulphatisation of most of the samples amount to over 100%, what means that the sulphur is not fully combined as alkali sulphate and its excess reacts with CaO and forms or CaSO_4 or mixtures of K_2SO_4 and CaSO_4 . Therefore, in this case it is worth to consider the sulphate vaporisation and its pressures from the binary system $\text{K}_2\text{SO}_4 - \text{CaSO}_4$, taking into account the activities obtained in the section 5.6.1.

According to present investigation it is also worth to consider the vaporisation of alkali not only as $M\text{Cl}(\text{g})$ and $M_2\text{SO}_4(\text{g})$ species, where $M=\text{Na}, \text{K}$, but also as mixed and polymeric species such as $\text{K}_2\text{Cl}_2(\text{g})$, $\text{NaKCl}_2(\text{g})$ and $\text{NaKSO}_4(\text{g})$. The role of the latter species for alkali transport in the kiln was modelled before [43]. Mixed and polymeric samples are significantly responsible for

alkali transport. According to previous researches [43], the atom K is the major alkali metal transported in the kiln, mostly by $K_2SO_4(g)$ molecule, whereas presence of $NaKSO_4$ molecule has significant influence for transport of atom Na, figure 5.16. That was also confirmed in the presented results of the industrial samples vaporisation studies.

It is also worth to discuss the influence of the alternative fuels on the vaporisation rate. In the case of materials coming from cement plants II and I, where enormous amounts of alternative fuels are used, the vaporisation of the volatilities is the highest from all the materials under investigation. The intensities of sulphur and alkalis were the highest in the case of those two cement plants. Also high vaporisation of sulphur and alkalis was detected in the case of materials coming from cement plant III. The lowest quantity of alkali sulphate/chloride vaporisation was detected in the case of cement plant IV, where mostly brown coal and brow coal dust and the low fluff content as alternative fuel are used. The chlorides vaporisation are the highest in the case of cement plant II, where the highest amount of fluff is used that is one of the main sources of chloride.

The special attention was drawn to the lead vaporisation. The highest vaporisation of lead from hot meal sample was detected in the case of the cement plant III and from hot meal coming from cement plant II vaporising as sulphates.

The enormous content of lead is caught by bypass installation in the cement plant II, and cement plant I, where the most alternative fuels as the lead sources are used. The most alternative fuels is used in cement plant II, therefore the intensities of Pb^+ vaporising as chloride from bypass dust sample are the highest.

Summarising, the vaporisation of volatiles could be combined with the quantity of the alternative fuels used. The vaporisation of alkalis should be considered as three different processes, from which the chloride vaporisation does not influence on alkali sulphate and alkali oxide vaporisation from clinker melt. Also the mixed species and polymeric species should be considered by modelling of the alkali transport in the gas phase.

7. Outlook

Some of the industrial samples, that are bypass dust and hot meal sample coming from the cement plant II, were investigated by the new developed experimental method, the commercial skimmer coupled mass spectrometer with simultaneous thermal analysis (DTA/TG).

The investigation of the materials by this method was originally not a part of the project, therefore the principle of the method and the experiment will be presented only briefly. The measurements were carried out for a trial to determine the possibility of the further application of the method into the characterization of the vaporisation of the industrial materials. The investigations of the industrial samples were carried out in the FZ Jülich [74].

7.1. The principle of the method

By skimmer coupled mass spectrometer (MS) with simultaneous thermal analysis (DTA/TG) method, the amounts of gases generated by the volatilization of the materials can be detected as the function of temperature when the temperature of the sample is increased at the predetermined heating rate. The gaseous products are flushed out of the furnace chamber operated at 1 atm thereby simulating the technology regime used in the industrial installation. Gas products are flushing out with help of pure gas for example air, N₂ etc. The involved gas is introduced in MS detector through a coupling system which acts both as MS inlet and pressure reduction system [75]. The coupling takes place directly in the furnace and is arranged right above the sample container. Since the entire system has sample temperature, no condensation during the gas emanation changes the condition of the vapour phase of the sample [76]. The schematic diagram of a skimmer coupled mass spectrometer with simultaneous thermal analysis (DTA/TG) is presented in figure 7.1 [77].

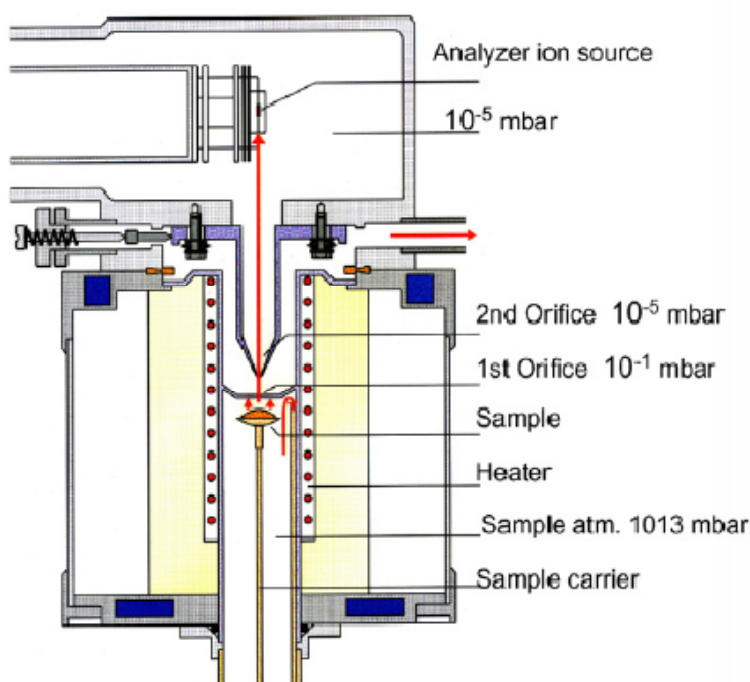


Figure 7.1. Scheme of skimmer coupled mass spectrometer with simultaneous thermal analysis (DTA/TG) apparatus [77].

The coupling system presented in figure 7.1, consists of two orifices in tandem, which are held at the same temperature as the sample. The coupling system lies right inside the thermobalance furnace. The first orifice serves as a divergent nozzle and creates a compression zone into which the second orifice, the so-called Skimmer, extends and creates a parallel molecular beam, which is directed at the ion source of the QMS [77]. Entering the ion source, the molecules are ionized by electron impact ionization with nominal electron energy of 70 eV. The ions are filtered in a quadrupole mass analyzer by their mass-to-charge (m/z) ratio and the intensity of the ion current is detected by a secondary electron multiplier. Kobertz et al. [76] in his work describes Skimmer coupled mass spectrometer with simultaneous thermal analysis (DTA/TG) in details showing also the possibilities of combining this method with Knudsen effusion mass spectrometry, what was also the aim of presented investigations.

7.2. Experimental section

The measurements were carried out in FZ Jülich with a thermal analysis instrument Netzsch STA 409 CD TG/DSC connected to a Balzers quadrupole Mass Spectrometer QMG422 (0–300 amu) by a special Coupling System. The measurements were carried out in the Pt crucibles in air

atmosphere. The temperature was increased from the temperature of 100 °C to 1400 °C with heating rate of 10 °C /min.

The obtained results of the investigation show the potential of the method for its application for the investigation of the vaporisation of industrial materials, but are not reliable enough for publishing at this stage.

The Skimmer coupled mass spectrometer with simultaneous thermal analysis (DTA/TG) could be a compliment for Knudsen effusion mass spectrometry because it enables the kinetically oriented identification of vaporisation by various atmospheres. The connection of Knudsen effusion mass spectrometry and Skimmer coupled with mass spectrometer and a simultaneous thermal analysis (DTA/TG) could in the future potentially fulfil the characterization of the vaporisation processes in the cement kiln through the determination of the partial species and their thermodynamic data together with the determination of kinetically oriented vaporisation by simulating the temperatures and atmospheres in the kiln oven.

8. Conclusions

This work focused on the thermochemical characterization of the gas circulation in the cement kiln and was undertaken due to the real industry problems during clinker production. Nowadays engineers can deal with some of the gas recirculation problems, but mechanism of such processes is not known. For this purpose the studies by the Knudsen effusion mass spectrometry was applied for gas vaporisation investigations. These studies widely implement KEMS as a tool for studying the vaporisation of volatilities occurring during clinker production and are in accordance with the previous investigation made in this field [1] completed before the aforementioned results were obtained.

The aim of the presented investigation was a better understanding of the volatile cycles in cement production technology by studying the thermodynamics of gas-gas and gas-solid reactions between chemicals occurring in the cement kiln, focused mostly on alkali sulphates vaporisation.

The first part of the project was the investigation of pure sulphate compounds, Na_2SO_4 , K_2SO_4 and CaSO_4 and the quasi binary system $\text{Na}_2\text{SO}_4 - \text{CaSO}_4$, $\text{K}_2\text{SO}_4 - \text{CaSO}_4$. By renewed pure alkali sulphates vaporisation, the thermodynamic characteristic of pure sulphates was determined and the fragmentation path of the gaseous species explained. The results are in accordance with the literature data. In the renewed investigation of $\text{K}_2\text{SO}_4 - \text{CaSO}_4$ system, the activities of the compounds were obtained with a higher accuracy. By the measurement of $\text{Na}_2\text{SO}_4 - \text{CaSO}_4$ system, the activities of Na_2SO_4 were obtained by Na_2SO_4 – rich samples, but the experiments did not compile the system exhaustively. In the measurement many difficulties were encountered due to creeping and therefore those experiments need to be repeated for better accuracy of the data.

The second part of the project was the determination of volatiles over the samples taken directly from the kiln from four different cement plants. The industrial materials were collected from four different cement plants, at four different kiln stages to characterize the dependence of volatilities vaporisation on various parameters such as atmospheres and temperature.

The obtained results showed the three vaporisation stages of volatilities alkali chlorides from all the industry materials; at the low temperature ranges 700 – 900 °C as alkali chlorides vaporisation, alkali sulphates vaporisation at 1000 – 1200 °C and vaporisation of alkali oxides from clinker phases at the temperature above 1200 °C. The present investigation showed that the vaporisation of alkali chlorides and alkali sulphates do not influence each other and the alkali chloride disappears from the vapour completely over 1000 °C, before sulphates start vaporizing at a high content; therefore, it is not possible that the chlorides could reach 1 bar in the sintering zone in the cement kiln, as it was considered before. Present investigation showed the similar temperature ranges of vaporisation of alkali sulphates and alkali oxides from clinker phases. These vaporisation processes were difficult to distinguish. The further investigation of vaporisation of alkali sulphates together with alkali oxides solved in the clinker melt will be needed to complete the characterization of alkali circulation in the clinker kiln.

The presented investigation described also the importance of the polymeric and mixed species such as NaKSO_4 in the gas transport processes and should be therefore considered by every modelling of the alkali transport, chemical reactions and equilibrium constants equations.

In this work, the first investigations of the industrial materials by skimmer coupled mass spectrometer with simultaneous thermal analysis (DTA/TG) were undertaken, indicating a great potential of this method combined with Knudsen effusion mass spectrometry for the investigation of the gaseous processes during clinker production.

9. References

1. Eguia, G.E., *Chemische und thermodynamische Untersuchung von kreislauffrelevanten Verbindungen bei der Zementherstellung durch Knudsen-Effusionmassenspektrometrie*, in *Institut für Nichtmetallische Werkstoffe*. 2006, Technische Universität Clausthal: Clausthal-Zellerfeld.
2. Bucchi, R., *Influence of the nature and preparation of raw materials on the reactivity of raw mix*, in *7. Intern. Congr. Chem. Cem.* 1980: Paris. p. I-3-43.
3. Bhatti, J.I., *Role of Minor Elements in Cement Manufacture and use*. PCA Research and Development Bulletin, 1995. **RD 109.03T**: p. 1-39.
4. Taylor, H.F.W., *Cement Chemistry*, ed. T. Telford. 1997, London.
5. Locher, F.W., ed. *Cement - Principles of production and use*. 2006: Düsseldorf.
6. Fidaros, D.K., et al., *Numerical modelling of flow and transport processes in a calciner for cement production*. Powder Technology, 2007. **171**: p. 81-95.
7. Eysel, W., *Crystal chemistry of the system $\text{Na}_2\text{SO}_4\text{-K}_2\text{SO}_4\text{-K}_2\text{CrO}_4\text{-Na}_2\text{CrO}_4$ and the glaserite Phase*. American Mineralogist, 1973. **58**: p. 736-747.
8. Rowe, J.J., G.W. Morey, and I.D. Hansen, *The binary system $\text{K}_2\text{SO}_4\text{-CaSO}_4$* . Journal of Inorganic and Nuclear Chemistry, 1965. **27**: p. 53-58.
9. Wolter, A., *Minor constituent recirculation in kiln system*, in *European Cement Conference*. 2001: Dresden.
10. Miller, M., *Thermodynamics investigations of the metal halide systems by Knudsen effusion mass spectrometry*. Scientific Papers of the Institute of Inorganic Chemistry and Metallurgy of Rare Elements of the Technical University of Wrocław. Vol. 66. 1997, Wrocław: Oficyna Wydawnicza Politechniki Wrocławskiej.
11. Ionov, N.I., *Doklady Akademii Nauk SSSR*, 1948. **59**(467-469): p. 467.
12. Chupka, W.A. and M.G. Inghram, *Journal of Physical Chemistry*, 1955. **59**: p. 100-1004.
13. Honig, R.E., *Journal of Chemical Physics*, 1954. **22**: p. 126-131.
14. Miller, M. and K. Armatys, *Twenty Years of Knudsen Effusion Mass Spectrometry: Studies Performed in the Period 1990 - 2010*. accepted for publication, 2011.
15. Inghram, M.G. and J. Drowart, *Mass Spectrometry Applied to High Temperature Chemistry*, in *High Temperature Technology*. 1960, McGraw-Hill Book Company: New York.
16. Knudsen, M., *Annalen Der Physik*, 1909. **29**: p. 75-130.
17. Margrave, J.L., *The Characterisation of High-Temperature Vapours*. 1967, New York London Sydney: John Wiley&Sons INC.
18. Clausius, P., *Über die Stromung sehr verdünnter Gase durch Röhren von beliebiger Länge*. Annalen Der Physik, 1932. **404**(8): p. 961-989.
19. Motzföldt K., *The thermal decomposition of sodium carbonate by the effusion method*. 1955. **59**: p. 139-147.
20. Whitman, C.I., *On the measurement of the pressures by effusion*. The Journal of Chemical Physics, 1952. **20**(1): p. 161-164.
21. Ramsey, N.F., *Z. Phys. D. - Atoms, Molecules, Clusters*, 1988. **10**: p. 121-125.
22. Carlson, K.D., P.W. Gilles, and R.J.J. Thorn, *Journal of Chemical Physics*, 1963. **38**(11): p. 2725-2735.

23. Rosenblatt, G.M., *Journal of The Electrochemical Society*, 1963. **110**(6): p. 563-569.
24. Vande, J.E. and C.I. Whitman, *Journal of Chemical Physics*, 1951. **19**(6): p. 744-748.
25. Stern, J.H. and N.W. Gregory, *The Condensation Coefficient of Iodine*. *Journal of Physical Chemistry*, 1957. **61**(9): p. 1226-1232.
26. Hilpert K., *Potential of mass spectrometry for the analysis of inorganic high-temperature vapors*. *Fresenius J Anal Chem*, 2001. **370**: p. 471-478.
27. Hilpert K., *High-temperature mass spectrometry in materials research*. *Rapid Communications in Mass Spectrometry*, 1991. **5**: p. 175-187.
28. Hilpert K., *Chemistry of Inorganic Vapors*, in *Structure and Bonding*. 1990: Berlin. p. 97-198.
29. Sidorov, L.N., *Inorganic Chemistry, Applications of Mass Spectrometry*, in *Encyclopedia of Spectroscopy and Spectrometry*. 2000, Elsevier Science. p. 915-923.
30. Drowart, J. and P. Goldfinger, *Die massenspektrometrie anorganischer systeme bei hohen Temperaturen*. *Angewandte Chemie*, 1967. **79**(13): p. 589-604.
31. Copland, E.H. and N.S. Jacobson, *Measuring Thermodynamic Properties of Metals and Alloys With Knudsen Effusion Mass Spectrometry*. NASA/TP—2010-216795, 2010.
32. Drowart, J., et al., *High-temperature mass spectrometry: instrumental techniques, ionization cross-sections, pressure measurements, and thermodynamic data*. *Pure and Applied Chemistry*, 2005. **77**(4): p. 683-737.
33. Stolyarova, V.L. and G.A. Semenov, *Mass Spectrometric Study of the vaporization of Oxide Systems*, ed. J.H. Beynon FRS. 1994, Chichester: John Wiley & Sons.
34. Skudlarski, K., *Spektrometria mas i parowanie nadrenianow litowcow*. Vol. 20. 1973, Wroclaw: Prace naukowe Inst. Chem. Nieorg. i Met. Pierw. Rzadkich Politechniki Wroclawskiej.
35. Mann, J.B., *Ionization Cross Sections of the Elements Calculated from Mean-Square Radii of Atomic Orbitals*. *The Journal of Chemical Physics*, 1967. **46**(5): p. 1646-1651.
36. Freund, R.S., R.C. Wetzel, and R.J. Shul, *Measurements of electron-impact-ionization cross sections of N₂, CO, CO₂, CS, S₂, CS₂ and metastable*. *Physical Review A*, 1990. **41**(11): p. 5861-5868.
37. Freund, R.S., et al., *Cross-section measurements for electron-impact ionization of atoms*. *Physical Review A*, 1990. **41**(7): p. 3575-3595.
38. Shul, R.J., R.S. Freund, and R.C. Wetzel, *Electron-impact-ionization cross sections of GaCl, GeCl, and SnCl*. *Physical Review A*, 1990. **41**(11): p. 5856-5860.
39. Otvos, J.W. and D.P. Stevenson, *Journal of the American Ceramic Society*, 1956. **78**: p. 546-551.
40. IVTANTHERMO, ed. *A Thermodynamic database and Software System for the Personal Computer*, . ed. M.V.A. Yungman V.S., Veits I.V. and Bergman G.A. 1993, CRS Press and Begell House, Boca Raton, FL,.
41. Belton, G.R. and R.J. Fruehan, *The determination of activities by mass spectrometry. I. The liquid metallic system iron-nickel and iron-cobalt*. *The Journal of Physical Chemistry*, 1967. **71**(5): p. 1403-1409.
42. Goldmann, W., W. Kreft, and R. Schutte, *Cyclic phenomena of sulphur in cement kilns*. *World Cement Technology*, 1981. **11**: p. 424-430.

43. Armatys, K., et al., *Vaporization study of sodium sulphate - potassium sulphate binary system by Knudsen effusion mass spectrometry*. accepted for publication, 2011.
44. Halle, J.C. and K.H. Stern, *Vaporization and decomposition of Na₂SO₄. Thermodynamics and kinetics*. Journal of Physical Chemistry, 1980. **84**: p. 1699-1704.
45. Lau, K.H., et al., *Studies of the vaporization/decomposition of alkali sulfates*. Journal of the Electrochemical Society: Solid States science and Technology, 1985. **132**(12): p. 3041-3048.
46. Lau, K.H., D. Cubicciotti, and D.L. Hildenbrand, *Effusion Studies of the vaporization/decomposition of potassium sulfate*. Journal of the Electrochemical Society: Solid States science and Technology, 1979. **126**(3): p. 490-495.
47. Halstead, W.D., *Saturated Vapour Pressure of Potassium Sulphate*. Transactions of the Faraday Society, 1970. **66**: p. 1966-1973.
48. Cubicciotti, D. and F.J. Keneshea, *Thermodynamics of Vaporization of Sodium Sulfate*. High Temperature Science, 1972. **4**: p. 32-40.
49. Powell, D.G. and P.A.H. Wyatt, *Vapour Pressures of Anhydrous Sulphates. Part 1. Knudsen Effusion Results between 560 and 1000 °C for Alkali-metal Sulphates*. Journal of the Chemical Society A, 1971: p. 3614-3617.
50. Ficalora, P.J., et al., *Mass spectrometric studies at high temperatures: XXIX, thermal decomposition and sublimation of alkali metal sulfates*. Journal of the American Ceramic Society, 1968. **51**(10): p. 574-577.
51. Fotiev, A.A. and B.V. Slobodin, Russian Journal of Inorganic Chemistry, 1965. **10**(3): p. 309-311.
52. Kosugi, T., *Measurements of the vapor and dissociation pressures of potassium sulfate and carbonate at high temperatures*. Bulletin of the Chemical Society of Japan, 1972. **45**: p. 15-19.
53. Uhlig, G.F., H.H. Davis, and H.C. Graham, *Vaporization Kinetic of Na₂SO₄ from 900° to 1200 °C*. Journal of the American Ceramic Society, 1975. **58**(5-6): p. 201-203.
54. Jagannathan, G.V. and P.A.H. Wyatt, Journal of Chemical Research S, 1978: p. 203.
55. Jagannathan, G.V., D.G. Powell, and P.A.H. Wyatt, Journal of Chemical Research S, 1978: p. 372-373.
56. Märk, T.D., *Cross section for single and double ionization of N₂ and O₂ molecules by electron impact from threshold up to 170 eV*. Journal of Chemical Physics, 1975. **63**(9): p. 3731-3736.
57. Orient, O.J. and S.K. Srivastava, *Mass spectrometric determination of partial and total electron impact ionization cross sections of 502 from threshold up to 200 eV*. Journal of Chemical Physics, 1984. **80**(1): p. 140-143.
58. Miller, M. and J. Kapała, *Niektóre aspekty fragmentacji jonowych cząsteczek gazowych w badaniach termodynamiki halogenków metali metoda spektrometrii mas*. Annales Universitatis Marie Curie-Skłodowska Lublin - Polonia, 1992. **XLVI/XLVII 28**(AAA): p. 283-296.
59. Bencze, L., e-mail correspondence.

60. Drowart J., et al., *High-temperature mass spectrometry: instrumental techniques, ionization cross-sections, pressure measurements, and thermodynamic data*. Pure and Applied Chemistry, 2005. **77**: p. 683-737.
61. Lau, K.H., D. Cubicciotti, and D.L. Hildenbrand, *Effusion studies of the thermal decomposition of magnesium and calcium sulfates*. The Journal of Chemical Physics, 1977. **66**(10): p. 4532 - 4539.
62. Zawadzki, J., *Zur Kenntnis des Systems Calcium-Schwefel-Sauerstoff*. Zeitschrift für Anorganische und Allgemeine Chemie, 1932. **205**: p. 180-192.
63. Freyer, D., W. Voigt, and K. Kohnke, *The phase diagram of the system Na_2SO_4 - CaSO_4* . European Journal of Solid State and Inorganic Chemistry, 1998. **35**: p. 595-606.
64. JCPDS - International Centre for Diffraction Data, ICDD cards.
65. Adaska, W.S. and D.H. Taubert, *Beneficial uses of cement kiln dust*, in *IEEE/PCA 50th Cement Industry Technical Conf.* 2008: Miami.
66. Ariyaratne, W.K.H., et al., *Meat and Bone Meal as a Renewable Energy Source in Cement Kilns: Investigation of Optimum Feeding Rate*, in *International Conference on Renewable Energies and Power Quality (ICREPQ'11)*. 2010: Spain.
67. Wolter, A. *Phase composition of calcined raw meal*. in *8th International Congress of Chemistry of Cement*. 1986. Rio de Janeiro.
68. *Isotope Calculator*. Available from: <http://www.sisweb.com/mstools/isotope.htm>.
69. Milne, T.A., H.M. Klein, and C. D., *Mass Spectrometer Analysis of the Vapor in Equilibrium with the Alkali- Metal Chlorides*. Journal of Chemical Physics, 1958. **28**: p. 718-719.
70. Van der Kemp W. J. M., et al., *The vapour composition and pressure over solid potassium chloride: new mass-spectrometric results and effusion masses*. J. Chem. Thermodynamics, 1991. **23**: p. 593-604.
71. Gesenhues U., Reuhl K., and W. H., *Vapour pressure and composition above mixed melts of alkali chlorides and aluminium chloride*. International Journal of Mass Spectrometry and Ion Physics, 1983. **47**: p. 251-252.
72. McPhail, D.S., M.G. Hocking, and J.H.E. Jeffes, *Metal halide vapour complexes: mass spectrometry*. International Journal of Mass Spectrometry and Ion Processes, 1984. **59**: p. 261-276.
73. Ritter, F., *Über den Flugstaub deutscher Portland - Zementwerke*. 1930: Jena.
74. FZ Jülich, IEK - 2.
75. Arii, T., *Involved Gas Analysis-Mass Spectrometry (EGA-MS) Using Skimmer Interface System Equipped with Pressure Control Function*. J. Mass Spectrom. Soc. Jpn., 2005. **53**(4): p. 211 - 216.
76. Kobertz, D., C. Gugushev, and M. Müller, *Investigations at High Temperature in Both Equilibrium and Kinetic State with Knudsen Effusion Mass Spectrometry (KEMS) and a Skimmer Integrated Coupling System of Mass Spectrometer and Thermal Analysis (STAMS)*. Open Journal, in press, 2011.
77. Senneceea, O., F. Scherillo, and A. Nunziata, *Thermal degradation of pesticides under oxidative conditions*. J. Anal. Appl. Pyrolysis, 2007. **80**: p. 61 - 76.

Eidesstattliche Erklärung

Hiermit erkläre ich an Eides Statt, dass ich die bei der Fakultät für Natur- und Materialwissenschaften der Technischen Universität Clausthal eingereichte Dissertation selbständig und ohne unerlaubte Hilfe verfasst und die benutzten Hilfsmittel vollständig angegeben habe.

Clausthal – Zellerfeld, September 2011

.....

Kamila Anna Armatys

Lebenslauf

Name: Kamila Armatys
Nationality: Polish
Date of birth: 07.12.1984
Place of birth: Wrocław, Poland

Education

2008 – 2011 PhD Student, Institute for Non- Metallic Materials, Clausthal University of Technology, Germany, DAAD Scholarship

2003 – 2008 Master of Science (engineer) at Wrocław University of Technology, Poland, Faculty Chemistry

1999 – 2003 Secondary School, Wrocław, Poland,
Profile: biology and chemistry